This is to certify that the

dissertation entitled

SINGLE CRYSTAL GROWTH OF CALCIUM OXALATE MONOHYDRATE IN VARIOUS AQUEOUS IONIC MEDIA

presented by

John D. DeLong

has been accepted towards fulfillment
of the requirements for

Ph.D. degree in CHE

Daina Briedis
Major professor

Date May 16, 1988

SINGLE CRYSTAL GROWTH OF CALCIUM OXALATE MONOHYDRATE IN VARIOUS AQUEOUS IONIC MEDIA

By

John D. DeLong

A DISSERTATION

Submitted to
Michigan State University
in partial fulfillment of the requirements
for the degree of

DOCTOR OF PHILOSOPHY

Department of Chemical Engineering

1988

ABSTRACT

SINGLE CRYSTAL GROWTH OF CALCIUM OXALATE MONOHYDRATE
IN VARIOUS AQUEOUS IONIC MEDIA

By

John D. DeLong

This study was undertaken to investigate the single crystal growth of calcium oxalate monohydrate (COM), a sparingly soluble salt that is a primary mineral constituent of kidney stones. Growth rates were measured under various solution conditions simulating those observed in urine.

Single crystal face growth rates of COM were measured using a photomicroscopic growth cell technique. COM growth rate was measured as a function of relative supersaturation, temperature, ionic strength, calcium to oxalate ratio, and polyelectrolyte concentration. The polyelectrolytes used, polyglutamate and heparin, are similar to urinary crystal growth modifiers thought to be important in the mechanism of kidney stone formation.

COM single crystal growth rate was found to have a second order dependence on the relative supersaturation with an activation energy for growth averaged over all crystal faces of 50.4 kJ/gmol, indicating a surface-integration-controlled growth mechanism with dehydration of the cation thought to account for the majority of the activation energy. The growth rate was greatest on the 110 faces; the 010 and $\underline{1}01$ faces showed slower, approximately equal growth rates. The faster rate of the 110 faces was reflected by the elongated growth habit seen for COM. At high relative supersaturation ($\sigma > 8$ at 25 °C) the growth habit showed a gradual transition as 010 faces were overcome by 011 faces.

COM growth rate measured as a function of ion ratio at ionic strength of 0.15 M buffered with KCl showed a maximum at equimolar ion ratio, with decreasing growth rate observed at low and high ion ratio. Results of the measurement of growth rate versus ion ratio with no added KCl showed no effect of ion ratio. The effect of ion ratio in the presence of the background electrolyte was most likely due to a non-constant driving force for crystal growth and indicates that relative supersaturation, maintained constant throughout the experiments, is not a complete expression of the driving force. COM growth rate increased with ionic strength towards an asymptotic maximum. This effect was similar to trends in double layer thickness as predicted by the Gouy-Chapman treatment of the electrical double layer suggesting that growth enhancement at increased ionic strength was due to compression of the electrical double layer at the solution/crystal interface.

Growth rate was inhibited by polyglutamate and by heparin. The shape of the curves of growth rate versus polyelectrolyte concentration indicated an inhibition mechanism by polyelectrolyte adsorbed on the crystal surface. When considered in the context of the different crystal lattice structure exposed on each crystal face, a lower degree of inhibition on the 010 face as compared to the $\underline{1}01$ face indicated an inhibition mechanism which involves incorporation of polyelectrolyte-bound calcium ions into the crystal lattice with anionic polyelectrolyte functional groups occupying oxalate lattice positions.

The results demonstrated the superiority of the photomicroscopic method over conventional methods in measuring crystal growth rates and offered new insights to the mechanism of electrolyte crystal growth.

TABLE OF CONTENTS

TABLE OF CONTENTS -- continued

TABLE OF CONTENTS -- continued

TABLE OF CONTENTS -- continued

LIST OF TABLES

LIST OF FIGURES

LIST OF FIGURES -- continued

LIST OF FIGURES -- continued

LIST OF FIGURES -- continued

Chapter 1. Introduction

This dissertation reports the results of a study of the single crystal growth of calcium oxalate monohydrate, a sparingly soluble salt that is a primary mineral constituent of kidney stones. This research was initiated to gain an understanding of the crystal growth mechanisms of calcium oxalate monohydrate (COM) under various solution conditions. Growth rates were measured using the photomicroscopic method, a technique not previously used in studies of sparingly soluble salts. Solution parameters varied included relative supersaturation of the precipitating species, temperature, ionic strength, calcium to oxalate ratio, and the presence of polyelectrolyte crystal growth modifiers. The effects of each of these parameters on single crystal growth in solution were studied over a wide range of their values. Analyses of the data presented evidence of the causes of interesting effects of these solution parameters on COM single crystal growth.

1.1 Research Motivation and Goals

Research of the single crystal growth of COM and the effects of various solution parameters was initially motivated by the occurrence of COM in kidney stones (Finlayson, 1978). A study of some of the literature dealing with kidney stones revealed that the role of COM crystallization in kidney stone disease was not well understood. In particular, the focus of investigation in many of the reports was the effect of urinary polyelectrolytes on nucleation, crystal growth, and crystal agglomeration in the mechanism of kidney stone formation (Fleisch, 1978). The present study was undertaken in an effort to further define the role of urinary polyelectrolytes and COM crystal

growth in the overall mechanism of kidney stone formation. This was to be done by investigating the effect of some model polyelectrolytes on COM single crystal growth.

Application of the experimental results of this research reaches beyond understanding the role of COM growth in kidney stone disease to understanding electrolyte crystal growth mechanisms in general. Study of solution parameters other than polyelectrolyte concentration is necessary to understand the role of COM growth in kidney stone formation. An understanding of the effects of relative supersaturation, temperature, ionic strength, and calcium to oxalate ratio on COM single crystal growth offers a good basis from which to develop an understanding of the changes that occur in growth behavior upon addition of polyelectrolyte growth modifiers. The study of the effects of these parameters on COM single crystal growth reveal interesting growth phenomena that may be unique to electrolyte crystal growth or are characteristic of growth of sparingly soluble salts in general (Nielsen, 1984a, 1984b).

1.2 Photomicroscopic Technique for Measurement of Single Crystal Growth

Study of the effects of the various solution parameters on COM single crystal growth was undertaken using a photomicroscopic method for the measurement of single crystal growth rates from solution. This method differs from other methods in that it allows for the direct measurement of growth rates of individual crystal faces. Growth rates measured using other methods including batch, semi-batch, and continuous crystallizers are bulk-average growth rates that do not reflect growth

rates of any one crystal face. In addition, crystal growth rates measured by other methods often reflect interfering effects of crystal nucleation and/or agglomeration, a problem not experienced with the photomicroscopic method.

A second feature of the photomicroscopic method is the measurement of crystal face growth rates at constant relative supersaturation. Crystal growth rate equations (Garside, 1984a) often express the growth rate of a crystal face in terms of the relative supersaturation, a measure of the concentration of the precipitating species in excess of equilibrium. In order to utilize rate equations of this type, growth rates of crystal faces should be measured under conditions of constant relative supersaturation. In some of the other methods used to measure crystal growth rates the relative supersaturation does not remain constant, as in batch techniques, or cannot be experimentally controlled, as in continuous crystallization.

Chapter 2. Background and Literature Review

2.1 The Occurrence of Calcium Oxalate in Nature

Calcium oxalate, CaC_2O_4, is a sparingly soluble salt found in animals, plants, and in mineral deposits in certain areas of the world. Three hydrated form of the salt are known including the monohydrate, dihydrate, and trihydrate. In animals, calcium oxalate occurs as a precipitate in the urinary tract and is a primary constituent in kidney and bladder stones. In plants, calcium oxalate is found in cells and serves as an immobile form of oxalic acid, a waste product of plant metabolism. The calcium oxalate found in mineral deposits in the earth is the result of the accumulation of dead plants and animals, usually from prehistoric seas (Leavens, 1968). As a sparingly soluble salt, calcium oxalate serves as a study model for other salts with low solubility in water such as calcium sulfate and calcium carbonate.

The study of the occurrence of calcium oxalate in nature involves several disciplines: the anatomy and physiology of both plants and animals, the thermodynamics and kinetics of crystal formation, crystallography, and geology among others. Of primary concern in this dissertation is the study of the kinetics of calcium oxalate crystal growth from ionic aqueous solution, specifically the study of the single crystal growth of calcium oxalate monohydrate. A thorough understanding of this growth is an important prerequisite to the complete understanding of the natural occurrence of calcium oxalate.

2.2 Calcium Oxalate Crystal Growth in Kidney Stones

Calcium oxalate is the primary mineral constituent in 73 percent of the incidences of kidney stones (Rose, 1982). Several other compounds contribute to the mineral portion of stones and are listed in Table 2.1. Stones are mostly mineral in composition; about 2.5 percent of the weight of a typical stone is due to organic compounds from the urine known as stone matrix (Boyce, 1968). Calcium oxalate monohydrate (COM), dihydrate (COD), and trihydrate (COT) are all found in kidney stones with COM occuring most frequently followed by COD (Rose, 1982). COT occurs least often, and has been reported in only a few cases (Heijnen, 1982, 1985).

Three theories of the formation of kidney stones have been given considerable attention in the literature. These include the inhibitor/ promoter theory (Fleisch, 1978), the matrix theory (Boyce, 1968), and the hyperexcretion/ supersaturation theory (Robertson, 1976a). In all cases, the formation of the mineral fraction of a stone depends on the thermodynamics and kinetics of crystallization of sparingly soluble urinary salts from solution. The theories of kidney stone formation differ mainly in their respective explanations of how the crystallization process begins or is prevented and how a heterogeneous kidney stone forms.

Crystallization from solution, which includes crystal nucleation and subsequent individual crystal growth, depends on several solution conditions. The concentrations of the precipitating species, the solution temperature, the pH, the ionic strength, and the concentrations of certain growth-modifying species all affect crystallization kinetics. These effects include increases or decreases in the following: 1) the

Table 2.1 Common Precipitates in Kidney Stone Disease

Chemical Name	Mineral Name	Formula
calcium oxalate monohydrate	whewellite	$CaC_2O_4 \cdot H2O$
calcium oxalate dihydrate	weddelite	$CaC_2O_4 \cdot 2H_2O$
calcium oxalate trihydrate		$CaC_2O_4 \cdot 3H_2O$
basic calcium hydrogen phosphate	hydroxyapatite	$Ca_5(PO_4)_3(OH)$
calcium hydrogen phosphate	brushite	$CaHPO_4 \cdot 2H_2O$
β-tricalcium phosphate	whitlockite	$\beta \cdot Ca_3(PO_4)_2$
magnesium ammonium phosphate hexahydrate	struvite	$Mg(NH_4)(PO_4) \cdot 6H_2O$
uric acid		$C_5H_4N_4O_3$
uric acid dihydrate		$C_5H_4N_4O_3 \cdot 2H_2O$
monosodium urate monohydrate		$NaC_5H_4N_4O_3 \cdot H_2O$
l-cystine		$S_2C_6H_{12}N_2O_4$
octacalcium phosphate		$Ca_8H_2(PO_4)_6 \cdot 5H_2O$
magnesium hydrogen phosphate trihydrate	newberyite	$MgHPO_4 \cdot 3H_2O$

Reference: Rose, 1982

numbers of crystals nucleated per solution volume, 2) the time required for the first crystal nuclei to form, or the induction time (Walton, 1967), and 3) the rate at which the individual faces of a crystal grow. In addition, the crystal habit and the crystal phase formed (monohydrate, dihydrate, or trihydrate, in the case of calcium oxalate) also depend on solution conditions. Subsequent agglomeration (the formation of multi-crystal masses) of growing crystals also depends on the various solution conditions. The effects of several solution parameters on nucleation, growth, and agglomeration have been reviewed by Finlayson (1978a).

2.2.1 The Hyperexcretion/ Supersaturation Theory of Kidney Stone Formation

The hyperexcretion/ supersaturation theory of kidney stone formation (Robertson, 1976a) suggests that calcium oxalate kidney stone formation is wholly due to an increased supersaturation of calcium oxalate in the urine. This increase is thought to be the result of higher output of calcium and oxalate ions by the kidneys either because of greater ingestion of these substances or through some metabolic malfunction in the body. The high supersaturation of calcium oxalate leads to nucleation of crystals in either free solution or on the luminal walls.

These two modes of nucleation suggest two possible mechanisms for the initiation of stone growth, the free particle mechanism and the fixed particle mechanism (Finlayson, 1978b). Rapidly growing crystals flowing freely in solution can, after reaching sufficient size, become trapped somewhere in the urinary tract forming the nidus of a stone.

According to the free particle theory, other crystals and urinary debris collide with the entrapped crystal and stick to it, and the stone continues to grow in this manner. In the fixed particle mechanism, a crystal nucleated on a luminal wall grows and attracts urinary debris. Accumulation of organic and mineral matter gradually leads to stone formation. Alternatively, the crystals may agglomerate together freely in the urine solution forming a multi-crystal mass which becomes too large to pass. The agglomerate then acts as a nidus for stone growth in much the same way as a single crystal.

The supersaturation levels of both stone-forming and non-stone-forming urines are high enough for crystals to form (Robertson et al. 1968), yet crystals occasionally lead to stone formation in the former while they harmlessly pass from the latter. Even though stone-forming urines often show a greater volume of crystals than that observed in non-stone-forming urine (Robertson et al., 1971), at the supersaturation level commonly observed for stone-forming urine, calcium oxalate growth rates are not fast enough to cause blockage of the urinary tract solely due to crystal growth (Finlayson, 1978b). Therefore, the hyperexcretion/supersaturation theory does not fully explain stone formation. Rather, this theory simply suggests one causative factor in the disease-- solution conditions conducive to rapid crystal nucleation and growth. The other two theories, the matrix theory and the promoter/inhibitor theory, attempt to explain how crystal nucleation, growth, and agglomeration are affected by solution conditions other than supersaturation.

2.2.2 The Matrix Theory of Kidney Stone Formation

The matrix theory of kidney stone formation (Boyce, 1968; Hallson and Rose, 1979) suggests that the nucleation of calcium oxalate crystals is promoted by the existence of a mucous organic matrix deposited in the urinary tract. This matrix is composed of various organic macromolecules such as glycosaminoglycans and glycoproteins that are thought to precipitate from urine. As they precipitate, they form a loose mucous mass in the tract. This mucous matrix serves as a substrate for crystal nucleation. Crystal nuclei form over the matrix and subsequently grow causing encrustation and hardening of the forming kidney stone. The tendency for deposition of the matrix is thought to be one factor that separates stone-formers from non-stone-formers and is thought to be a function of the excretion of macromolecules into the urine from various sources in the body.

The matrix theory lacks credibility in that there is a lack of evidence supporting the idea of large-scale deposition of the organic macromolecules prior to encrustation. A more plausible explanation, and one that seems to be more verifiable, is the promoter/inhibitor theory.

2.2.3 The Promoter/Inhibitor Theory of Kidney Stone Formation

The promoter/inhibitor theory of kidney stone formation (Fleisch, 1978) is based on the fact that the tendency for calcium oxalate crystals to nucleate and grow in urine is greater for stone-formers than for non-stone formers. This is not, however, necessarily due to a greater calcium oxalate supersaturation in stone-forming urine, as noted above. Rather, there are certain chemical species in urine that modify the nucleation, growth, and/or agglomeration of calcium oxalate.

Various substances have been implicated as growth modifiers, including macromolecular species such as glycosaminoglycans and glycoproteins. The modification may be inhibitory or promotional depending on the substance present, the amount present, and the process being considered. Normal urine contains macromolecules that inhibit crystal growth but promote the nucleation of crystals (Drach et al., 1982a). There is apparently a greater concentration of these macromolecules in normal urine than in stone-forming urine (Robertson et al., 1981). The creation of many small, slowly growing crystals in normal urine allows excretion of the precipitate before stone formation can occur. Urinary macromolecules may also inhibit the agglomeration of crystals (Ryall et al., 1986). Enhancement of nucleation by urinary macromolecules and the apparent increase in the probability of agglomeration due to a higher concentration of crystals in urine is offset by the inhibition of agglomeration by urinary macromolecules. Thus, the promoting effect of certain urinary macromolecules on crystal nucleation is offset by their inhibiting effect on crystal growth and agglomeration. The net effect is that crystals pass from the urinary tract before stone formation can occur. The low concentration or lack of these macromolecules in stone-forming urine is one possible cause of an increased tendency to form kidney stones.

The promoter/inhibitor theory is actually an extension of hyperexcretion/supersaturation theory in that high levels of calcium oxalate supersaturation are still required to form crystals and consequent stones. The overall mechanism of stone formation, whether by a fixed or free particle mechanism, is still a matter for debate and can only be resolved by experiments simulating the complete environment of

the kidney, including the flow characteristics, luminal walls, and insoluble debris. The plausibility of the theory can be and has been tested by simple experiments of solution crystallization in the presence of various modifiers. Experiments such as these, while intended to explain kidney stone formation, also contribute to the general understanding of crystal growth.

2.3 Calcium Oxalate Crystal Growth in Plants

Calcium oxalate is often seen as crystalline deposits in vacuoles of plant tissue with over 74 percent of the families of seed plants reported to have calcium oxalate deposits (Arnott, 1982). The crystals occur intracellularly often in specialized cells called crystal idioblasts. Two calcium oxalate phases commonly occur in plants with the monohydrate more prevalent that the dihydrate.

Two mechanisms have been proposed to explain the presence of these crystals in higher plants (Whitney and Arnott, 1986; Frey-Wyssling, 1981). The crystals may serve as a means of decreasing the concentration of oxalic acid, which otherwise might accumulate to toxic levels. Precipitation of the relatively insoluble crystal would in this way reduce the plant's exposure to toxic substances. Another suggestion is that the crystals act to detoxify calcium ions, reducing their concentration to safe levels. The crystals might later through some dissolution mechanism release their calcium to the plant as needed. The formation of crystals does not occur as a random event, but is highly controlled so that from 1 to 2,000 or more entirely separate crystals can develop with a single vacuole (Arnott, 1982).

Calcium oxalate crystals may act in a more passive role in lower plants. The presence of a considerable amount of calcium oxalate crystals in the fungus G. persicaria suggests that the crystals may serve as an exoskeletal system (Whitney and Arnott, 1986). The extensive array of crystals may also provide a physical or chemical barrier against insects.

2.4 Calcium Oxalate as a Sparingly Soluble Salt

Calcium oxalate monohydrate is a sparingly soluble salt with a very low solubility product of 2.00×10^{-9} $mole^2/liter^2$ at 25 °C (Nancollas and Gardner, 1974). COM precipitates from solution at low concentrations. The other kidney stone precipitates listed in Table 2.1 are also sparingly soluble salts (except for uric acid, uric acid monohydrate and l-cystine) and are also likely to precipitate from a solution containing relatively low concentrations of their respective constituent ions.

Such a description is typical of sparingly soluble salts in general. Precipitates of these salts from low concentration solutions occur in various circumstances including industrial water systems and in the aforementioned biological phenomena. In particular, precipitates of the sparingly soluble salts calcium carbonate, $CaCO_3$, and calcium sulfate dihydrate, $CaSO_4 \cdot 2H_2O$ (gypsum), are often seen as unwanted scale in boilers, reactors, and cooling water systems. This scaling reduces heat transfer coefficients and often leads to the obstruction of piping. The removal of scale from process surfaces and the treatment of raw water to reduce its scaling tendency is done at considerable expense to industry. In order to develop cost-effective means of reducing scale,

it is desirable to develop an understanding of the mechanisms of crystallization of sparingly soluble salts.

As a sparingly soluble salt, COM is fairly typical when considering its crystallization characteristics. It follows second-order crystal growth kinetics, which is also true of a many other sparingly soluble salts (Nielsen, 1982). The solubility product of COM is typical of sparingly soluble salts; it is low enough to allow ready nucleation and growth of crystals, but it is not so low as to lead to uncontrolled precipitation at low ion concentrations. Additionally, the availability of many COM crystal growth studies which have used other measurement techniques makes comparison of results easy. The study of COM crystal growth is therefore useful for gaining information about the crystal growth of sparingly soluble salts in general, as well as for understanding the role of COM as it occurs in biological systems.

The importance of the single crystal growth of calcium oxalate monohydrate as it occurs naturally is apparent. Before we can completely understand the role of calcium oxalate crystal growth in kidney stones and in plants and understand sparingly soluble electrolyte crystal growth in general, the effects of individual solution conditions on growth must be studied. To this end, a considerable body of literature dealing with the question has developed. Some of the literature to date which is relevant to the single crystal growth of calcium oxalate monohydrate is reviewed in the following sections.

2.5 Theories of Single Crystal Growth Kinetics

Growth of a single crystal from solution can be thought of as a series of steps of movement of dissolved species from solution to a

crystal surface. Bennema (1967a) has suggested that the mechanism of crystal growth consists of four steps, each of which contributes to the overall rate of crystal growth. These steps are: 1) convective and diffusive transfer of growth units from the bulk solution to the vicinity of the crystal surface, 2) the adsorption of the growth units from the liquid phase onto the solid crystal surface, 3) surface migration of the growth units to crystal lattice growth sites, and 4) the incorporation of growth units into the crystal lattice. These growth units may be individual molecules, ions, or a complex of the precipitating species.

A few theories attempting to explain the growth of single crystals from solution have been proposed. Growth can be divided into two regimes, bulk solution mass transfer-limited growth and surface integration limited growth. Bulk solution mass transfer-limited growth equations are derived from elementary material balances, while surface integration theories are more complex. Two of these surface integration theories have received considerable attention in the literature, the screw dislocation theory of Burton, Cabrera, and Frank (BCF), and the two-dimensional nucleation or birth and spread theory. The rate laws for crystal face growth given by both theories are functions of the relative supersaturation, a measure of the concentration of precipitating species in excess of equilibrium. The following section discusses the definition of the relative supersaturation and summarizes the mass transfer-limited and surface integration growth theories in the context of electrolyte crystal growth.

2.5.1 Relative Supersaturation

Garside (1984a) has stated that the driving force for precipitation of dissolved chemical species in solution is the growth affinity, ϕ, the difference in the chemical potential between the solution and the crystal, given by

$$\phi = -\Delta\mu = \mu_{soln} - \mu_{cryst} \qquad (2\text{-}1)$$

where the chemical potential μ is defined by

$$\mu = \mu^\circ + R_g T \ln (i) \qquad (2\text{-}2)$$

Here, (i) is the chemical activity of species i, R_g is the gas constant, T is the absolute temperature, and μ° is the standard state chemical potential. Using (2-1) and (2-2), the fundamental dimensionless driving force for crystallization, σ_a, is given by

$$\sigma_a = \phi/RT = \ln (i)/(i)_{eq} \qquad (2\text{-}3)$$

where the activity of crystalline i is equal to the equilibrium activity. Equation (2-3) can be rewritten as

$$\sigma_a = \ln [((i)-(i)_{eq})/(i)_{eq} + 1] = \ln (\sigma + 1) \qquad (2\text{-}4)$$

where

$$\sigma = ((i) - (i)_{eq})/(i)_{eq} \qquad (2\text{-}5)$$

The quantity σ is the relative supersaturation and is one of the most commonly used expressions for supersaturation in crystal growth kinetic equations. The general expression for σ given by equation (2-5) will be used in this work.

2.5.2 Relative Supersaturation for Electrolytes

The definition of σ given by (2-5) is expressed in terms of a theoretical "growth unit" of species i. For a substance that dissolves into single molecular units, such as sucrose, i refers to the single

molecule in solution. However, for an ionic salt such as calcium oxalate, a calcium oxalate "molecule" dissolves into two distinct ionic units, Ca^{2+} and $C_2O_4^{2-}$. Although the exact nature of the calcium oxalate growth unit is not known, many studies (e.g., Tomazic and Nancollas (1980a), Nielsen (1984a)) use a growth unit based on stoichiometric co-precipitation of the individual ions. This treatment will be used in this thesis. The activity of an ionic growth unit then must include contributions from both cations and anions. The development of the expression for the relative supersaturation of an ionic solute is presented next.

The ionic activity of a given ion is related to the concentration of that ionic species, in this example Ca^{2+}, by

$$(Ca^{2+}) = [Ca^{2+}]\gamma \qquad (2\text{-}6)$$

where $[Ca^{2+}]$ denotes the molar (moles/liter) concentration of the divalent calcium ion and γ is the ionic activity coefficient given by Debye-Huckel theory, to be discussed in Chapter 3.

The activity at which precipitation of the solid phase of a given ionic species will occur depends on the thermodynamic solubility product, K_a. For calcium oxalate, this product is defined as

$$K_a = (Ca^{2+})_o(C_2O_4^{2-})_o \qquad (2\text{-}7)$$

Using (2-6), (2-7) is rewritten as

$$K_a = [Ca^{2+}]_o[C_2O_4^{2-}]_o\gamma^2 \qquad (2\text{-}8)$$

In these equations, $(Ca^{2+})_o$ and $[Ca^{2+}]_o$ denote the activity and concentration, respectively, of Ca^{2+} at the condition of equilibrium between the solid and dissolved species. The solubility product represents the minimum product of the calcium and oxalate activities required for precipitation to occur. A solution at its K_a is saturated

with respect to the solid precipitate. At an ionic activity product greater than K_a, a solution is said to be supersaturated with respect to the solid, and spontaneous nucleation and crystal growth can theoretically occur.

K_a is characteristic of a given compound. For a multi phase-forming solid such as calcium oxalate, each phase has a different solubility product. The K_a values for each of the calcium oxalate phases are given in Table 2.2. Solubility products are functions of temperature, and Table 2.2 gives K_a at several temperatures for each phase of calcium oxalate. Subsequent discussion will focus on the monohydrate phase.

Table 2.2 Thermodynamic Activity Products for Calcium Oxalate

Phase	K_a, moles^2/liter^2 x 10^9			
	15 °C	25 °C	37 °C	50 °C
$CaC_2O_4 \cdot H_2O$	1.58	2.00	2.49	3.17
$CaC_2O_4 \cdot 2H_2O$	-	2.82	-	-
$CaC_2O_4 \cdot 3H_2O$	3.30	4.81	7.19	10.17

References: COM, Nancollas and Gardner (1974); COD, Babic-Ivancic, et al (1985); COT, Tomazic and Nancollas (1979a).

For growth of a hypothetical ionic crystal $A_\alpha B_\beta$, the dissolution mass balance is given by (Nielsen, 1984b)

$$A_\alpha B_\beta \rightleftharpoons \alpha A^{a+} + \beta B^{b-} \qquad (2\text{-}9)$$

The driving force for crystal growth, similar to (2-3), is

$$\Delta\mu = R_g T \ln S \qquad (2\text{-}10)$$

Here, S is the supersaturation ratio defined by

$$S = ((A^{a+})(B^{b-})/K_a)^{1/\nu} \qquad (2\text{-}11)$$

where ν is the sum of the stoichiometric coefficients

$$\nu = \alpha + \beta \qquad (2\text{-}12)$$

For COM, (2-9) and (2-11) become

$$CaC_2O_4 = Ca^{2+} + C_2O_4^{2-} \qquad (2\text{-}13)$$

$$S = ([Ca^{2+}][C_2O_4^{2-}]\gamma^2/K_a)^{1/2} \qquad (2\text{-}14)$$

where (2-6) has been substituted for the ionic activities. The relative supersaturation σ is related to the supersaturation ratio S by

$$\sigma = S - 1 \qquad (2\text{-}15)$$

Combining (2-14) and (2-15) gives the final expression for the relative supersaturation of COM as

$$\sigma = ([Ca^{2+}][C_2O_4^{2-}]\gamma^2)^{1/2} - K_a^{1/2}) \; / \; K_a^{1/2} \qquad (2\text{-}16)$$

The method used to calculate values of the relative supersaturation will be described in Chapter 3.

The relative supersaturation or similar expressions of the supersaturation of a dissolved species are used in crystal growth rate laws. Three theories describing rate laws are discussed next.

2.5.3 Mass Transfer-Limited Crystal Growth

Of the four steps that constitute the simple model of the mechanism of crystal growth described earlier, only the last three contribute to the surface integration kinetics of crystal growth, i. e., the kinetics directly attributable to the surface chemistry of the crystal. The transfer of growth units from bulk solution to the vicinity of the crystal is influenced largely by the shear rate-controlled mass transfer resistance in solution. Garside (1984a) has given the mass transfer-limited rate equation based on a simple material balance around a

growing crystal as

$$R = (\rho_f D_{AB} / \rho_s \delta) \ln [(1-w_\infty)/(1-w_i)] \qquad (2\text{-}17)$$

where ρ_f and ρ_s are the fluid and solid mass densities, respectively, D_{AB} is the diffusion coefficient of the growth unit through the fluid, w_∞ and w_i are the mass fractions of the growth unit in the bulk solution and at the solution/crystal interface, respectively, and δ is the thickness of the boundary layer region near the crystal where the mass fraction varies from w_∞ to w_i. Writing the concentration term in (2-17) as

$$(1-w_\infty)/(1-w_i) = (w_i-w_\infty)/(1-w_i) + (1-w_i)/(1-w_i) \qquad (2\text{-}18a)$$

$$= (w_i-w_\infty)/(1-w_i) + 1 \qquad (2\text{-}18b)$$

and noting that for $(w_i-w_\infty)/(1-w_i) \ll 1$,

$\ln [(w_i-w_\infty)/(1-w_i) + 1] \approx (w_i-w_\infty)/(1-w_i)$, (2-17) becomes

$$R = (\rho_f D_{AB} / \rho_s \delta) (w_i - w_\infty)/(1-w_i) \qquad (2\text{-}19)$$

The interfacial concentration, w_i, is assumed equal to the equilibrium concentration, which, for a sparingly soluble salt such as calcium oxalate, makes $(1 - w_i) \approx 1$. Then (2-19) becomes

$$R = (\rho_f D_{AB} / \rho_s \delta) (w_i - w_\infty) \qquad (2\text{-}20)$$

The term $(w_i - w_\infty)$ in (2-20) is another way of expressing supersaturation of the precipitating species; (2-20) can be rewritten as

$$R = (\rho_f D_{AB} w_i / \rho_s \delta) (w_i - w_\infty) / w_i \qquad (2\text{-}21)$$

The concentration driving force term $(w_i - w_\infty)/w_i$ is in the same form as the relative supersaturation as can be seen by comparing (2-21) with (2-5) and (2-16).

The expression for the growth rate as given by (2-21) is the result of both convective and diffusive contributions to mass transfer from solution to the solid. As the shear rate near a crystal in the solution

is increased, either by stirring or by a greater throughput of solution, the diffusion boundary layer, δ, becomes thinner, thus effectively reducing the resistance to mass transfer and increasing the growth rate, R. The growth rate cannot, of course, increase indefinitely.

In deriving the material balance (2-17), it is assumed that the incorporation of growth units into the crystal lattice is instantaneous. At conditions of high mass transfer resistance, the resistance to surface integration of growth units is negligible compared to the mass transfer resistance, mass transfer through the solution is rate-limiting, and the assumption of instantaneous integration is valid. At high shear rates, however, where the mass transfer resistance is low, adsorption, surface migration, and/or integration become rate-limiting, and it is necessary to account for surface integration kinetics in growth rate expressions.

2.5.4 BCF Theory of Crystal Growth

One comprehensive theory of the surface integration kinetics of single crystals is that of Burton, Carbrera, and Frank (BCF) (1951), who developed their theory for growth from the vapor but theorized that a similar treatment would be applicable for growth from liquid solution. Bennema (1967a, b) has extended the BCF theory to growth from solution and attempted to describe the dependence of the rate of growth of single crystal faces as a function of relative supersaturation.

Considering the three crystal growth steps, adsorption from solution, surface migration, and lattice incorporation, to be important in the growth mechanism, the BCF theory as modified by Bennema suggests that the linear growth of a crystal face may be described by

$$R = C\ (\sigma^2 / \sigma_c)\ \tanh\ (\sigma_c / \sigma) \qquad (2\text{-}22)$$

where R is the linear growth rate of a crystal face. C is a combination of physical constants of the system including adsorption, surface diffusion, and growth unit incorporation factors

$$C = \beta\ C' \qquad (2\text{-}23)$$

where

$$\beta = [1 + (D_s\ t_k / a_s\ x_d)\ \tanh\ (\sigma_c/\sigma)]^{-1} \qquad (2\text{-}24)$$

and

$$C' = D_s\ n_{so}\ \Omega / x_s^2 \qquad (2\text{-}25)$$

Definitions of the variables used in the BCF equations are given in Table 2.3. Garside (1984a) has suggested that β is usually assumed to be unity, meaning the resistance to incorporation of growth units into the crystal lattice is negligible compared to the other effects. The parameter σ_c is a characteristic relative supersaturation to be discussed later and is given by

$$\sigma_c = 9.5\ \gamma_e\ a_s / s\ k\ T\ x_s \qquad (2\text{-}26)$$

By this theory, crystal growth is assumed to proceed by the incorporation of growth units into growth sites visualized as kinks in the steps of a surface spiral. The growth rate of a crystal face is the product of the rate of advance of the steps and the number of steps per unit area of crystal surface. Both the rate of advance of a step and the number of steps per unit area are linearly increasing functions of the relative supersaturation.

The mean diffusion distance, x_d, of a growth unit on the surface is compared to the mean distance between steps, x_s. At $x_d >> x_s$, the Diffusion fields of adjacent steps overlap leading to a competition for growth units. At $x_d << x_s$, steps are sufficiently spaced so that their

Table 2.3 Notation used in BCF equations

a_s	lattice spacing
C	a measure of unimpeded growth rate
C'	value of C when $\beta = 1$
D_s	surface diffusion coefficient
k	Boltzmann constant
n_{so}	equilibrium value of surface solute
R	linear growth rate
s	number of co-operating spirals or strength of the step source
T	absolute temperature
t_k	relaxation time for entering kinks from the surface
x_d	mean diffusion distance of adsorbed growth units on surface
β	retardation factor
γ_e	edge energy
σ	relative supersaturation
σ_c	characteristic relative supersaturation
Ω	molecular volume in crystal

diffusion fields do not interact. Assuming x_d constant, the degree of step interaction depends on x_s. As the relative supersaturation increases, the number of steps per area increases, thus decreasing x_s. It follows that as the relative supersaturation increases, the interaction between steps increases. At low relative supersaturations, the lack of interaction between steps suggests that the growth rate will depend on the relative supersaturation squared as both the number of kinks and the number of steps per area are dependent linearly on the relative supersaturation. At high relative supersaturations, the interaction of steps implies that the rate of advance of steps is independent of the relative supersaturation, and the growth rate will depend only on the first power of the relative supersaturation.

This can be seen by considering the form of the BCF equation given above. At low relative supersaturations, where $\sigma \ll \sigma_c$, $\tanh(\sigma_c/\sigma) \rightarrow 1$, and the BCF equation reduces to

$$R = C\,\sigma^2/\sigma_c \qquad (2\text{-}27)$$

which is known as the parabolic rate law. At high relative supersaturations, where $\sigma \gg \sigma_c$, $\tanh(\sigma_c/\sigma) \rightarrow \sigma_c/\sigma$ and the BCF equation reduces to

$$R = C\,\sigma \qquad (2\text{-}28)$$

which is known as the linear rate law. Thus σ_c/σ is a measure of the degree of step interaction, given from BCF theory as

$$\sigma_c/\sigma = x_s/2x_d \qquad (2\text{-}29)$$

σ_c represents a characteristic transition relative supersaturation below which growth follows the parabolic rate law and above which growth follows a linear rate law.

2.5.5 Birth and Spread Theory of Crystal Growth

Another theory of crystal growth is the birth and spread model described by Hillig (1966). As with the BCF theory, this theory assumes the four steps in the growth mechanism, i. e., bulk diffusion, adsorption, surface diffusion, and incorporation. As opposed to the BCF theory, this theory assumes that surface growth proceeds by the formation of two-dimensional nuclei on the crystal surface. Adsorbed growth units join an existing surface nucleus or form a new nucleus which then grows through the addition of other growth units. The rate of growth is expressed as

$$R = A\, \sigma^{5/6} \exp(-B/\sigma) \qquad (2\text{-}30)$$

where

$$A = (2\pi C_o / 3)^{1/3} (2 x_d / a_s) C' \qquad (2\text{-}31)$$

and

$$B = (\pi / 3) (\gamma_e / k T)^2 \qquad (2\text{-}32)$$

C_o is the fraction of the crystal surface occupied by separate growth units, C′ is defined by (2-25), and all other parameters are as defined for the BCF equations.

At low relative supersaturations, the exponential term of (2-30) will dominate giving a region analogous to the parabolic region of the BCF curve. At high relative supersaturations, the exponential will die out leaving the growth rate, R, proportional to $\sigma^{5/6}$; this is analogous to the linear region of the BCF curve.

2.5.6 Comparison and Contrast of Theories and Empirical Treatment of Data

Although the form of the birth and spread model appears much different from the BCF model, Garside (1984a) has shown that it is often

difficult to discriminate between these models in order to determine the growth mechanism. This being the case, one needs a considerable amount of good data before attempting to classify a given crystal system as following one of these models or some other model. Indeed, the BCF and birth and spread theories may not accurately predict crystal growth for a given system, especially electrolyte crystal growth since electrolyte crystal growth does not appear to follow either theory.

Nielsen (1984b) has stated that elementary crystal growth mechanisms may be classified according to three types of relative supersaturation dependence: 1) linear, 2) parabolic, and 3) exponential. He suggests that these three kinds of kinetics are explained by the following rate-determining mechanisms, respectively, 1) solution mass transfer or adsorption from solution, 2) surface spiral growth, including surface diffusion and lattice integration, and 3) surface nucleation. The first order relative supersaturation dependence of the bulk solution mass transfer limited rate equation given by (2-21) is an example of linear kinetics.

This view of the mechanistic source of the growth rate dependence on relative supersaturation does not take into account the unique nature of electrolyte crystal growth. Chiang and Donohue (1987) have shown that a second-order dependence of crystal growth rate on relative supersaturation can be derived by considering ionic adsorption in the context of electrical double layer theory.

It often occurs that rate expressions reveal mixed rate control, i. e., they show transitions from one relative supersaturation dependence to another. This is the case for both the BCF and the birth and spread mechanisms given by (2-22) and (2-30), respectively. Nielsen

has stated further that the BCF mechanism is a combination of adsorption (first order dependence) and surface diffusion (second order dependence) rate control at high and low relative supersaturation, respectively.

Often it is sufficient to model data using an empirical power-law model of the form

$$R = k_n \sigma^n \qquad (2\text{-}33)$$

where k_n represents an empirical intrinsic rate constant, and n is the empirical reaction order. The reaction order allows classification of the rate mechanism according to the three types given above. It is important and necessary, however, to measure growth over a wide range of relative supersaturation to determine if a change in reaction order occurs at any relative supersaturation.

Additional information about the nature of the growth mechanism can also be obtained by measuring growth as a function of temperature, thereby obtaining k_n as a function of temperature. Data of this type may be plotted using the Arrhenius equation

$$k_n = A_o \exp(-E_a / R_g T) \qquad (2\text{-}34)$$

The activation energy for growth E_a can be found from a plot of ln (k_n) versus 1/T. The magnitude of the activation energy then gives an indication of which steps in the growth mechanism are rate-controlling. For example, at low relative supersaturations a BCF crystal follows the parabolic rate law given by (2-27). An empirical model for growth of such a crystal would have $n = 2$ and a rate contant given by $k_n = C/\sigma_c$. Of the possible stages in crystal growth for a BCF crystal, adsorption, surface diffusion, and surface integration, only surface diffusion- and surface integration-controlled mechanisms should have a second order rate law. By comparing the magnitude of the activation energy for k_n

with those typical of surface diffusion and lattice integration phenomena, it is possible to conjecture a rate-determining step in the crystal growth mechanism.

2.6 Methods Used to Measure Calcium Oxalate Crystal Growth Rates: Advantages and Disadvantages

Although crystal growth theories suggest how single crystal face growth rates should depend on the relative supersaturation, the actual dependence of growth rates on various solution variables must be valuated experimentally. Relative supersaturation, temperature, ionic strength, calcium to oxalate ratio, and growth modifiers all have important effects on growth, so an experimental method should be flexible enough to allow measurement of growth under wide ranges of all of these variables. The results obtained in various studies of calcium oxalate crystal growth depend to a large degree on the experimental method used to measure growth. These methods include batch and continuous crystallization methods. The advantages and disadvantages of the several methods commonly used will be discussed.

2.6.1 Batch Crystallization

Simple batch crystallization techniques have been used many times in investigations of the crystallization of calcium oxalate. Generally, these techniques involve the use of a batch crystallizer, usually a glass beaker or flask, into which the calcium and oxalate solutions are added, either gradually or all at once. The combined solutions are mixed using either an impeller or magnetic stirring bar or are shaken. The crystallization is initiated either by the use of seed crystals or

by spontaneous nucleation. As the crystals grow, calcium and oxalate ions disappear from solution decreasing the relative supersaturation driving force. A crystallization rate is then measured by one of various techniques. Since the relative supersaturation falls throughout the experiment, the measured rate is not characteristic of any one value of relative supersaturation. Batch crystallization methods offer simple ways of measuring crystallization rates. The rate obtained using spontaneous nucleation, however, is a non-specific, bulk average rate reflecting contributions from nucleation, single crystal growth, and sometimes agglomeration. Seeded batch techniques offer an improvement over spontaneous nucleation if the supersaturation is kept low enough to preclude nucleation of additional crystals. The rate measured by such seeded methods is a bulk-average crystal growth rate, not a true single crystal growth rate.

Nielsen (1960) has measured the rate of formation of calcium oxalate precipitate in a batch crystallizer by measuring the change in electric conductance of the solution. He did not specify the crystal phase formed. Nancollas and Gardner (1974), Nielsen (1984a), and Rizkalla and Moawad (1984) have measured the rate of growth of COM seed crystals conductimetrically in a batch crystallizer. Because a stable supersaturated calcium oxalate solution was used, the authors of these studies suggest that no spontaneous nucleation occurred during their experiments, and that, therefore, the kinetics measured reflected only crystal growth. Due to the nature of the conductivity measurements, these experiments were limited by the fact that no background electrolyte could be added to determine the effect of ionic strength. In addition, the concentrations of calcium and oxalate were necessarily

kept low in an attempt to prevent spontaneous nucleation.

Desmars and Tawashi (1973) have followed the rate of growth of COM in a seeded batch crystallizer using a Coulter Counter®. They determined an average growth rate by measuring the shift in the crystal size distribution as a function of time. In order to eliminate spontaneous nucleation effects, the authors took special precautions with the order in which solutions were mixed and with the method used to bring the reactants together. However, the possibility still exists that the growth rate results were affected by agglomeration of crystals. Meyer and Smith (1975a) and Tomazic and Nancollas (1980a) have measured the rate of disappearance of calcium ion from a stirred COM-seeded batch crystallizer. Calcium ion was detected using atomic absorption spectroscopy. The growth solutions were stable with respect to spontaneous nucleation, but were limited to low concentrations. This technique had an advantage over the conductimetric method in that high ionic strength solutions could be used. Will et al. (1983) have measured the rate of uptake of radioactive ^{45}Ca by COM seed crystals in a shaken batch crystallizer. By measuring the uptake of tracer by crystals rather than its disappearance from solution, this method offered a direct measurement of crystal growth, but still measured only an average growth rate over a changing supersaturation. This method was not limited either by low concentrations or by ionic strength.

In each of the studies above, the accurate measurement of a batch growth rate requires an accurate measurement of crystal surface area. Therefore, if seed crystals are not very well characterized, growth rate results will vary depending upon the nature of the seeds.

The major drawback to batch techniques is the inability to maintain a constant supersaturation during crystallization. Continuous crystallization techniques, on the other hand, are by design constant condition methods. Three continuous methods are particularly well-suited to studying calcium oxalate growth and are discussed next.

2.6.2 Constant Composition Method

A semi-batch crystallization method used in the measurement of calcium oxalate crystal growth rates is the constant composition method developed by Sheehan and Nancollas (1980). The constant composition method is a modification of the seeded batch technique. Calcium and oxalate solutions and crystal seeds are added to a stirred crystallization vessel at the beginning of the experiment and concentrated calcium and oxalate solutions are titrated into the vessel throughout the experiment. Instead of following the depletion of an ion from solution, the amounts of concentrated calcium and oxalate solutions titrated to maintain a constant supersaturation during crystallization are recorded. The calcium concentration is monitored using a calcium-specific electrode, with the measurement of oxalate obviated by the assumption of equimolar co-precipitation of the oxalate ion.

The constant composition method allows for the measurement of crystal growth rates at constant solution conditions, particularly constant supersaturation. Assuming that no additional crystals nucleate during the experiment, the amounts of calcium and oxalate ions titrated contribute exclusively to crystal growth of seed crystals and not to nucleation. This condition of no spontaneous nucleation limits to fairly low values the range of concentrations that can be used. The

crystal growth rates measured are averages for crystal populations. The method does not allow for the measurement of the growth rates of individual crystal faces.

2.6.3 MSMPR Crystallizer

The mixed-suspension, mixed-product removal (MSMPR) crystallizer is a continuous crystallization method that has been used to study calcium oxalate crystallization. Results may be analyzed using the population balance model (Randolph and Larson, 1971) for a continuous crystallizer. In this method, separate streams of calcium and oxalate solutions are added continuously to a well-stirred crystallization vessel. The well-mixed crystallization suspension is withdrawn continuously so as to maintain a constant solution volume in the crystallizer. Upon initial addition of the concentrated calcium and oxalate solutions, nucleation and subsequent single crystal growth begin. Nucleation and crystal growth continue, and a steady-state crystal size distribution is reached within about 10 crystallizer residence times (Garside et al., 1982).

The rates of nucleation and single crystal growth are determined by measuring the crystal size distribution (number of crystals versus crystal size) in the crystallizer. This is done by withdrawing a sample of the solution containing crystals and examining the crystal population in terms of length, mass, or volume distributions using techniques such as electronic solution particle counting or image analysis.

Randolph and Larson (1971) have shown that the solution to the steady-state population balance on an MSMPR crystallizer is given by

$$n = n^{\circ} \exp(-L/Gr) \qquad (2\text{-}35)$$

where n is the number of crystals of size L at steady state, n° is the

number of vanishingly small embryonic crystals, G is the size-independent crystal growth rate, and τ is the residence time of the crystallizer, given as the ratio of the crystallizer holding volume to the solution throughput rate. In order to determine a crystal growth rate, the crystal size distribution (n vs. L) is measured for a wide range of crystal sizes. The bulk averaged growth rate G can then be calculated by plotting equation (2-35) as ln (n) versus L. The slope of the line is given by $-1/(G\tau)$ and for a known residence time the growth rate is calculated. Randolph and Larson have further shown that the nucleation rate B° is given by

$$B^\circ = n^\circ G \qquad (2\text{-}36)$$

The intercept of the ln (n) versus L plot is given by ln (n°) and multiplication of n° by G gives the nucleation rate B°.

Finlayson (1972) has measured the crystal size distribution of MSMPR crystallizer samples photomicroscopically and used the results to derive a growth rate. The results obtained represented average growth rate values and not facial growth rates. He did not specify the crystal phase grown. Rodgers and Garside (1981) also used an MSMPR crystallizer system to measure calcium oxalate growth rates. A Coulter Counter® was used to measure the crystal size distribution. Crystal phase was identified by x-ray diffraction, and results for pure COM were obtained. They did not account for the non-linearity in their ln (n) vs L plots so the results may have been affected by agglomeration, growth rate dispersion, and/ or size dependent growth. Garside et al. (1982) have used an MSMPR crystallizer system with a Coulter Counter® to measure the temperature dependence of COM growth rates. Non-linearities in plots of ln (n) vs L were assumed to be caused by agglomeration at crystal sizes

greater than forty microns and by growth rate dispersion and/ or size dependent growth at sizes less than five microns. The slope of the size distribution was measured in a fairly linear intermediate range of crystal sizes to determine crystal growth rate. The crystal phase was identified using x-ray diffraction of filtered precipitate. As in earlier studies cited, the growth rate results obtained represented average growth rates of entire crystals and not facial growth rates. In addition, both COM and COT were identified in the precipitate, so the results may not have been truly representative of COM growth.

The MSMPR crystallizer method offers a method of calculating crystal growth rates over a wide range of solution conditions. The accuracy of these measurements, however, depends on the validity of the model used in the calculation of the growth rate. As described previously, the measurement of the crystal growth rate depends on the measurement of the slope of a ln (n) vs L plot. The determination of the slope is often a matter of judgement, thus leading to ambiguity in the actual growth rate reported. Furthermore, the growth rate measured is an average for many crystals, rather than the more physically significant facial growth rate of a single crystal. It is also often difficult to obtain results for a single crystal phase due to multiple phase formation in the crystallizer and the inability to distinguish their growth rates. Thus, while the MSMPR method is an improvement over batch methods in that it allows measurement of crystal growth rates at constant solution conditions, the results obtained are still equivocal.

2.6.4 Photomicroscopic Growth Cell Method

The photomicroscopic growth cell technique is a continuous crystallization method specific for the measurement of single crystal face growth rates. This technique, based on a design first used by Valcic (1975), has not been used previously for calcium oxalate. Similar methods have been utilized by others including Berglund (1981) and Garside and Ristic (1983). This method, which has been previously reported by DeLong and Briedis (1985) and will be described in detail in Chapter 4, involves the use of a small growth cell. Calcium and oxalate solutions, which are mixed immediately before entering the growth chamber of the cell, flow continuously through the cell providing constant solution conditions. Calcium oxalate monohydrate crystals nucleate spontaneously within the cell and are held stationary on a flat glass surface mounted in the middle of the flow field. The growth of the individual crystals is followed by time-sequenced photographs taken through an optical microscope.

The photomicroscopic technique allows the direct measurement of the growth rates of not only individual crystals but of each crystal face. The distinct advantage of this method over other continuous or batch methods is that it permits the direct measurement of facial growth rates in the units of length per time. No conversion from concentration depletion (as in batch or constant composition methods) or crystal volume units (as in MSMPR crystallizer methods) is necessary. Measurement of facial growth allows comparison of the effects of various solution conditions on the growth of different faces which expose different configurations of the crystal lattice to solution and hence grow at different rates. Facial growth rate data can then be used to

accurately model the growth. A second advantage of this method is the ability to visually or spectroscopically identify the phase of individual crystals, which is important in multi-phase-forming systems such as calcium oxalate.

2.7 Results of Previous Studies of COM Crystal Growth Kinetics

Existing data on the single crystal growth of calcium oxalate monohydrate are the result of studies done using batch, MSMPR crystallizer, and constant composition experiments. The means of expressing the data in each case depends on the experimental method used. In general, however, it is desirable to express all results on a common basis. The logical choice is that used in theories of crystal growth kinetics-- the linear crystal face growth rate. Often, it is impossible to express reported data in terms of a single face, and only an average growth rate can be determined. In some studies, in lieu of measured growth rates other data such as rate constants are given.

In the following sections, the results from previous studies of calcium oxalate growth studies are given.

2.7.1 Effect of Calcium Oxalate Concentration

Several studies have been published which report the effect of calcium oxalate concentration on COM crystal growth rate. The concentration has been expressed in various ways including molarity, saturation ratio, supersaturation, and relative supersaturation. The data reported are, therefore, not directly comparable to each other. However, in most cases the reported growth rate, R, (not always a true

crystal growth rate) is proportional to a term related to the relative supersaturation squared, i.e., $R \alpha \sigma^2$.

Nielsen (1960) has measured a "calcium oxalate precipitation" rate, dl/dt, where l is a calculated crystal length and t is time, as a function of calcium oxalate concentration and has found two distinct regions of concentration dependence. For $c < 10^{-3}$ M, he found that $dl/dt \alpha c^4$, where $c = [Ca^{2+}] = [C_2O_4^{2-}]$, or $dl/dt \alpha ([Ca^{2+}][C_2O_4^{2-}])^2$, which was explained as describing the deposition of calcium oxalate onto crystal surfaces. For $c > 10^{-3}$ M, the result was $dl/dt \alpha c^2$, or $dl/dt \alpha [Ca^{2+}][C_2O_4^{2-}]$, which he described as diffusion controlled growth. These findings took into account the formation of an aqueous calcium oxalate complex, but the phase of the solid precipitate was not identified. The growth rates ranged from approximately .06 microns/minute at $.3 \times 10^{-3}$ M to 2.4 microns/minute at 10^{-3} M to 19 microns/minute at 4×10^{-3} M. It is probable that the values of the rates measured are too high and reflect contributions from both crystal growth and nucleation since the experiments were done using a batch crystallizer with spontaneous nucleation.

Nancollas and Gardner (1974) have found that the rate of change of the calcium concentration in a seeded batch crystallizer followed the form

$$-d[Ca^{2+}]/dt = ks([Ca^{2+}] - [Ca^{2+}]_o)^2$$

where k is the observed rate constant for crystal growth, s is the surface area of the added seed crystals and is a function of the density of added seeds (mg seed/100 ml solution), $[Ca^{2+}]$ is the concentration of calcium ions at time t, and $[Ca^{2+}]_o$ is the ionic solubility under the experimental conditions. Data were taken over a range of

supersaturations $S = ([Ca^{2+}]_i - [Ca^{2+}]_o)/[Ca^{2+}]_o = 0.2$ to 4.0 where $[Ca^{2+}]_i$ was the initial free calcium concentration. The results depended on the method of seed crystal formation with rate constants at 25 °C in a solution without added background electrolyte averaging 5.9 $M^{-1}min^{-1}(mg\ seed/100\ ml)^{-1}$ for their type A seeds and 0.82 $M^{-1}min^{-1}(mg\ seed/100\ ml)^{-1}$ for their type B seeds. Due to differences in their preparation, type A seeds apparently had a greater surface area than did type B. Rizkalla and Moawad (1984) found similar results using the same method.

Meyer and Smith (1975a) have investigated the growth of calcium oxalate monohydrate in a COM-seeded batch crystallizer. Using a 0.15 M NaCl electrolyte and taking into account the formation of only the CaC_2O_4 and $HC_2O_4^-$ aqueous complexes, they measured the rate of disappearance of Ca^{2+} from solution during precipitation and found, similar to the results of Nancollas and Gardner, a second order dependence of growth rate on the supersaturation of the form

$$-dCa^{2+}/dt = k\,[(Ca^{2+}) - (Ca^{2+})_\infty]^2$$

where (Ca^{2+}) and $(Ca^{2+})_\infty$ are the free calcium activities at time t and saturation, respectively, and k is the rate constant with units of $M^{-1}min^{-1}$. The authors have reported that the rate constant k was independent of the stirring rate but dependent on the mass of seeds used. When the rate constant was corrected for the amount of added seed, a fairly seed-concentration-independent constant was found with an average value of 64.5 $M^{-1}min^{-1}(mg\ seed/100\ ml)^{-1}$ at 37 °C. Since the supersaturated solutions without seeds were stable for at least six hours, the authors suggested that the results represented the crystal growth rate without spontaneous nucleation.

Sheehan and Nancollas (1980) have measured the rate of addition of calcium and oxalate solutions to a constant composition crystallizer. COM seed crystals were used, and the surface area of these seeds was measured. NaCl was used as a background electrolyte to maintain an ionic strength of 0.15 M, and pH and temperature were held at 6.00 and 37 °C, respectively. Taking care to prevent spontaneous nucleation by keeping the calcium oxalate concentration fairly low, they found the rate of crystal growth, R, to follow a second-order law of the form

$$R = -dm/dt = k\ s\ (m - m_o)^2$$

where R has the units of $(l \cdot mol)/(min \cdot m^2)$, the rate constant, k, has units of $l/(mol \cdot min \cdot (m^2/l))$, and the seed surface area s has units of m^2/l. The symbol m is the equimolar concentration of calcium or oxalate in molar units at time t, i.e., $m = [Ca^{2+}] = [C_2O_4^{2-}]$, and m_o is the saturation value. The authors have taken into account the formation of the aqueous complexes $NaC_2O_4^-$ and CaC_2O_4. They reported a rate constant of $k \approx 525\ l^2/(mol \cdot min \cdot (m^2/l))$ at 37 °C (from their Figure 3).

Tomazic and Nancollas (1980a) have used a COM-seeded batch crystallizer and have followed the depletion of calcium from solution to measure the growth rate, taking care to prevent spontaneous nucleation. They found that the rate could be expressed in the second-order form

$$-dT_{Ca}/dt = k_g\ S\ [([Ca^{2+}][C_2O_4^{2-}]\ y_2^2)^{1/2} - K_{so}^{1/2}]^2$$

where T_{Ca} is the total molar concentration of calcium including all ionic forms of calcium, k_g is the rate constant in units of $l^2/(mol \cdot min \cdot m^2)$, S is a surface parameter proportional to the surface area of the growing material, y_2 is the divalent activity coefficient, and K_{so} is the activity product. The growth experiments were done in 0.15 M NaCl at 37 °C. The aqueous complexes $NaC_2O_4^-$ and CaC_2O_4 were

accounted for. They reported a rate constant $k_g = 5920\ l^2/(mol \cdot min \cdot m^2)$.

Garside et al. (1982) have performed experiments using an MSMPR crystallizer with an Coulter Counter®. They found that the crystal growth rate, G, followed a second-order law of the form

$$G = k_g \sigma^2$$

where k_g is a rate constant with units of m/s and σ is their supersaturation driving force defined as

$$\sigma = ([Ca^{2+}][C_2O_4^{2-}]\gamma^2 - K_{so})/K_{so}$$

Here, γ is the divalent ionic activity coefficient, and K_{so} is the COM thermodynamic activity product. They accounted for the $H_2C_2O_4$, $HC_2O_4^-$, CaC_2O_4, and $Ca(C_2O_4)_2^{2-}$ aqueous complexes. The pH was held at 6.5, and no background electrolyte was added. Their growth rates at 37 °C were in the range of approximately $.003 < G < .03$ μm/s for a supersaturation range of $10 < \sigma < 30$, which corresponds to a rate constant of $k_g = 2.92 \times 10^{-5}$ μm/s. They noted problems with multi-phase precipitation of COM and COT.

Will et. al (1983) have followed the uptake of ^{45}Ca by COM seeds in a batch crystallizer. They expressed their results in terms of the second-order equation based on enzyme kinetics

$$dU_t/dt = U_\infty/t_m\ ((U_\infty - U_t)/U_\infty)^2$$

where the fractional uptake of ^{45}Ca at time t, U_t, is given by

$$U_t = (T_{Ca,i} - T_{Ca})/T_{Ca,i}$$

U_∞ is the fractional uptake of ^{45}Ca at $t = \infty$, t_m is the time when $U_t = 1/2\ U_\infty$, $T_{Ca,i}$ is the initial total molar calcium concentration, and T_{Ca} is the calcium concentration at time t. Their results have also shown a second order response of growth to supersaturation.

2.7.2 Effect of Temperature

Two studies are known in which the effect of temperature on COM growth has been measured. Nancollas and Gardner (1974) have determined the response of growth rate to concentration over a range of temperatures from 15 °C to 45 °C. Using a rate law of the form

$$-dCa/dt = k\ s\ ([Ca^{2+}] - [Ca^{2+}]_o)^2$$

they measured the rate constant k for temperatures of 15 °C, 25 °C, 35 °C, and 45 °C. They have found an activation energy for COM growth of Ea = 11.7 ± 1.0 kcal/mole, and suggested that this magnitude for E_a supports an interface mechanism for COM growth.

Garside et al. (1982) have measured COM growth at temperatures of 30 °C, 37 °C, and 45 °C. Using a rate law of the form

$$G = k_g\ ([Ca^{2+}][C_2O_4^{2-}]\gamma^2 - K_{so})/K_{so}$$

they found an activation energy for COM growth of E_a = 6.7 kcal/mole. They noted that this is a higher value than would be found for the corresponding mass transfer controlled dissolution process, which they cited to be 3.1 kcal/mole.

2.7.3 Effect of Polelectrolyte Growth Modifiers

As discussed earlier in this dissertation, various organic macromolecules have been implicated in kidney stone disease. Their role in the formation of kidney stones is the subject of debate; the matrix theory contradicts the inhibitor/promoter theory in explaining how these urinary macromolecules influence the formation of stones. The basic premise of the inhibitor/promoter theory suggests that the urinary macromolecules interact with the calcium oxalate crystals in such a way as to interfere with the crystallization process. It has been suggested

that these macromolecules act both as inhibitors and promoters of crystallization depending upon which type of crystallization is being affected.

The exact nature of urinary crystal growth modifiers has been the subject of much research. Magnesium, pyrophosphate, and citrate ions were originally identified as urinary crystal growth modifiers (Smith et al. 1973), but subsequent work has indicated that other, as of then unidentified, compounds were responsible for the bulk of the crystal growth inhibitory activity in urine. Meyer and Smith (1975b) have found that magnesium, citrate, and pyrophosphate contributed little to urinary inhibitory activity and have ascribed the major part of the activity to undefined compounds. Robertson et al. (1976b) have shown that most of the urinary crystal growth modifier activity is due to anionic, macromolecular compounds with hydroxyl, carboxyl, and sulfate residues in the molecular weight range of 10,000 to 50,000. In that work, urinary crystal growth modifiers were shown to inhibit the formation of calcium oxalate precipitate in batch crystallizers. The individual effects of these compounds on nucleation, crystal growth, and crystal agglomeration were not demonstrated.

Many other studies have reported on the ability of unknown urinary compounds to affect the crystallization of calcium oxalate including those by Randolph and Drach (1981), Gill et al. (1977), Robertson et al. (1981), Azoury et al. (1985), Drach et al. (1980), and Gardner and Doremus (1978).

Various urinary compounds have been suggested as being crystallization modifiers. Several studies have reported on the crystallization-modifying ability of glycosaminoglycans, a group of

polysaccharides that include heparin and the urinary compounds chondroitin sulfate and hyaluronic acid. Their molecular structures are shown in Figure 2-1. These compounds have molecular weights greater than 10,000 (Sallis and Lumley, 1979), and their carboxylic and sulfate functional groups are largely dissociated at normal urinary conditions. Robertson et. al (1973) have reported that heparin and chondroitin sulfate are effective in inhibiting calcium oxalate precipitation in a batch crystallizer. Robertson et al. (1984) have measured the rates of crystal growth and nucleation in a continuous crystallizer and have found that heparin and chondroitin sulfate both decrease the growth rate of calcium oxalate but increase the nucleation rate. Sallis and Lumley (1979) and Kitamura et al. (1982) have isolated glycosaminoglycans from urine and have found that they inhibit the formation of calcium oxalate crystals in batch crystallizers. Robertson et al. (1981) have fractionated the macromolecules in urine and have found that the glycosaminoglycan fraction contributes the major fraction of the crystal growth inhibitory activity. Gjaldbeck (1982) has found that heparin inhibits COM crystal growth, but chondroitin sulfate does not. Crawford et al. (1968) have shown that heparin and chondroitin sulfate both inhibit the formation of calcium oxalate precipitate. Drach et al. (1982a) have found that heparin significantly decreases calcium oxalate crystal growth rates.

Nakagawa and his co-workers have published a series of articles (Nakagawa, et al., 1978, 1981, 1983, 1984, Lopez, et al., 1986) in which they report isolating crystallization modifiers from urine and kidney tissue and identifying them as anionic glycoproteins. They suggest that these compounds account for as much as 90 percent of the crystal growth

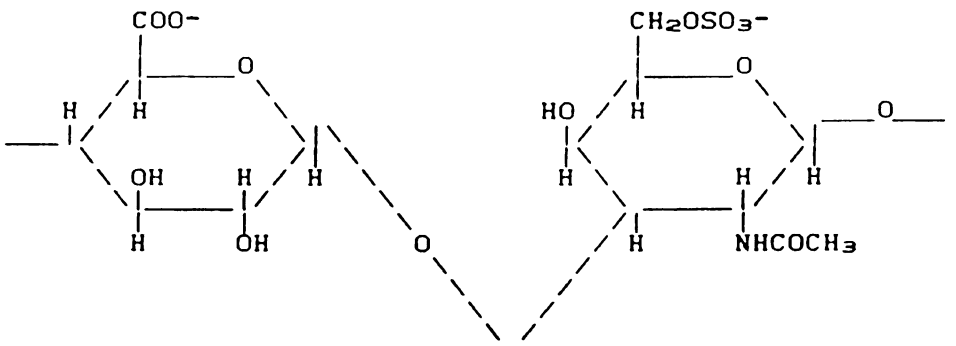

Chondroitin 6-sulfate

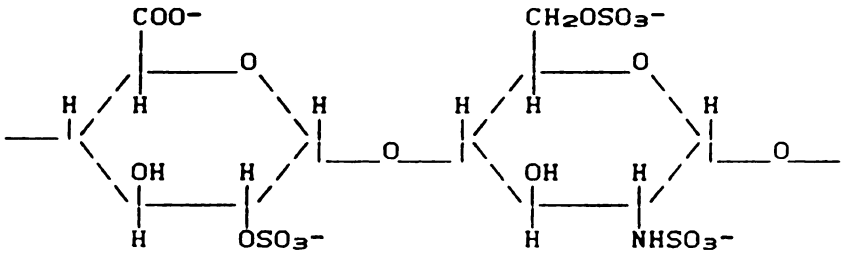

Heparin

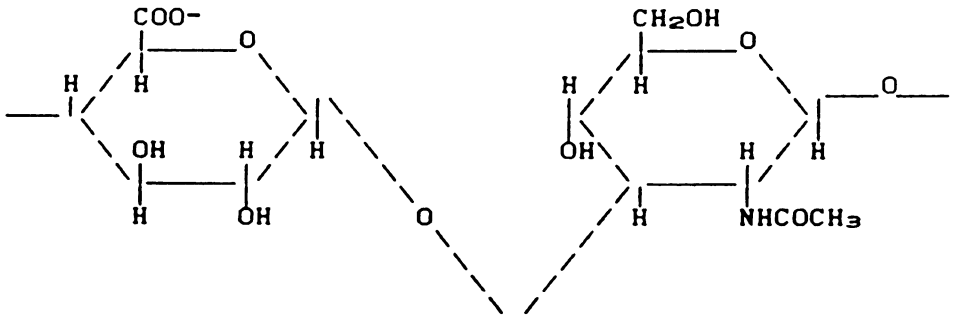

Hyaluronate

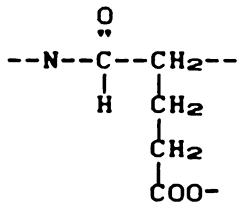

Polyglutamate

Figure 2-1. Repeating Units of Some Polyelectrolyte Crystal Growth Modifiers

inhibitory activity of urine. These inhibitors have molecular weights of about 14,000, and the majority of their structures consist of various amino acids with a high percentage of glutamic acid and aspartic acid residues. The balance consists of various saccharide units. Kitamura et al. (1982) have fractionated urinary macromolecules and have also found that some inhibitory activity was due to glycoproteins.

Other specific urinary anionic polyelectrolyte compounds have been suggested as growth modifiers including RNA (Ito and Coe, 1977) and Tamm-Horsfall mucoprotein (Robertson et al., 1981).

In addition to the naturally occurring urinary polyelectrolytes, various synthetic polyelectrolytes have been shown to inhibit calcium oxalate crystallization. Crawford et al. (1968) have measured the induction time for calcium oxalate precipitation and found that various copolymers of styrene and polyacrylic acid increased the induction time, indicating an inhibition of precipitation. Sheehan and Nancollas (1980) have reported that polyacrylic acid inhibited the crystal growth of COM. Garti et al. (1980) have found that the rate of disappearance of Ca^{2+} from a calcium oxalate solution was retarded in the presence of polyglutamic acid and polyaspartic acid. Drach et al. (1982a) have studied the crystallization of calcium oxalate in the presence of polylysine and polyglutamate. The cationic polylysine showed no effect, while anionic polyglutamate was a potent inhibitor of crystal growth.

The particular step of calcium oxalate precipitation, i.e., nucleation or growth, that is affected by a given modifier has often been left out of reports on crystal growth inhibitors. Some workers have made efforts to isolate the effects of various polyelectrolytes on nucleation and crystal growth and have found that modifiers can inhibit

one aspect while promoting another. This seeming paradox is outlined by Drach et al. (1982a) who have shown that both heparin and polyglutamate inhibit the crystal growth of calcium oxalate dihydrate, but enhance crystal nucleation. Thus, reports of crystallization "inhibition" in studies using bulk crystallization techniques such as batch crystallizers are often misleading.

The way in which polyelectrolytes interact with calcium oxalate crystals to inhibit their growth has been considered in some of the studies described above. Most of these analyses suggest that polyelectrolytes adsorb onto the crystal surface and interfere with the surface growth mechanism. Efforts to fit inhibited growth data to a simple Langmuir adsorption isotherm have proven successful (Meyer and Smith, 1975b, Nakagawa et. al., 1983, and Sheehan and Nancollas, 1980). Leal and Finlayson (1977) and Hlady (1984) have measured the adsorption of various polyelectrolytes onto COM crystal surfaces using solution depletion methods.

The way in which the adsorbed polyelectrolyte interferes with the crystal growth mechanism is not well understood. In explaining the growth inhibition of calcium sulfate by adsorbed polymers, Smith and Alexander (1970) have suggested that the adsorbed polymer molecules act as immobile impurities on the crystal surface reducing the step velocity and therefore the crystal growth rate. Equally as uncertain is an understanding of the way in which the adsorbing polymer is associated with the crystal surface. Gill and Varsanik (1986) have proposed a model in which the distance between carboxylate groups of polyacrylic acid is similar to the spacing between the calcium atoms in the calcium carbonate crystal lattice, thus suggesting that the carboxylate groups

somehow associate with the calcium atoms upon adsorption. There is a lack of evidence as to how polyelectrolytes associate with the calcium oxalate monohydrate lattice and subsequently interfere with the crystal growth mechanism.

2.8 COM Crystal Structure and Growth Habit

The crystal structure and solution growth habit of calcium oxalate monohydrate have been well documented. The growth habit can be used for ready visual identification of growing crystals without resorting to more sophisticated, and possibly inappropriate, instrumental techniques such as x-ray diffraction. Knowledge of the crystal structure is useful as an aid in interpreting observed differences in the growth kinetics of the various crystal faces.

2.8.1 COM Crystal Structure

The crystal structure of COM has been reviewed by Tazzoli and Domeneghetti (1980). COM belongs to the space group $P2_1/c$ with a unit cell having the dimensions a = 6.290 Å, b = 14.583 Å, and c = 10.116 Å, with β = 109.46° where β is the angle between sides a and c. The structure is shown in Figures 2-2 and 2-3. These diagrams show that in the COM crystal the coordination number for each calcium atom is eight. Each calcium is associated with eight oxygen atoms, seven of which are from five oxalate ions, the other from a water molecule. The oxalate ions are arranged in two sets of parallel planes. The first set, as shown in Figure 2-2, consists of planes of oxalate ions whose oxygen atoms are associated exclusively with calcium ions. The calcium ions are arranged in a hexagonal pattern in the first set of planes with a

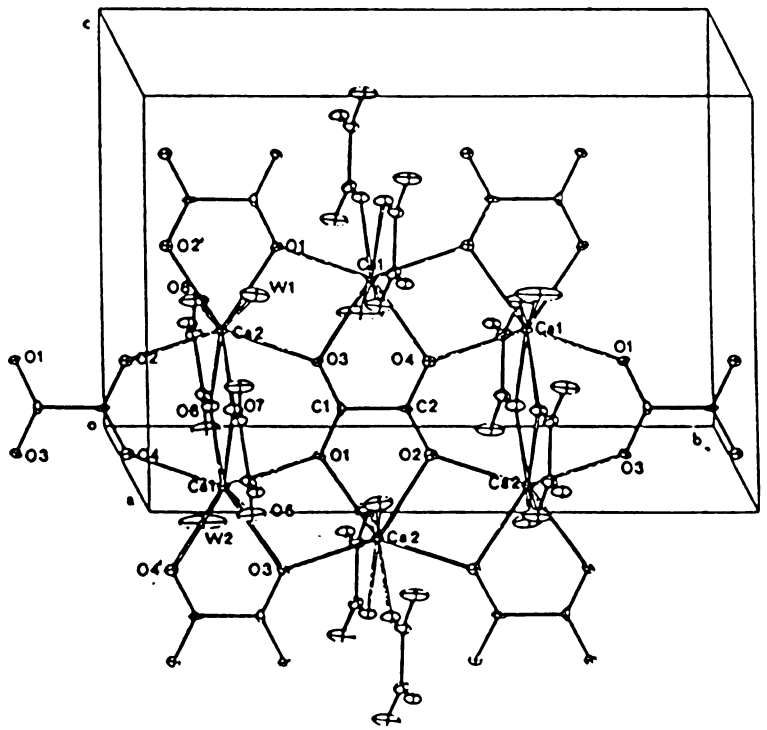

Figure 2-2. Crystal Lattice Structure of Calcium Oxalate Monohydrate: 100 Face (Tazzoli and Domeneghetti, 1980)

single oxalate ion in the center of each hexagon. These planes of oxalate ions are nearly parallel to the 100 plane of the crystal lattice. The second set of oxalate ion planes, as shown in Figure 2-3, serves as a framework for connecting together the first set of oxalate planes. Each oxalate in the second set is associated with four calcium ions and two water molecules. These planes are parallel to the 010 plane of the crystal lattice. The two sets of oxalate planes are interconnected through the calcium ions; each calcium is associated with four oxalate oxygens from the first set of planes, three oxalate oxygens from the second set, and one water oxygen from the second set.

2.8.2 COM Solution Growth Habit

The growth habit of COM crystals is dependent on the conditions used for growth. A few studies report on the habits observed at various solution conditions including those by Burns and Finlayson (1980) and Babic-Ivancic et al. (1985). A particularly revealing review of the growth habit and its relationship to the crystal structure has been given by Frey-Wyssling (1981). In describing the forms of COM crystals observed in plant tissues, he has noted that COM exhibits a variety of growth habits. These habits show only four types of faces, however, and he has identified them according to their crystallographic indices as $\bar{1}01$, 010, 011, and 110 (as will be seen in Chapter 5, these are also the faces seen in COM crystals grown by the photomicroscopic growth cell method). Various growth habits seen for COM are shown in Figure 2-4. The simplest form is the form with two $\bar{1}01$ faces and four 011 faces, (Figure 2-4a). Frey-Wyssling has noted that this form is normally seen at crystal sizes less than 50 microns. At sizes greater than 50

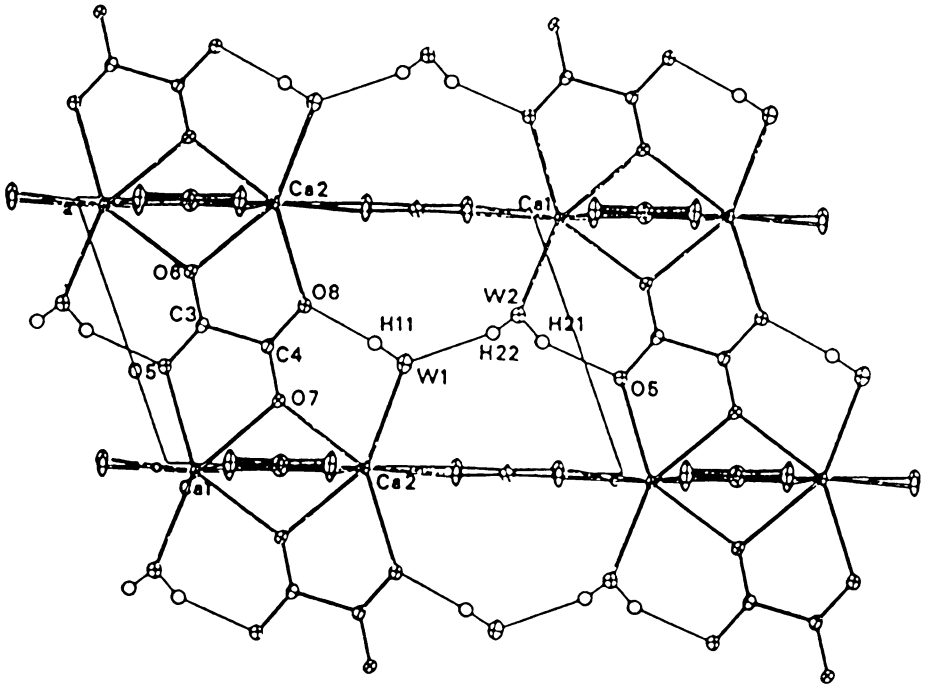

Figure 2-3. Crystal Lattice Structure of Calcium Oxalate Monohydrate: 010 Face (Tazzoli and Domeneghetti, 1980)

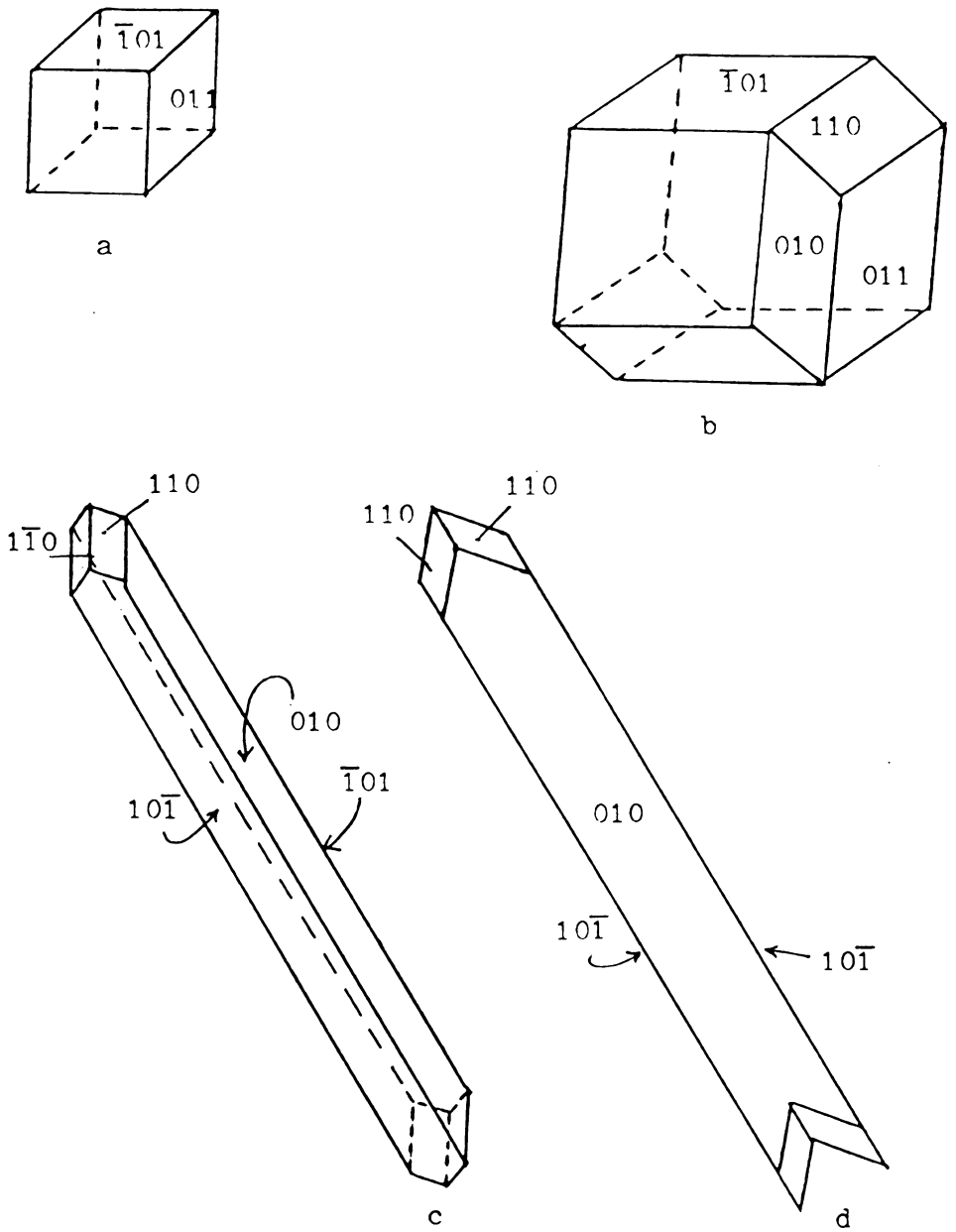

Figure 2-4. Crystal Growth Habits of Calcium Oxalate Monohydrate (Frey-Wyssling, 1981)

microns, the other crystal faces become apparent. In Figure 2-4b, a COM crystal form with all four types of crystal faces is shown. Another form exists (Figure 2-4c) in which the 010 and 110 faces grow at the expense of the 011 faces, which are no longer apparent. $\bar{1}01$ and 010 faces are dominant and 110 faces are smaller. Frey-Wyssling called this form a styloid, a designation to be used in this dissertation. A common form of the styloid is a twin along the $\bar{1}01$ face as shown in Figure 2-4d.

Comparison of the growth habits and face designations of Figure 2-4 with the crystal structure shown in Figures 2-2 and 2-3 may allow the understanding of crystal face growth phenomena in terms of the crystal structure of different faces. Specifically, it may be possible to explain differences in the growth rates seen for different faces of the same crystal under identical solution conditions. The explanation would theoretically focus on the difference in the crystal structure at the different faces.

The observed crystal habit for COM is often distorted from normal forms in the presence of growth modifiers. Good examples of the effect of growth modifiers on habit are seen in crystals taken from urine samples. Elliot and Rabinowitz (1980) have noted that COM crystals observed in the urine of 27 patients show oval and "dumbbell" shapes. Werness et al. (1981) have observed dumbbell and twinned oval forms, but note that urinary inhibitors of COM growth do not alter the crystal habit. Berg et al. (1976) also have reported seeing dumbbell and oval shapes, but these ovals are very similar in shape to the 010 COM face seen in Figure 2-4c. The effect of urinary growth modifiers definitely seems to extend beyond the inhibition of growth to gross alteration of

the growth habit.

2.9 Summary

The entire body of literature on both kidney stone formation and crystal growth studies is vast; this review has only presented the work most closely related to this investigation. It is apparent that deficiencies exist in batch, semi-batch, and MSMPR crystallizer techniques for measurement of crystal growth kinetics. These deficiencies include most significantly their ability to only measure a bulk average crystal growth rate, whereas most crystal growth theories address face growth. The effect of crystal growth modifiers is significant in inhibiting the rate of crystallization, but the methods used in the cited works clearly do not give unequivocal results.

The goal of this work is to understand the growth kinetics of single COM crystals through use of the photomicroscopic method. This method allows direct observation of growth on individual crystal faces and facilitates the measurement of the effects of relative supersaturation, temperature, ionic strength, ion ratio, and growth modifiers on COM single crystal growth kinetics. Results of studies of these parameters on single growth are reported in the following chapters, but first, the methods used to calculate the relative supersaturation and the experiment methods employed in the photomicroscopic technique are discussed.

Chapter 3. Calculation of Relative Supersaturation

3.1 Definition of the Relative Supersaturation

In Chapter 2, the relative supersaturation was defined for a hypothetical salt $A_\alpha B_\beta$ that dissociates in solution according to

$$A_\alpha B_\beta \rightleftharpoons \alpha A^{a+} + \beta B^{b-} \qquad (3\text{-}1)$$

The relative supersaturation σ was given as

$$\sigma = ((A^{a+})(B^{b-}))^{1/\nu} - K_a^{1/\nu})/ K_a^{1/\nu} \qquad (3\text{-}2)$$

For calcium oxalate monohydrate, (3-2) becomes

$$\sigma = ([Ca^{2+}][C_2O_4^{2-}]\gamma^2)^{1/2} - K_a^{1/2})/K_a^{1/2} \qquad (3\text{-}3)$$

where the cationic and anionic activities are expressed in terms of the molar concentrations and activity coefficients. In this chapter, the method used to calculate σ for a variety of solution conditions will be discussed.

3.2 Distribution of Calcium and Oxalate in Ionic Species

When $CaCl_2 \cdot 2H_2O$ and $K_2C_2O_4 \cdot H_2O$ are dissolved in water along with other electrolytes such as KCl, the calcium and oxalate ions exist in various ionic forms in solution (Nancollas, 1974). In addition to the free Ca^{2+} and $C_2O_4^{2-}$ ions, various ion pairs are also formed. In the approach used in this work, only the free Ca^{2+} and $C_2O_4^{2-}$ species are assumed to contribute to the COM relative supersaturation. In order to calculate σ correctly and, in turn, correctly specify the reagent amounts required for a given experiment, it is necessary to account for all of the ionic species through a species balance approach.

The terms $[Ca^{2+}]$ and $[C_2O_4^{2-}]$ in (3-3) refer to the molar concentration of free calcium and oxalate ions in aqueous solution,

whereas total concentration of the respective ions dissolved in solution is expressed as T_{Ca} and T_{Ox}. Ion-pairs and free ion concentration both contribute to T_{Ca} and T_{Ox}. For an aqueous solution close to neutral pH containing KCl and equimolar $CaCl_2 \cdot 2H_2O$ and $K_2C_2O_4 \cdot H_2O$, Tomazic and Nancollas (1979a) suggest that the significant ion-pairs are CaC_2O_4 and $KC_2O_4^-$. For more general non-equimolar, variable pH solutions, the ion-pairs $Ca_2C_2O_4^{2+}$, $Ca(C_2O_4)_2^{2-}$, $H_2C_2O_4$, and $HC_2O_4^-$ must be taken into account (Curreri et al. 1979). The total ion concentrations for calcium and oxalate are then given by

$$T_{Ca} = [Ca^{2+}] + [CaC_2O_4] + 2[Ca_2C_2O_4^{2+}] + [Ca(C_2O_4)_2^{2-}] \qquad (3\text{-}4)$$

$$T_{Ox} = [C_2O_4^{2-}] + [CaC_2O_4] + [Ca_2C_2O_4^{2+}] + 2[Ca(C_2O_4)_2^{2-}] + [H_2C_2O_4] + [HC_2O_4^-] + [KC_2O_4^-] \qquad (3\text{-}5)$$

Equations (3-4) and (3-5) are the species balances necessary in the calculation of σ.

3.3 Ion-Pair Stability Constants

The activities of each of the ion-pairs given in (3-4) and (3-5) are expressed in terms of a stability constant K. For an equilibrium such as

$$Ca^{2+} + C_2O_4^{2-} \rightleftharpoons CaC_2O_4 \text{ (aq)} \qquad (3\text{-}6)$$

the stability constant is defined as

$$K_1 = (CaC_2O_4)/(Ca^{2+})(C_2O_4^{2-}) \qquad (3\text{-}7)$$

with the subscript on K indicating the ion-pair. The subscripts on the stability constants to be used in the following are 1 = CaC_2O_4, 2 = $KC_2O_4^-$, 3 = $HC_2O_4^-$, 4 = $Ca(C_2O_4)_2^{2-}$, 5 = $H_2C_2O_4$, 6 = $Ca_2C_2O_4^{2+}$, and 7 = $LiC_2O_4^-$.

Expressing the activities in terms of molarities and activity coefficients gives

$$K_1 = [CaC_2O_4]/([Ca^{2+}][C_2O_4^{2-}]\gamma_2^2) \qquad (3\text{-}8)$$

where the subscript on γ indicates the activity coefficient for a divalent ion, which is discussed in section 3.4. Similarly for the other ion-pairs

$$K_2 = [KC_2O_4^-]\gamma_1/([K^+]\gamma_1[C_2O_4^{2-}]\gamma_2) \qquad (3\text{-}9)$$

$$K_3 = [HC_2O_4^-]\gamma_1/([H^+]\gamma_1[C_2O_4^{2-}]\gamma_2) \qquad (3\text{-}10)$$

$$K_4 = [Ca(C_2O_4)_2^{2-}]\gamma_2/([CaC_2O_4][C_2O_4^{2-}]\gamma_2) \qquad (3\text{-}11)$$

$$K_5 = [H_2C_2O_4]/([H^+]\gamma_1[HC_2O_4^-]\gamma_1) \qquad (3\text{-}12)$$

$$K_6 = [Ca_2C_2O_4^{2+}]\gamma_2/([Ca^{2+}]\gamma_2[CaC_2O_4]) \qquad (3\text{-}13)$$

Equations (3-8) through (3-13) are the equilibrium relationships required for the calculation of σ. If other reagents are added to the crystal growth solution, additional equilibrium relationships may be required. For example, if LiCl is used instead of KCl, (3-9) becomes

$$K_7 = [LiC_2O_4^-]\gamma_1/([Li^+]\gamma_1[C_2O_4^{2-}]\gamma_2) \qquad (3\text{-}14)$$

and $[LiC_2O_4^-]$ replaces $[KC_2O_4^-]$ in the oxalate species balance, (3-5).

Stability constants for each of the relevant ion pairs are given in Table 3.1. Stability constants, as other equilibrium constants, are functions of temperature. When available, data for stability constants versus temperature have been fitted using the van't Hoff equation (Levine, 1978)

$$d \ln K / d T = \Delta H^\circ / R_g T^2 \qquad (3\text{-}15)$$

where ΔH° is the standard enthalpy of ion-pair formation, R_g is the gas constant, and T is the absolute temperature. Where temperature-dependent data were unavailable, the same value of K was used for all temperatures. Error introduced in this way was insignificant. As seen

Table 3.1 Ion-Pair Stability Constants

Ion-pair	K			
	15 °C	25 °C	37 °C	50 °C
CaC_2O_4	1289	1537	1869	2279
$Ca_2C_2O_4^{2+}$	-	-	71.4	-
$Ca(C_2O_4)_2^{2-}$	-	-	17.3	-
$H_2C_2O_4$	17.73 (9°C)	17.86	19.40	19.72 (45°C)
$HC_2O_4^-$	16440 (9°C)	18450	21010	23390 (45°C)
$KC_2O_4^-$	6.9	8.2	10.0	12.2
$LiC_2O_4^-$	-	-	23	-

See equilibrium equations (3-8) through (3-14) for units of K.

References: CaC_2O_4, $KC_2O_4^-$, Tomazic and Nancollas (1979a, values calculated using same temperature dependence as for $NaC_2O_4^-$); $Ca_2C_2O_4^{2+}$, Curreri et al. (1979); $Ca(C_2O_4)_2^{2-}$ Burns et al. (1981); $H_2C_2O_4$, $HC_2O_4^-$, Garside et al. (1982); $LiC_2O_4^-$, Danielle et al. (1983).

in Table 3.1, the ion-pairs for which there was a value of K known for only a single temperature of 37 °C were $Ca_2C_2O_4^{2+}$, $Ca(C_2O_4)_2^{2-}$, and $LiC_2O_4^-$. The activities of the species $Ca_2C_2O_4^{2+}$ and $Ca(C_2O_4)_2^{2-}$ were significant only when the calcium and oxalate ion concentrations were far from equimolar, which occurred in some experiments performed at 37 °C, as discussed in Chapter 4. All experiments done using LiCl were carried out at 37 °C.

3.4 Ionic Strength and Activity Coefficients

Ionic activity coefficients γ_z were calculated using the Davies extension of the Debye-Huckel equation (Levine, 1978)

$$-\log \gamma_z = A\, z_j^2\, [\sqrt{I}/(1+\sqrt{I}) - .3I] \qquad (3\text{-}16)$$

where A is the Debye-Huckel parameter which is a function of temperature, z_j is the ionic valence, and I is the ionic strength of the solution. Values of A for several different temperatures are given in Table 3.2

Table 3.2 Values of the Debye-Huckel Parameter A

Temperature, °C	A
15	.5028
25	.5115
37	.5230
50	.5373

Reference: Tomazic and Nancollas (1979a)

For a solution containing many different ions, the ionic strength I is defined as (Levine, 1978)

$$I = 1/2 \Sigma M_j z_j^2 \qquad (3\text{-}17)$$

M_j is the molar concentration of the j^{th} ion, and z_j is the valence of the j^{th} ion.

3.5 Algorithm for Calculation of Relative Supersaturation

An algorithm for the calculation of the COM relative supersaturation σ was developed using the SuperCalc III® spreadsheet program (Sorcim Corp., 1983) for the IBM personal computer. The equations used in the algorithm include the material balances (3-4) and (3-5), the equilibrium equations (3-8) through (3-12) and (3-13) (when KCl was used) or (3-14) (when LiCl was used), the Debye-Huckel equation for activity coefficients (3-16), the ionic strength expression (3-17), and the relative supersaturation expression (3-3). The stability constants were taken from Table 3.1 and fitted as a function of temperature using the van't Hoff equation (3-15) when possible. The thermodynamic activity product K_a for COM was taken from Table 2.2 and fitted as a function of temperature using the Arrhenius equation (2-34).

The general strategy for calculating σ centered on the oxalate species balance (3-5). Using the equilibrium equations, the calcium species balance, and a potassium (or lithium) balance, each of the concentration terms in (3-5) was expressed in terms of $[C_2O_4^{2-}]$. An equation containing $[C_2O_4^{2-}]$ and $[Ca^{2+}]$ as the only dependent variables was subsequently developed, containing also the input independent variables of T_{Ca}, T_{Ox}, [KCl] or [LiCl], T, and $[H^+]$ (as pH).

The resulting expression for $[C_2O_4^{2-}]$ is

$$[C_2O_4^{2-}] = T_{Ox} / D \qquad (3\text{-}18)$$

where the denominator D is given by

$$\begin{aligned} D = 1 &+ K_1\gamma_2^2 T_{Ca}/(1 + K_1\gamma_2^2[C_2O_4^{2-}] + K_1K_4\gamma_2^2[C_2O_4^{2-}]^2 \\ &\quad + 2K_1K_6\gamma_2^2[Ca^{2+}][C_2O_4^{2-}]) \\ &+ K_1K_6\gamma_2^2 T_{Ca}^2/(1 + K_1\gamma_2^2[C_2O_4^{2-}] + K_1K_4\gamma_2^2[C_2O_4^{2-}]^2 \\ &\quad + 2K_1K_6\gamma_2^2[Ca^{2+}][C_2O_4^{2-}])^2 \\ &+ K_2\gamma_2 T_K/(1 + K_2\gamma_2[C_2O_4^{2-}]) \\ &+ K_3\gamma_2[H^+] \\ &+ K_3K_5\gamma_1^2\gamma_2[H^+]^2 \\ &+ 2K_1K_4\gamma_2^2[C_2O_4^{2-}]T_{Ca}/(1 + K_1\gamma_2^2[C_2O_4^{2-}] \\ &\quad + K_1K_4\gamma_2^2[C_2O_4^{2-}]^2 \\ &\quad + 2K_1K_6\gamma_2^2[Ca^{2+}][C_2O_4^{2-}]) \end{aligned} \qquad (3\text{-}19)$$

In (3-19), T_K refers to the total concentration of potassium in solution, given by

$$T_K = [K^+] + [KC_2O_4^-] \qquad (3\text{-}20)$$

Equations (3-18) and (3-19) were solved iteratively as follows. The total calcium and total oxalate concentrations, T_{Ca} and T_{Ox}, were known from the input amounts of reagents $CaCl_2 \cdot 2H_2O$ and $K_2C_2O_4 \cdot H_2O$. T_K was known from the input amount of KCl and $K_2C_2O_4 \cdot H_2O$. $[H^+]$ was known from the solution pH. The temperature was known which determined the values of the stability constants and K_a. As a first guess, $[Ca^{2+}]$ and $[C_2O_4^{2-}]$ were set equal to T_{Ca} and T_{Ox}, respectively, and the ionic strength was set equal to [KCl]. Activity coefficients were calculated using (3-14). The new value of $[C_2O_4^{2-}]$ was calculated using (3-19). All other ion concentrations were calculated using the equilibrium

equations, the calcium balance, and the potassium balance. The ionic strength was recalculated using the calculated ion concentration values, and the activity coefficients were recalculated. A new value of $[C_2O_4^{2-}]$ was calculated using (3-19), and all other ion concentrations were subsequenty recalculated. This process was repeated until the calculated concentrations stopped changing; convergence typically occurred within five to ten iterations. The COM relative supersaturation, σ, was then calculated from (3-3) using the converged values of $[Ca^{2+}]$ and $[C_2O_4^{2-}]$.

Results of relative supersaturation calculations using the computer algorithm are given in Chapter 4 and Appendix A.

Chapter 4. Photomicroscopic Method for Single Crystal Growth of Calcium Oxalate Monohydrate

In Chapter 2, the advantages of the photomicroscopic technique for single crystal growth rate measurement over other methods were discussed. In this chapter, the procedures used in the crystal growth experiments are described in detail. First, the preparation of growth solutions and methods used to measure the ion concentrations in solution are discussed, followed by a summary of the experimental solution conditions calculated using the relative supersaturation algorithm. This is followed by a description of the growth cell and crystal growth flow system. Next, the process of inducing crystal nucleation, growth, and dissolution in the cell is described. The chapter ends with a discussion of the procedures involved in measuring single crystal facial growth rates.

The methods described in this chapter have been reported previously for use in crystal growth (DeLong and Briedis, 1985a) and dissolution (DeLong and Briedis, 1984).

4.1 Solution Preparation

Three types of ionic solutions were prepared each using a different background electrolyte (KCl, LiCl, or $KClO_4$). In each case, separate solutions of Ca^{2+} and of $C_2O_4^{2-}$ were prepared using reagent grade chemicals. For solutions with KCl, the cationic solutions consisted of calcium chloride dihydrate, $CaCl_2 \cdot 2(H_2O)$, and potassium chloride, KCl, while the anionic solutions contained potassium oxalate monohydrate, $K_2C_2O_4 \cdot H_2O$, and KCl. For LiCl solutions, the calcium solution consisted

of $CaCl_2 \cdot 2H_2O$ and lithium chloride, LiCl, and the oxalate solution consisted of oxalic acid dihydrate, $H_2C_2O_4 \cdot 2H_2O$, lithium hydroxide monohydrate, $LiOH \cdot H_2O$, and LiCl. For $KClO_4$ solutions, the calcium solution contained $CaCl_2 \cdot 2H_2O$ and potassium perchlorate, $KClO_4$, and the oxalate solution contained $K_2C_2O_4 \cdot H_2O$ and $KClO_4$.

Dry reagents were weighed fresh daily in required amounts using a Mettler AE 100 analytical balance. The weighed reagents were then dissolved in doubly distilled, freshly deionized water to the required concentration. The pH of both the Ca^{2+} and $C_2O_4^{2-}$ solutions was adjusted to 6.00 ± 0.01 using 0.05 M HCl (or $HClO_4$) and 0.05 M KOH (or LiOH). A Fisher model 800 MP millivolt meter with a glass pH and reference electrodes or a double-junction glass electrode were used to monitor the pH during adjustment. The solutions were stirred to homogeneity using a magnetic stirrer.

Solution preparation was complicated by the need to eliminate carbon dioxide from the growth cell. Any significant amount of CO_2 in solution tended to volatilize due to warming as it passed through the flow system; this lead to the problem of gas bubbles blocking the field of view of the microscope. For this reason, it was necessary to remove CO_2 from solution before introducing the solution into the cell. This was accomplished by drawing doubly distilled, deionized water directly from the deionizer (Cole-Parmer 1506-15, 1506-35) into 2 or 4 liter Erlenmeyer flasks containing the weighed dry reagents and a magnetic stir bar. Each Erlenmeyer flask was equipped with a rubber stopper pierced by two 1/4-inch ID glass tubes. One tube extended to the bottom of the flask and was connected to a flexible plastic tube external to the flask. This plastic tube was connected to either the deionizer

while the flask was filling or the crystal growth apparatus while emptying. The other, shorter glass tube was open to the atmosphere to allow pressure equilibration in the flask. The Erlenmeyer flasks were calibrated using 2000 ml volumetric flasks. By pumping water directly from the deionizer into the Erlenmeyer flask, it was possible to reduce exposure of the relatively CO_2-free water to air. Earlier attempts to prepare the solutions in volumetric flasks and then transfer the solutions to Erlenmeyer flasks resulted in a significant air exposure and subsequent absorption of CO_2. With a solubility of CO_2 in water of 1.45 grams per liter at 25 °C and 0.97 grams per liter at 40 °C (CRC Handbook, 1977), volatilization of the dissolved gas upon heating from 25°C to 40 °C could have lead to formation of 240 ml of CO_2 per liter of solution. Pumping freshly deionized water directly into calibrated Erlenmeyer flasks was chosen over degassing with nitrogen as the more convenient and reasonably reliable method of solution preparation.

For growth experiments in which a growth modifier was used, the anionic biopolymer was added to the anionic oxalate solution. The biopolymers used included sodium poly-L-glutamate of various molecular weights (Sigma P 4636, P-4761, P-4886) and sodium heparin (Sigma H-3125).

4.2 Measurement of Solution Ion Concentrations

In order to ensure accurate calculation of the relative supersaturation, it was necessary to measure concentrations of ions in the growth solution. Measurement of calcium ion [Ca^{2+}] was fairly straightforward, but measurement of low concentrations of oxalate [$C_2O_4^{2-}$] presented greater difficulty and was not attempted. Calcium

concentrations were therefore measured in an effort to verify the theoretical calculation of relative supersaturation as presented in Chapter 3.

The calcium concentration was measured in both the stock growth solution and in the effluent from the growth cell using atomic absorption spectroscopy (Varian AA-375) or a calcium selective electrode (Orion 93-20). The instruments in both methods were standardized using a standard calcium solution, and all samples and standards were adjusted to a constant ionic strength using the appropriate background electrolyte.

4.3 Design of Crystal Growth Experiments Using the Supersaturation Algorithm

The algorithm described in Chapter 3 was used to calculate the relative supersaturation for a variety of solution conditions. Relative supersaturation could be easily varied by changing total calcium or oxalate concentrations, ionic strength, pH, or temperature. This allowed the design of a series of crystal growth experiments with identical ionic strengths, temperatures, pH values, and ratios of total calcium to total oxalate concentration, but with different relative supersaturations. This approach facilitated the determination of the dependence of COM single crystal growth rate on the relative supersaturation. In turn, it was possible to design a series of experiments in which one of the independent solution variables other than σ was varied while the others were held constant. It was therefore possible to test the effect of solution variables on growth beyond their effect on the relative supersaturation. It was also possible to

determine the effect of various electrolytes on growth kinetics, e. g., as with parallel series of experiments using LiCl in one and KCl in the other, but with identical calculated solution properties.

The relative supersaturation algorithm was used to specify the solution conditions for several series of crystal growth experiments which are described in the following section.

4.3.1 Variation of Relative Supersaturation

Experiments to determine the dependence of crystal growth rate on relative supersaturation were designed using solution conditions typical of human urine (Isaacson, 1968; Gains, 1968). The temperature was specified as 37 °C, the ionic strength I = 0.15 M, and the pH = 6.00. Potassium chloride was the background electrolyte. Although not typical of urine, the total calcium and total oxalate concentrations were set equal in this "base" series of experiments. The relative supersaturation was varied by varying the equimolar ion concentrations in the range $T_{Ca} = T_{Ox} = 0.450 \times 10^{-3}$ M to 1.75×10^{-3} M. These conditions gave a range of σ resulting in growth rates easily evaluated with the photomicroscopic crystal growth technique. The calculated solution parameters for variable σ are given in Table A-1 of Appendix A. A summary of solution conditions used for all of the experiment series described in this section is given in Table 4-1.

4.3.2 Variation of Temperature

Three series of experiments were designed to complement the base case (T = 37 °C) shown in Table A-1. Each was conducted at a different temperature: 15 °C, 25 °C, and 50 °C. Conditions of pH, ionic

Table 4.1 Summary of Solution Conditions Used in Experiments

T,°C	σ	I, M	Electrolyte	T_{Ca}/T_{Ox}	$[Ca^{2+}]/[C_2O_4^{2-}]$	Table
37	var	0.15	KCl	1	-	A-1
15	var	0.15	KCl	1	-	A-2
25	var	0.15	KCl	1	-	A-3
50	var	0.15	KCl	1	-	A-4
37	3.71	var	KCl	-	1	A-5
37	3.71	var	LiCl	-	1	A-6
37	3.71	0.15	KCl	-	var	A-7
37	3.71	≈ 0	-	-	var	A-8
37	3.71	0.15	LiCl	-	var	A-9

var = variable

strength, and total calcium and oxalate concentrations were similar to those used in the base case. Results of the relative supersaturation algorithm are shown in Tables A-2, A-3, and A-4 for 15 °C, 25 °C, and 50 °C, respectively. These conditions were used in experiments to generate four isotherms of crystal growth rate versus relative supersaturation. These data were then used to calculate an activation energy for COM crystal growth, as will be discussed in section 6.4.

4.3.3 Variation of Ionic Strength

Two series of experiments were designed to determine the response of COM crystal growth rate to changes in the solution ionic strength. For these two series, background electrolyte was changed, but the relative supersaturation was maintained at $\sigma \approx 3.71$, the same σ as for the base case in Table A-1 ($T_{Ca} = T_{Ox} = 0.001$ M). For reasons to be described later, the ratio of the free calcium to free oxalate concentration, $[Ca^{2+}]/[C_2O_4^{2-}]$, was set equal to one. Since $[Ca^{2+}]/[C_2O_4^{2-}]$ was not an independent variable, T_{Ox} and T_{Ca}/T_{Ox} were altered in the algorithm until the desired conditions of $[Ca^{2+}]/[C_2O_4^{2-}] \approx 1$ and $\sigma \approx 3.71$ were found. The other fixed solution conditions were pH = 6.00, T = 37 °C. The ionic strength was varied in a range of approximately $0.002 \leq I \leq 0.5$ M.

As mentioned above, the difference between the two series of experiments was the background electrolyte used. In the first series, KCl was used, as shown in Table A-5. In the second, LiCl was used, as shown in Table A-6.

4.3.4 Variation of Calcium to Oxalate Ratio

Three series of experiments were designed in order to determine the effect of varying the free calcium to free oxalate ratio, $[Ca^{2+}]/[C_2O_4^{2-}]$. Experiments were designed for varying ion ratio in the presence of KCl as a background electrolyte at ionic strengths of I = 0.15 M and I ≈ 0 (no added KCl). This series is described in Tables A-7 and A-8, respectively. Another series was designed for varying ion ratio with LiCl as the background electrolyte at an ionic strength of I = 0.15 M. This series is described in Table A-9. In all of these experiments, the other conditions of the base case in Table A-1 (with $T_{Ca} = T_{Ox} = .001$ M) were used, i. e., the temperature was designated as T = 37 °C, the pH = 6.00, and $\sigma \approx 3.71$.

4.3.5 Experiments Using Polyelectrolytes

In experiments in which polyelectrolytes such as polyglutamate or heparin was added to the oxalate solution, no adjustment of solution parameters was made. Since the concentration of added polymer was low (≈ 10 mg/l), the small contribution by the polyelectrolyte to the ionic strength and the complexation of calcium ion by the polyelectrolyte were neglected.

4.4 Growth Cell

The growth cell used is shown diagramatically in Figure 4-1. The cell was designed after that of Valcic (1975). The cell consisted of three thin, stacked plexiglass sections with round pyrex windows inserted between the top and center sections and between the center and bottom sections. The three sections and the glass windows were held

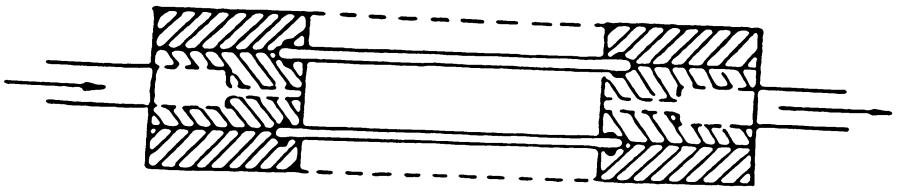

Side View

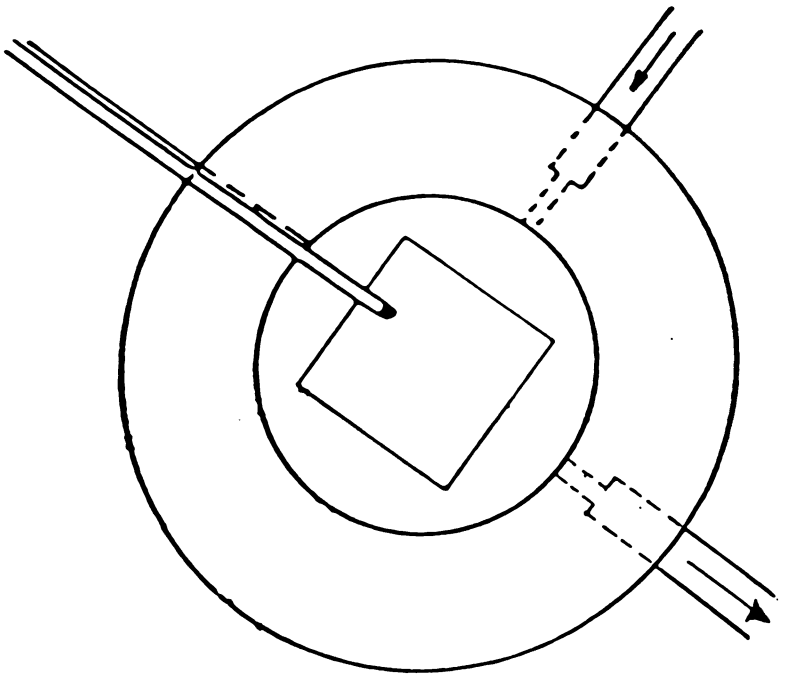

Top View

Figure 4-1. Isothermal Continuous Flow Crystal Growth Cell

together with four brass screws distributed about the periphery of the cell. When assembled, the cell contained a small cylindrical chamber of approximately 5 ml in volume.

The center section of the cell contained several threaded holes for access to the chamber. Two of these holes held threaded stainless steel ports for entry and exit of the mixed calcium oxalate solution. The ports were positioned at 90 degrees to prevent immediate exit of the entering solution. Another hole held a plastic-coated thermistor (Yellow Springs Series 700) used as a temperature monitor.

A fourth hole held a stainless steel rod onto which a thin glass microscope slide cover slip was attached using a cyanoacrylate glue. This slip provided the surface for calcium oxalate nucleation and growth and crystal observation. The rod was positioned such that the glass slip was centered both vertically and horizontally in the flow field of the calcium oxalate solution. This positioning ensured a more uniform solution concentration in the vicinity of the crystals and a more uniform temperature away from the effects of the walls of the chamber.

When not in use, the cell was kept disassembled in soapy water. Before each new growth experiment, the cell was thoroughly cleaned and a new glass cover slip was mounted on the stainless steel rod before assembly.

4.5 Crystal Growth System

4.5.1 Flow Scheme

The assembled growth cell was incorporated in a flow scheme as shown in Figure 4-2. The separate calcium and oxalate solution flasks were each connected to flexible plastic tubing (Tygon 1363) and the

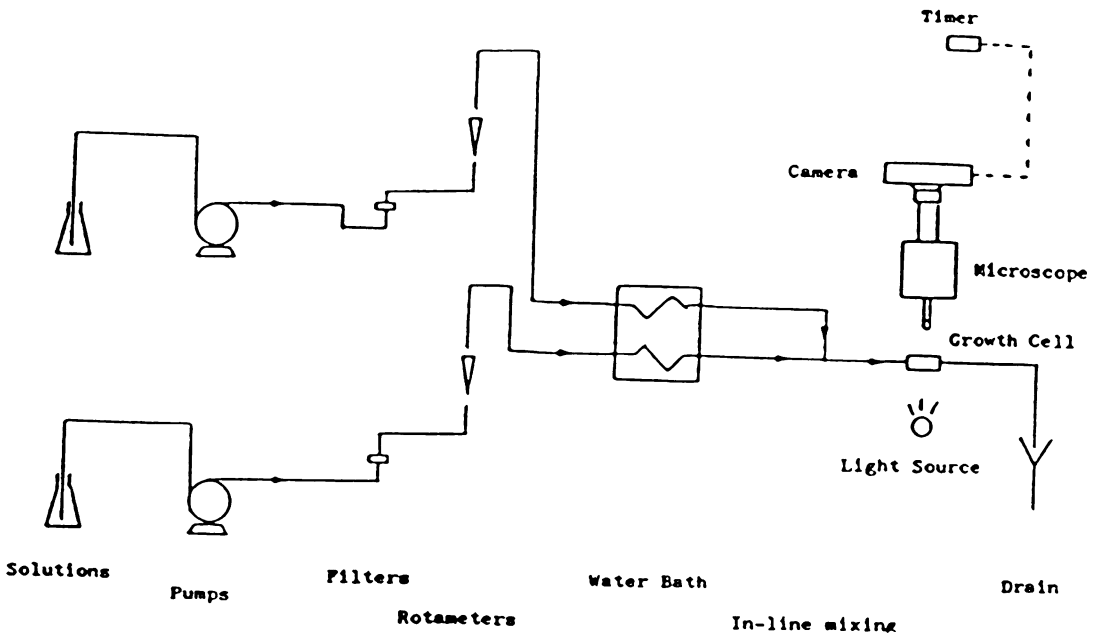

Figure 4-2. Flow Diagram for Single Crystal Growth Experiment

solutions were pumped through the system using positive-displacement pumps (Masterflex, Cole-Parmer 7553-10 and 7014-20). In order to remove any undissolved particulate matter, the solutions flowed through in-line, 25 millimeter diameter filters (Gelman Scientific) equipped with 0.45 micron pore size flexible membranes. The solutions then passed through rotameters (Cole-Parmer FM-092-04G) used to monitor the flow rates. Each solution passed through a 1/4-inch ID glass coil submerged in a constant temperature water bath (Haake NK 22) set at a temperature several degrees above that desired in the growth cell. The two solutions were mixed in an in-line, 1/8-inch ID T-joint immediately up stream of the growth cell, with a three-inch section of 1/8-inch ID plastic tubing leading into the cell. The mixed solution then entered the cell which was mounted on the observation stage of a light microscope. The solution flowed over the crystals growing on the glass cover slip in the cell, and then exited the cell to a drain. As is normally the case, the residence time of the solution in the cell was dependent on flow rate.

4.5.2 In-line Mixing of Solutions

The calcium and oxalate solutions were mixed in an in-line T-joint immediately upstream of the growth cell. It was suspected that combination in a T-joint would give better mixing of solutions than use of a Y-joint or by simply feeding the streams separately into the cell. Flow visualization in the growth cell with dyed water showed this to be true. In addition, the insertion of a short (three-inch) tube between the T-joint and the cell seemed to improve the degree of mixing. This flow configuration achieved thorough mixing of the two solutions and has been widely used in the study of rapid reactions in solution as

described by Caldin (1964). With regards to the thermodynamic state of the solution that reaches the crystals, it may be reasonably assumed that equilibrium for the ions and ion-pairs in solution is achieved between the instant of mixing and the time of contact between solution and crystals for the following reason: the kinetic constant of formation of the calcium oxalate ion-pair, $[CaC_2O_4]$, which may be thought of as representing the crystal growth units, has been found to be on the order of 108 s^{-1} for calcium ion-pairs (Eigen, 1963). Such rapid kinetics, coupled with the rapid mixing and the fact that small solution volumes were involved, provided for solution equilibrium within the cell.

Location of the cell exit port 90 degrees from the inlet rather than 180 degrees also promoted better mixing. When located at 180 degrees, a large portion of the incoming solution seemed to exit immediately without mixing with the solution in the cell. After moving the outlet to the 90 degree position, flow visualization demonstrated that the incoming solution stream impinged upon the opposite wall of the cell (the prior location of the outlet port) and flowed back, thereby providing a significant improvement in the mixing.

4.5.3 Solution Temperature and Flowrate Control

The temperature of the solution in the cell growth chamber was held at the desired level by flowing the separate solutions through glass coils in a constant temperature water bath. Since there were significant heat losses through the lines leading from the water bath to the cell and through the walls of the cell, it was necessary to set the bath temperature slightly higher (or slightly lower for sub-ambient

work) than the desired cell temperature. The required water bath temperature depended on the ambient temperature, the cell temperature, and the flowrate through the lines, and was usually set by trial and error. The solution lines leading from the bath to the cell were insulated with foam rubber to minimize heat loss. This method provided excellent temperature control, usually to within 0.2 °C.

The temperature in the cell was monitored using a temperature probe connected to a digital multimeter (Keithly 179A) that provided a readout of the probe's electrical resistance. This value was translated into a temperature using the calibration chart provided with the probe. The calibration chart was verified by measuring the resistance of the probe in ice water and in boiling water. Deviations from the temperature setpoint were noted visually and compensated for manually by adjusting the water bath temperature.

The flow rates of the calcium and oxalate solutions were controlled individually through the use of variable speed positive displacement pumps and rotameters. The rotameters were calibrated using a stopwatch and graduated cylinder. Prior to an experiment, the solution flowrates were initially set by increasing the pump speed until the rotameter reading corresponded to the desired flowrate as read from the rotameter calibration curve. The flowrate was then verified using a stopwatch and graduated cylinder. Fluctuations in the flow rates during experiments were compensated for by adjusting the pump speeds.

4.6 Nucleation, Growth, and Dissolution of Crystals

A typical experimental run started with the connection of the growth cell to the flow system and filling of the cell with distilled

water or a blank solution containing only the background electrolyte at the appropriate ionic strength. The cell was then placed on the microscope stage and the microscope objective focused on the top side of the glass cover slip. The desired solution flowrate was set and checked with a 10 ml graduated cylinder and a stopwatch. The temperature probe was connected to the multimeter and the temperature of the cell was allowed to equilibrate at the desired level with adjustments made to the water bath temperature as required. Typically, the temperature of the water bath was set several degrees above or below the desired cell temperature to compensate for heat losses in the plastic tubing between the water bath and the cell. The surface of the glass cover slip was then inspected for debris. A significant amount of debris was often the cause of excess crystal nucleation. If too many crystals formed, the crystal growth rates were retarded probably due to a reduced relative supersaturation caused by rapid growth ion depletion. In order to measure meaningful growth rates at the desired relative supersaturation, it was necessary to maintain a very clean nucleation surface. To this end, if a surface appeared too dirty, the cell was disassembled and cleaned again.

When the solution flowrate and the cell temperature were at the desired levels and the cover slip surface appeared sufficiently clean, the flow of the calcium and oxalate solutions was started. After an initial start-up period of several minutes to allow for replacement of the blank solutions in the lines with the growth solutions, the surface of the glass cover slip was observed with the microscope for the formation of crystals. If it appeared that too many nuclei had formed, the crystals were dissolved by running the blank solutions through the

cell, or, if necessary, the cell was disassembled and cleaned.

After it was confirmed that the nucleation was sufficiently sparse to preclude significant reduction of the relative supersaturation, the crystals were allowed to grow to a size at which crystal edges were distinguishable, generally about 5 to 10 microns in length at 200x magnification. At this point, the top of the cover slip was scanned to find several (approximately 3 to 5) well spaced crystals. This view was centered in the field of view of the camera (Olympus OM-10) mounted on the top of the microscope (American Optical MicroStar 110). A series of approximately 10 photographs was then taken. Time intervals between exposures were controlled by a remote automatic timer (Olympus Remote Controller 1), and the film (Kodak Ektachrome slide film, ASA 100) was advanced by an automatic camera winder (Olympus Winder 2). When the picture sequence was completed, blank solution was again run through the lines to remove the growth solution. After the growth solution was purged from the system, another series of photographs was sometimes taken while the crystals dissolved in the blank solution.

4.7 Measurement of Single Crystal Growth Rates

A series of photographs taken during growth runs was analyzed for single crystal growth rates as follows. Each picture in a series of developed photograph slides was projected onto a screen. A sheet of tracing paper was laid on the screen, and the crystal images along with the magnification scale were traced on the paper. This series of tracings was then analyzed using an image analysis sytem, the HiPad digitizing tablet (Houston Instruments) interfaced to an Apple IIe computer. The image analysis software package (Dapple Systems, Inc.)

was equipped with two modes for measuring image dimensions. In the first mode, the distance between parallel faces of the crystals could be measured leading to a calculation of the linear face growth rate. Second, for irregularly shaped crystals without parallel faces, the program calculated several parameters including the area of the projected crystal face. This area, A, was used to calculate an equivalent circular diameter, D_{eq}, defined as

$$D_{eq} = (4A/\pi)^{1/2} \qquad (4\text{-}1)$$

Depending on the mode of measurement, the relevant crystal dimension was plotted versus the growth time. A least-squares linear regression analysis was used to calculate the best-fit lines for the data. The slopes of these lines, dD_{eq}/dt, represented the growth rates for the crystals in units of length per time. Units of microns/min (μm/min) were typically used.

Chapter 5. COM Single Crystals: Identification and Growth Habit under Various Solution Conditions

5.1 Identification and Crystal Habit in Modifier-Free Solutions

The introduction of the mixed calcium and oxalate ionic solutions into the growth cell induced heterogeneous nucleation of calcium oxalate crystals on the glass surface mounted in the cell. In solutions with no added polymeric crystal growth modifiers, two general types of crystal habits were observed in the ranges of relative supersaturations and temperatures used, the monoclinic tabular habit of calcium oxalate monohydrate and the tetragonal bipyramidal habit of calcium oxalate dihydrate. In addition, some flat, elongated plate-like crystals that may have been the trigonal calcium oxalate trihydrate were occasionally seen. All of these crystal types were identified by comparing their habits with previously reported calcium oxalate crystal habits. COM crystals were identified further through comparison of their Raman spectra with that of commercially available analytical grade COM. Raman spectra of COD and COT crystals were also taken.

5.1.1 Calcium Oxalate Monohydrate Crystal Growth Habits

Over most of the ranges of relative supersaturation ($1 \leq \sigma \leq 8$) and temperature ($15\ ^{\circ}C \leq T \leq 50\ ^{\circ}C$), crystals formed with various monoclinic tabular habits as shown in Figures 5-1 through 5-9. These were identified as COM based on previous reports of COM crystal habits, such as that by Frey-Wyssling (1981) discussed in Chapter 3. Raman spectra of several crystals were taken, and spectra of crystals such as those in Figures 5-1 through 5-9 are shown in Figure B-1 of Appendix B.

The particular habit observed for COM depended upon the relative supersaturation at which the crystal was grown. Crystals grown at low relative supersaturations ($\sigma < 2$) showed habits such as that shown in Figure 5-1, grown at $\sigma = 1.49$ and T = 37 °C. Two views of COM crystals are shown in Figure 5-1, views A and B. View A shows a more prominent hexagonally-shaped face (parallel to the page) and four smaller parallelogram-shaped faces extending away from the prominent face (into the page). View B shows a prominent parallelogram-shaped face (parallel to the page), along with two smaller parallelogram-shaped faces. The prominent hexagonal and parallelogram faces are perpendicular to each other in a COM crystal of this type. This habit has been called a styloid by Frey-Wyssling (1980) as noted earlier in Section 2.8. The eight faces of the COM styloid crystal were identified in section 2.8 according to their crystallographic indices. A perspective drawing of a COM styloid is shown in Figure 5-2 with the crystallographic indices of the faces included.

Various styloid twins were observed, with increasing frequency at higher relative supersaturations. Crystal twins are composite crystals that appear to be composed of two intergrown individual crystals, similar in form, joined symetrically about a twin axis or a twin plane (Mullin, 1961). One type of twin is shown located between the 450 to 475 micron lines in Figure 5-1. This crystal revealed a twinned 010 face, with the additional plane of symmetry parallel to the $\underline{1}01$ face. A perspective drawing with crystallographic indices for the styloid twin of Figure 5-1 is given in Figure 5-3.

A second type of styloid twin observed is shown in Figure 5-4, grown at $\sigma = 2.07$ and T = 37 °C. This crystal appeared as a combination

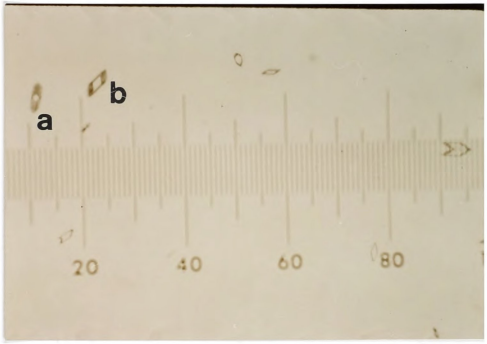

Figure 5-1. COM Crystals Grown at σ = 1.49, T = 37 °C.

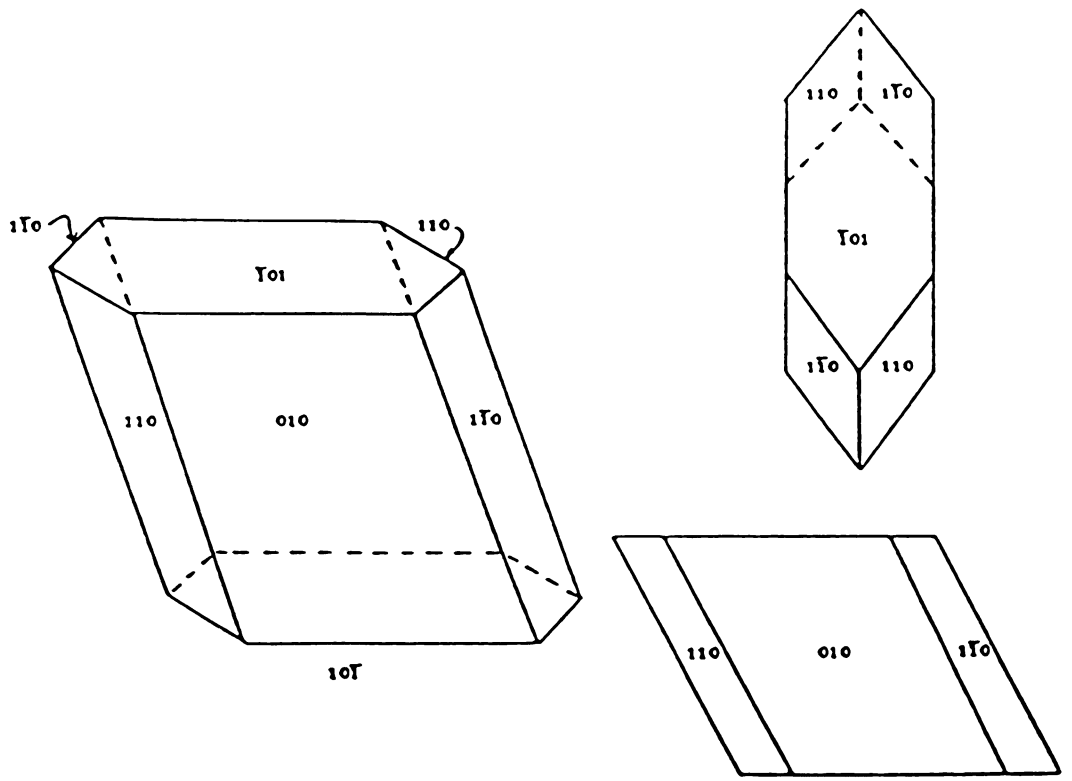

Figure 5-2. Perspective Drawing of Crystals in Figure 5-1.

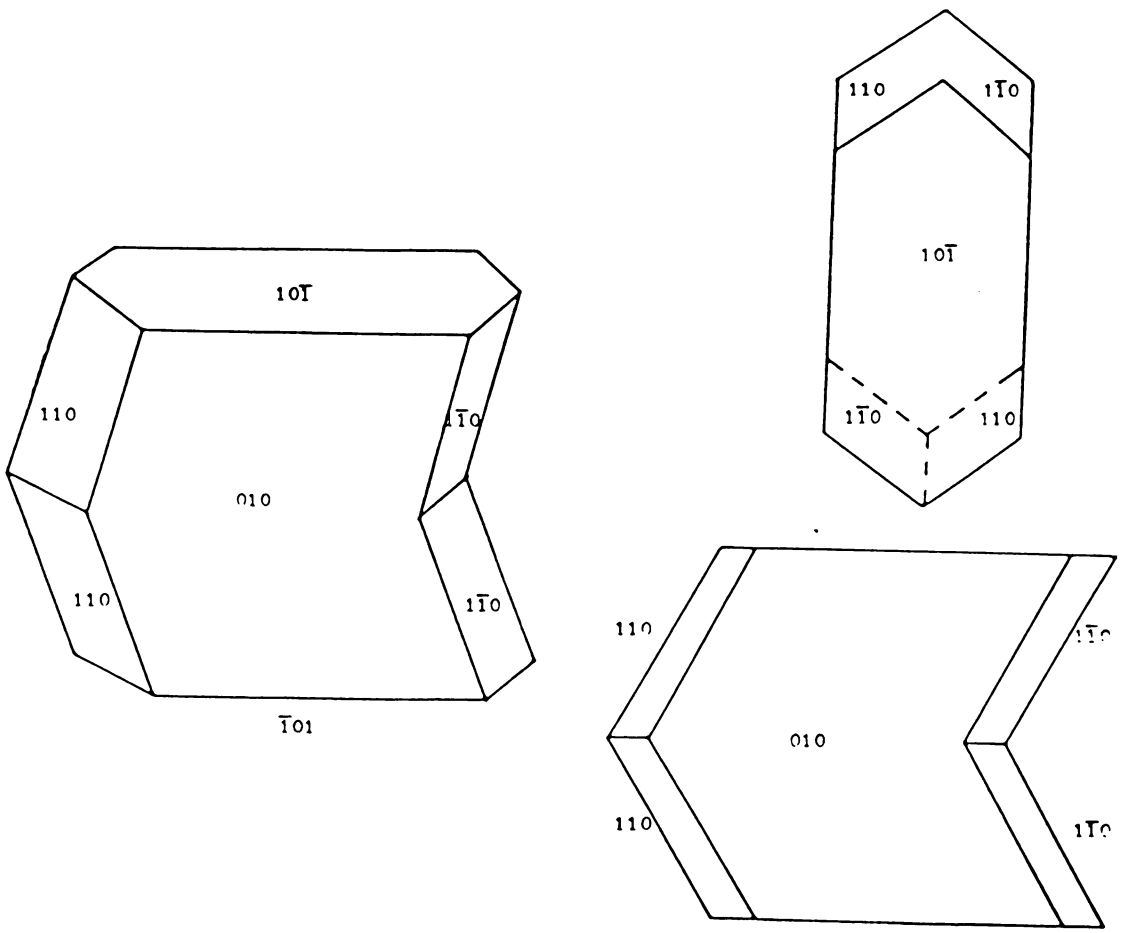

Figure 5-3. Perspective Drawing of Crystals in Figure 5-1.

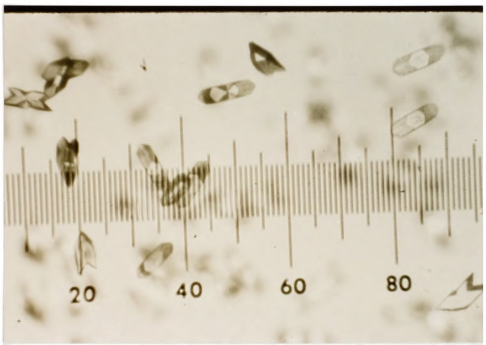

Figure 5-4. COM Crystals Grown at σ = 2.07, T = 37 °C.

of two normal styloids (Figure 5-1) with their 010 faces crossing in the center. Eight additional 110 and $1\underline{1}0$ faces were also apparent in this type of twin. A perspective drawing of this twinned styloid showing crystallographic indices is given in Figure 5-5.

At relative supersaturations greater than about $\sigma = 3$, the twinned styloids grew with the additional 110 and $1\underline{1}0$ faces absent. Crystals of this type grown at $\sigma = 3.71$ and T = 37 °C are shown in Figure 5-6, with a perspective drawing including crystallographic indices given in Figure 5-7. The styloid twins of Figures 5-6 and 5-7 were the most frequently seen COM crystal type.

At high relative supersaturations corresponding to the upper limit for nucleation of the monohydrate phase ($\sigma \approx 8$), COM crystals grew with a rhomboid prism habit as shown in Figure 5-8. View A of Figure 5-8 reveals a rhomboid $\underline{1}01$ face, and view B shows a rectangular 011 face similar to the COM habit shown in Figure 2-4a. Growth experiments demonstrated that the 010, 110, and $1\underline{1}0$ faces apparently did not grow at these conditions ($\sigma = 7.07$, T = 25 °C). A perspective drawing including the crystallographic indices for a crystal of the type shown in Figure 5-8 is given in Figure 5-9.

Results of the modifier-free experiments have shown a gradual transition in the type of crystal habit observed for COM crystals from the styloid to twinned styloid to the rhomboid prism with increasing relative supersaturation. In Figure 5-10, perspective drawings show the gradual habit transition from the twinned styloid to the rhomboid prism with crystallographic indices indicated on the crystal faces. As noted earlier, the styloid twin of Figure 5-6 was the most frequently observed crystal habit.

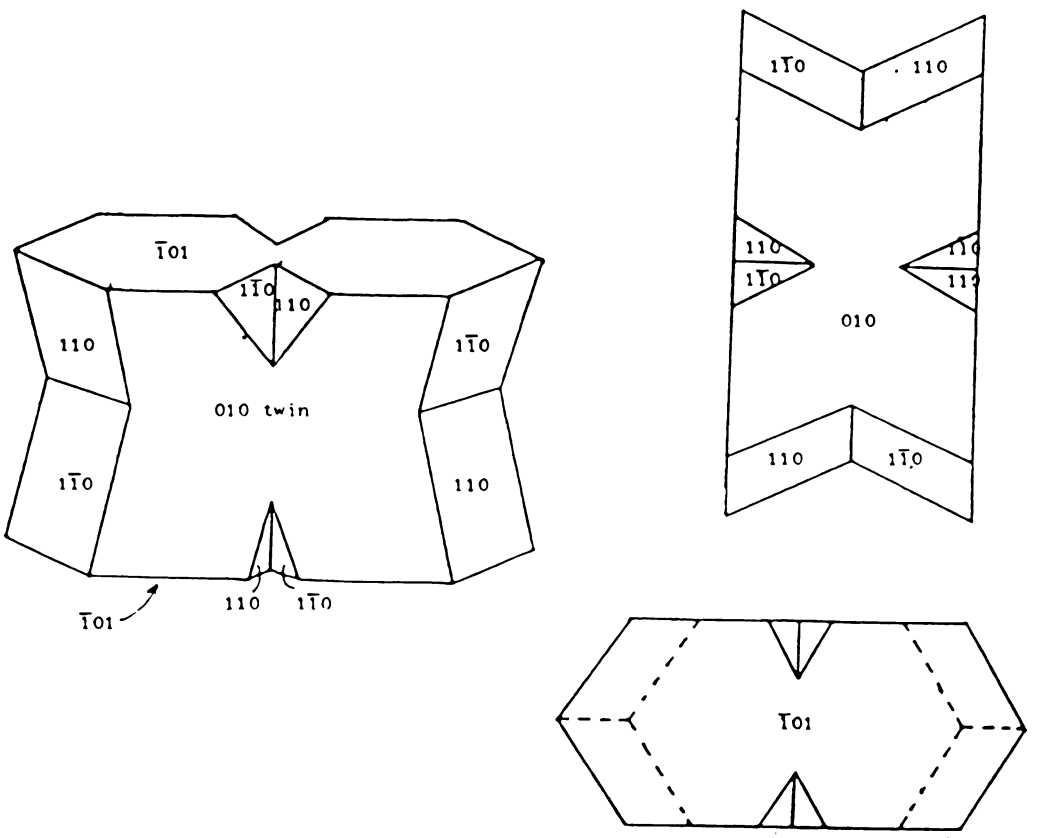

Figure 5-5. Perspective Drawing of Crystals in Figure 5-4.

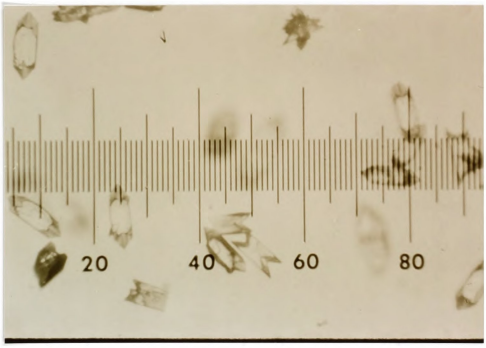

Figure 5-6. COM Crystals Grown at σ = 3.71, T = 37 °C.

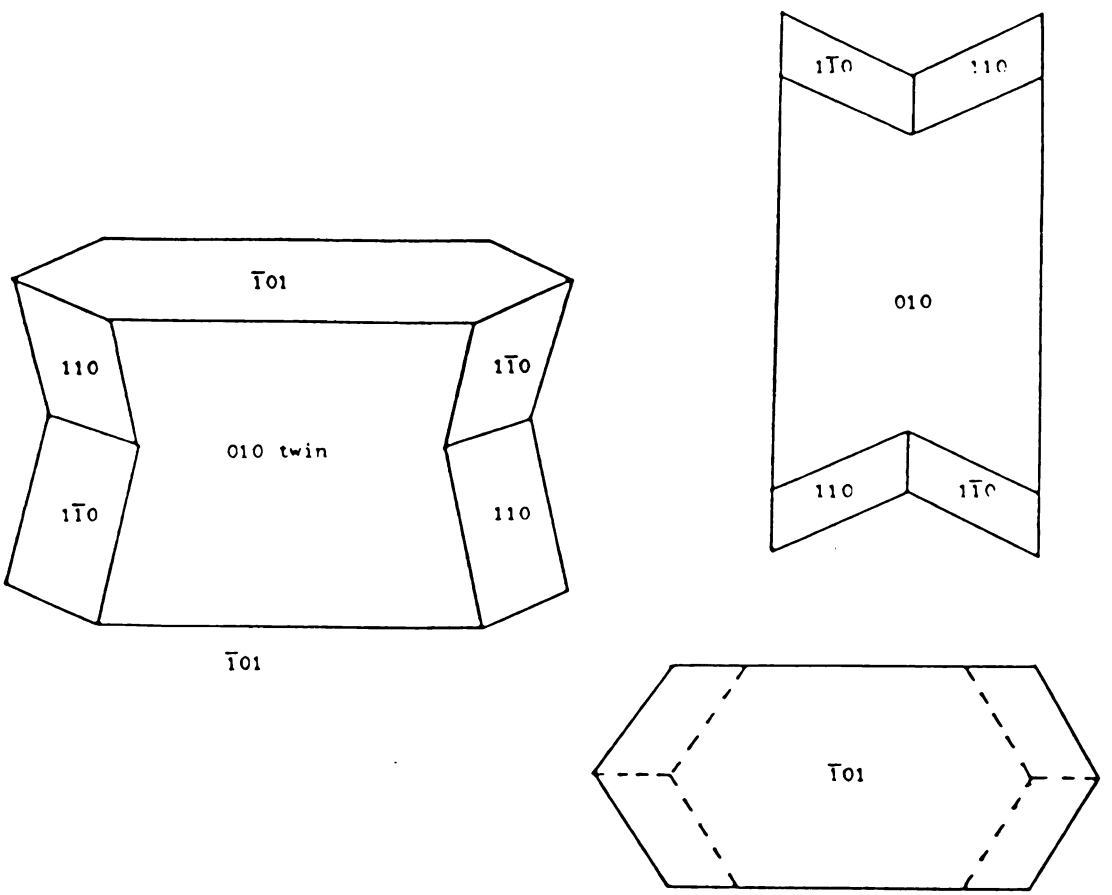

Figure 5-7. Perspective Drawing of Crystals in Figure 5-6.

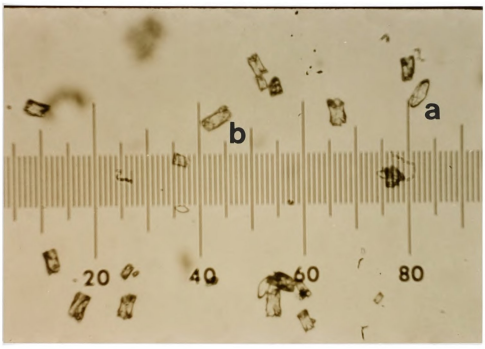

Figure 5-8. COM Crystals Grown at σ = 7.07, T = 25 °C.

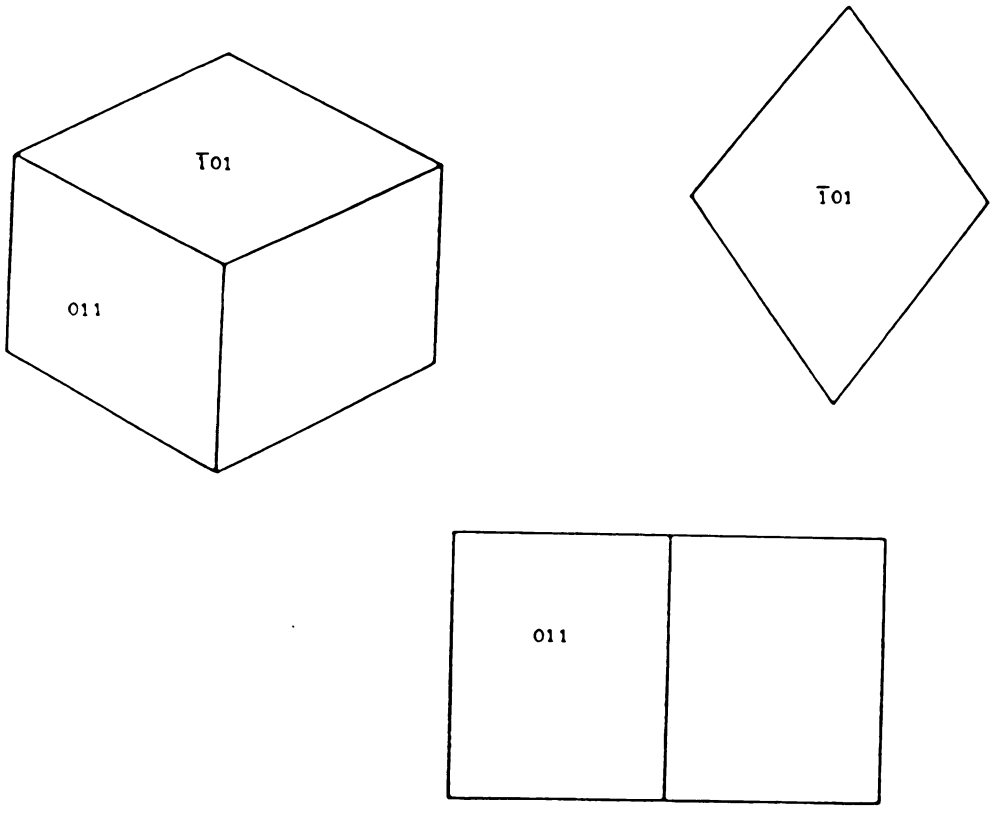

Figure 5-9. Perspective Drawing of Crystals in Figure 5-8.

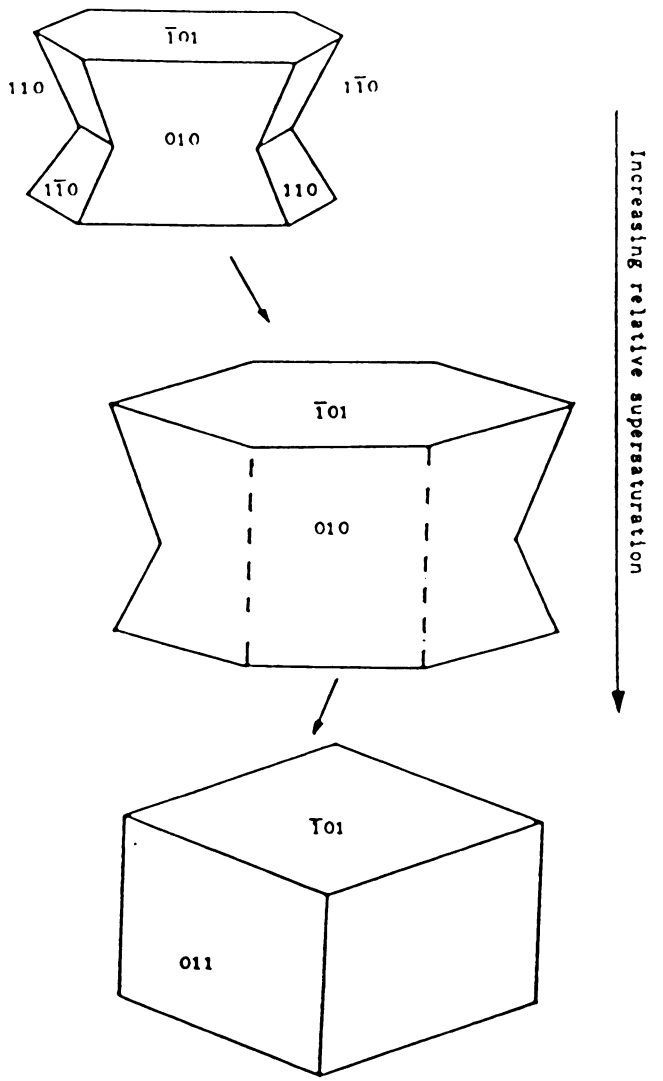

Figure 5-10. Transition in COM Growth Habit

The transition in crystal growth habit can be further illustrated using the ratio of the length of the long parallel edges of the $\underline{1}01$ face (representing the intersection of the 010 face with the $\underline{1}01$ twinned face) to the length of the major axis of the $\underline{1}01$ face (representing the distance between the intersections of the 110, $1\underline{1}0$, and $\underline{1}01$ faces at either end of the $\underline{1}01$ face). The length ratio for the $\underline{1}01$ face, a/b, is plotted versus relative supersaturation in Figure 5-11 for COM crystals grown at 25 °C. This ratio was higher for crystals grown at lower relative supersaturations, with a gradual decrease in this ratio reflecting a decrease in the prominence of the 010 face, which was completely absent at very high relative supersaturations. In addition, the 110 and $1\underline{1}0$ faces seemed to lose their integrity at higher relative supersaturations, finally being overcome by the formation of 011 faces. The sudden decrease in the $\underline{1}01$ length ratio in the relative supersaturation range of approximately $5 \leq \sigma \leq 8$ in Figure 5-11 is indicative of the decreased prominence of the 010 face. The formation of the rhomboid prism habits was observed at the upper extreme of this relative supersaturation range. At relative supersaturations higher than this, COD formation became more significant than COM formation. This result has been previously reported (DeLong and Briedis, 1986).

5.1.2 Calcium Oxalate Dihydrate Crystal Growth Habit

At relative supersaturations near and above the upper extreme of the range noted for COM formation, octahedral crystals were seen as shown in Figure 5-12. Figure 5-12 shows crystals grown at $\sigma = 7.07$ and T = 25 °C. These were identified as calcium oxalate dihydrate (COD) based on previous reports of COD crystal habits (Werness et al., 1979).

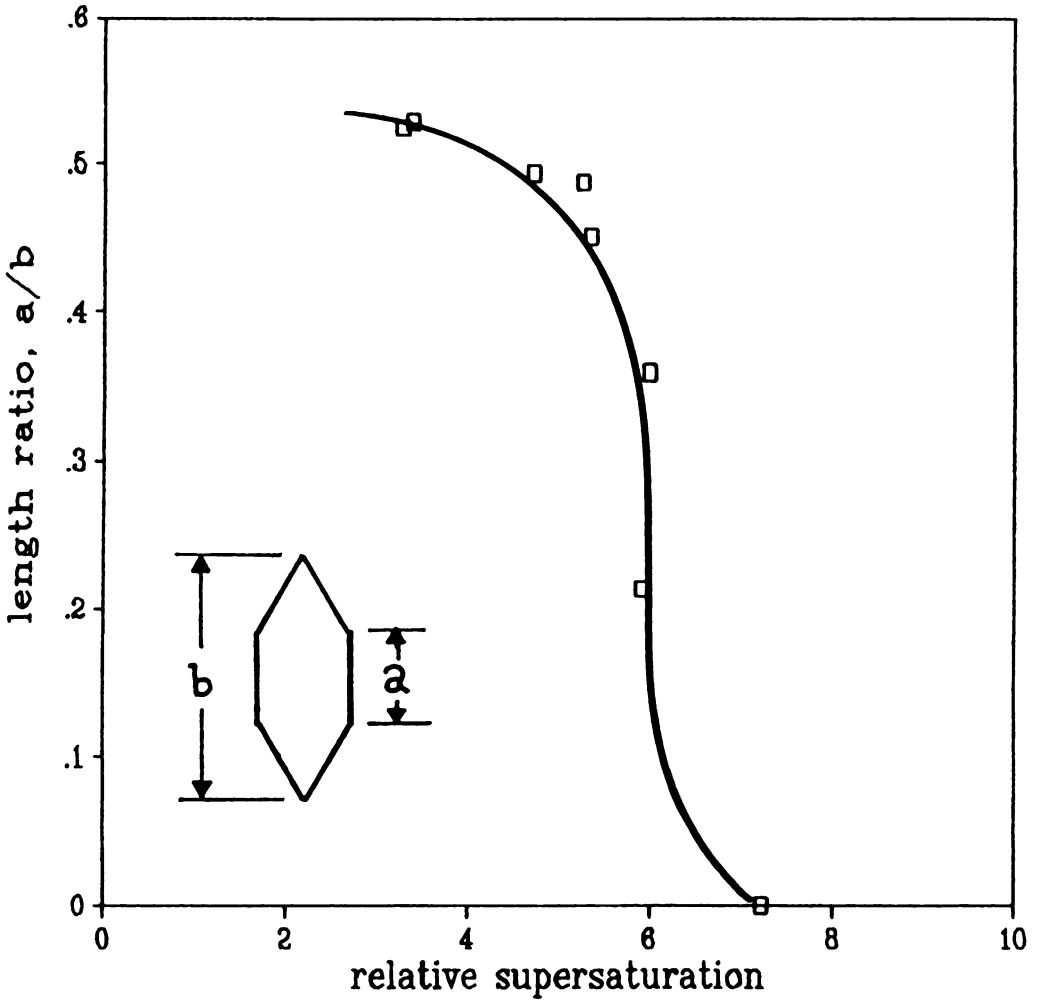

Figure 5-11. Transition in COM Aspect Ratio

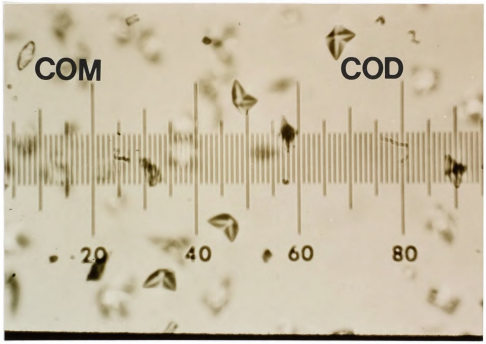

Figure 5-12. COD and COM Crystals grown at σ = 7.07, T = 25 °C.

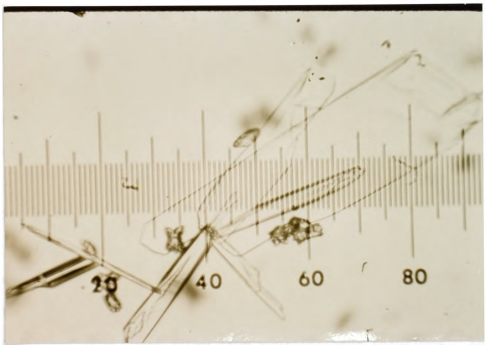

Figure 5-13. COT Crystal Grown at σ = 7.07 and T = 25 °C.

The Raman spectrum of a COD crystal such as those in Figure 5-12 is shown in Figure B-2 of Appendix B. At relative supersaturations of $\sigma \approx 8$ and above, both COM and COD crystals were formed from the same solution as shown in Figure 5-12. The fraction of COD crystals formed increased at higher relative supersaturations especially for the lower temperatures of 15 °C and 25 °C. Few COD crystals were seen at 37 °C and 50 °C even at very high relative supersaturations. Solution conditions for the growth of COM and COD crystals are given in Table 5.1.

As seen from Table 5.1, COD formation occurred at high relative supersaturations, with the relative supersaturation necessary for COD formation increasing with temperature.

5.1.3 Calcium Oxalate Trihydrate Crystal Growth Habit

A very few flat, plate-like crystals were seen at low temperatures (15 and 25 °C) and high relative supersaturations. These were tentatively identified as calcium oxalate trihydrate based on reports of the COT crystal habit (Brecevic et al., 1986; Djarova and Kovandjiev, 1984; Gardner, 1975). One such COT crystal is shown in Figure 5-13 which was grown at $\sigma = 7.07$ and T = 25 °C. The Raman spectrum of a COT crystal is shown in Figure B-3 of Appendix B.

5.2 Identification and Crystal Habits in Modified Solutions

Calcium oxalate monohydrate crystals were grown from solutions containing one of the known growth modifiers heparin or polyglutamic acid. These modified crystals often grew with habits distinctly different from those grown from modifier-free solutions. The effect of these polyelectrolytes on the growth morphology of COM was investigated

Table 5.1. Solution Conditions for Formation of COM and COD

Temp, °C	σ	COM	COD
15	3.28	+	-
15	4.08	+	+
15	5.61	+	+
15	6.35	+	+
25	1.98	+	-
25	3.35	+	-
25	4.65	+	-
25	5.27	+	+
25	5.89	+	+
25	7.07	+	+
37	3.71	+	-
37	4.74	+	-
37	6.64	+	+
50	5.31	+	-
50	6.74	+	+

+ denotes presence; - denotes absence

in two ways. First, crystals were nucleated and grown in the presence of the polyelectrolyte, and the resulting crystal habit was observed and compared with the habit seen for COM grown from polyelectrolyte-free solution. In the second method, COM crystals were nucleated from polyelectrolyte-free solution, then grown in dilute polyelectrolyte solution. The results of these two methods were then compared to determine the difference in effect, if any, of methods on the COM growth habit.

5.2.1 Crystal Habits in the Presence of Heparin

The dimensions of COM crystals nucleated and grown in the presence of heparin were significantly different than COM crystals nucleated and grown from heparin-free solution. Figures 5-14 through 5-19 show COM crystals grown at various heparin concentrations. At low concentrations of heparin, the COM crystals grew with the twinned styloid habit and were not visibly different from COM crystals nucleated and grown from heparin-free solution (Figure 5-14 for crystals grown at σ = 3.71, T = 37 °C, and 1 mg/l heparin). At higher concentrations of heparin, both the $\bar{1}01$ face and the twin 010 face retained their general shape, but were modified in their dimensions (Figure 5-15 for crystals grown at σ = 2.64, T = 37 °C, and 10 mg/l heparin). Figures 5-16 and 5-17 show heparin-modified COM crystals at higher magnification. The $\bar{1}01$ face appears less elongated and the 110-1$\bar{1}$0 interfacial angles less acute than for the unmodified case. The 010 twinned faces appeared much more elongated between the 110 faces and shorter between the $\bar{1}01$ and 10$\bar{1}$ faces than in the unmodified case. The greater extension of the 010 faces causes the crystals to become thinner than in the unmodified case.

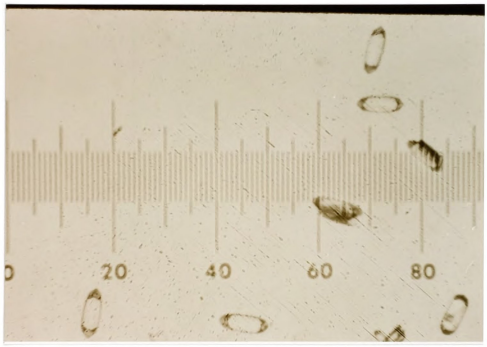

Figure 5-14. COM Crystals Grown at σ = 3.71, T = 37 °C, 1 mg/l Heparin

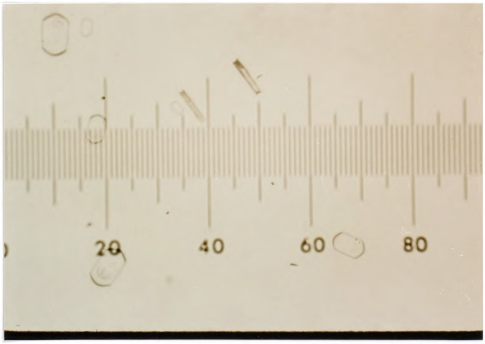

Figure 5-15. COM Crystals Grown at σ = 2.64, T = 37 °C, 10 mg/l Heparin

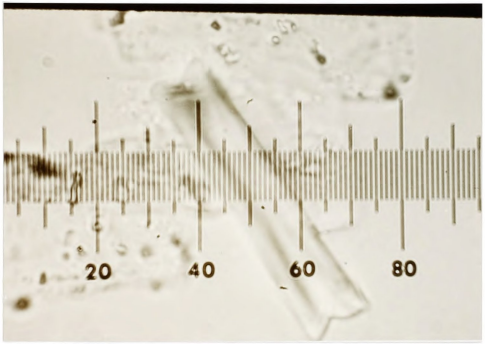

Figure 5-16. Heparin-modified COM Crystal Showing Twinned 010 Face at High Magnification (800x)

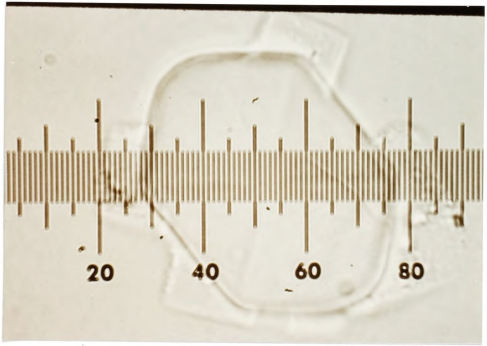

Figure 5-17. Heparin-modified COM Crystal showing 101 Face at High Magnification (800x)

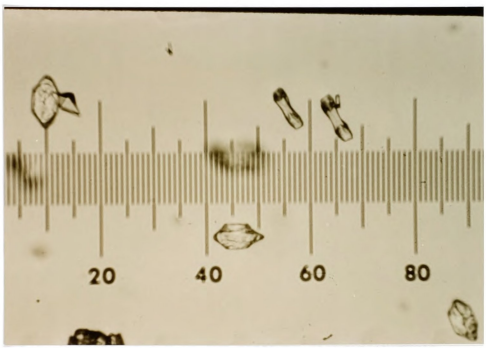

Figure 5-18. Heparin-modified COM Crystal Showing End-Bulging on 010 Twin Face

At a higher relative supersaturation, the $\bar{1}01$ and $10\bar{1}$ faces show slight bulging at the ends with the spaces between the 110 and $1\bar{1}0$ apparently becoming filled in as shown in Figure 5-18.

COM crystals nucleated in heparin-free solution but grown in the presence of 40 mg/l heparin are shown in Figures 5-19 and 5-20. Crystals grown under these conditions gradually develop habit characteristics similar to those of crystals nucleated and grown in the presence of heparin. The originally unmodified $\bar{1}01$ faces of crystals (Figure 5-19) became less elongated upon growth in the presence of heparin (Figure 5-20), and twinned 010 faces become thinner, thus developing proportions similar to those seen in Figures 5-17 and 5-18.

5.2.2 Crystal Habits in the Presence of Polyglutamate

COM crystals nucleated and grown in the presence of polyglutamate are shown in Figures 5-21 through 5-24. The crystals in Figures 5-21 through 5-24 were grown at the same relative supersaturations. At very low concentrations of polyglutamate, COM crystals appear essentially the same as for those grown in polyglutamate-free solution as seen in Figure 5-21. These crystals grew with a twinned styloid habit. At higher polyglutamate concentrations, the crystals grew with less discernible faces, as seen in Figure 5-22, 5-23, and 5-24. As was the case with heparin modified COM crystal habits, two faces of a typical COM crystal appeared less elongated while the other two major faces were elongated. The crystals appear long and thin in view A and rather oval-shaped in view B. As seen in Figure 2-1, both heparin and polyglutamate have deprotonated carboxylic groups free to associate with the crystal lattice. Assuming behavior by polyglutamate similar to that of heparin,

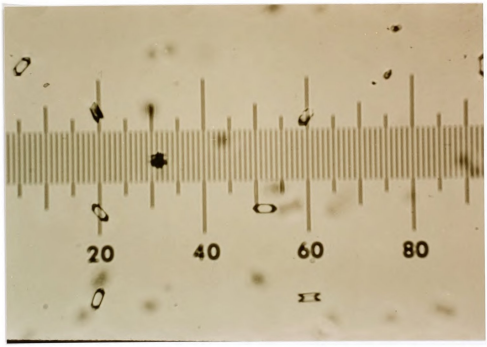

Figure 5-19. COM Crystals Nucleated at σ = 3.71, T = 37 °C at Beginning of Growth Run

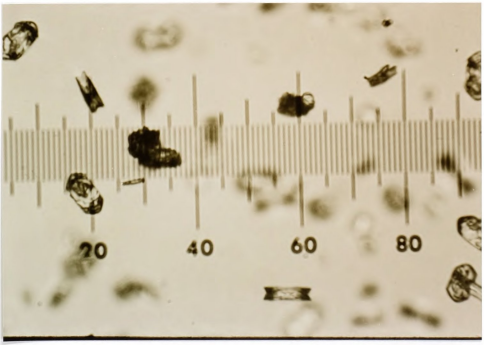

Figure 5-20. COM Crystals of Figure 5-19 After Growth in 40 mg/l Heparin at σ = 3.71 and T = 37 °C

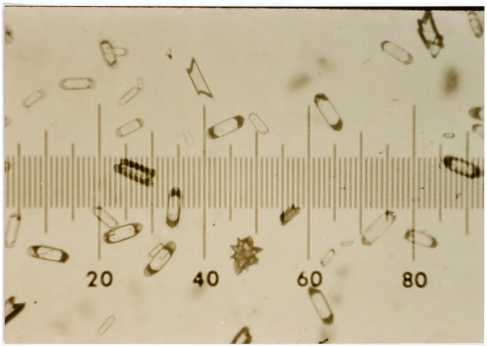

Figure 5-21. COM Crystals Grown at σ = 3.71, T = 37 °C, 1 mg/l Polyglutamate (MW = 32000)

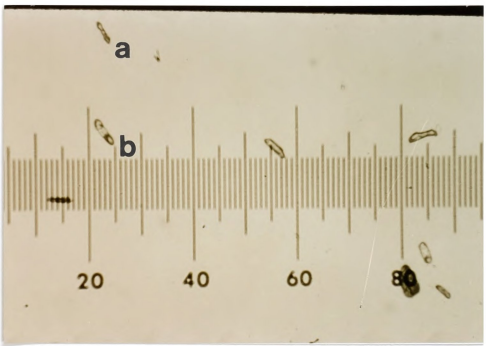

Figure 5-22. COM Crystals Grown at σ = 3.71, T = 37 °C, 5 mg/l Polyglutamate (MW = 32000)

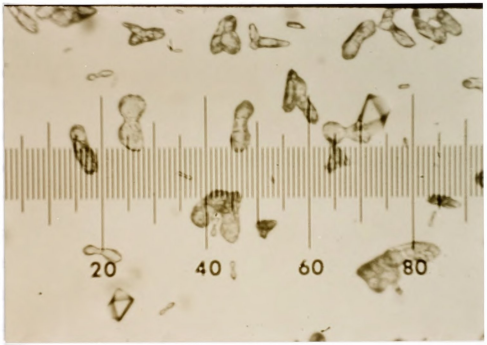

Figure 5-23. COM Crystals Grown at σ = 3.71, T = 37 °C, 10 mg/l Polyglutamate (MW = 32000)

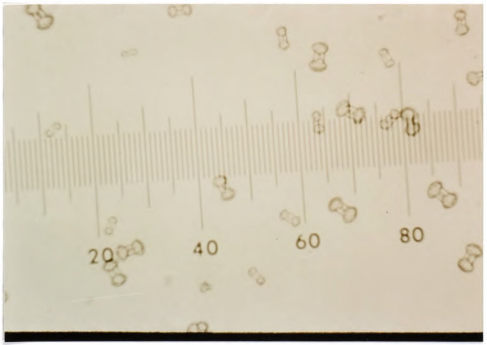

Figure 5-24. COM Crystals Grown at σ = 3.71, T = 37 °C, 46 mg/l Polyglutamate (MW = 46000)

the long, thin face of view B is probably the 010 face, and the oval-shaped face of view A is probably the $\underline{1}01$ face. The 110 and $1\underline{1}0$ faces are not recognizable. Figures 5-22 through 5-24 show that the crystals seem to be "pinched" in the middle. Comparison with the twinned styloid habits of Figure 5-5 suggests that these narrowed sections may be the result of the formation of additional 110 and $1\underline{1}0$ faces. Heparin-modified crystals with bulging ends shown in Figure 5-18 show a similar "pinched" shape, but there is no suggestion of additional faces. The pinched crystals are reminiscent of the "dumbbell" COM crystals frequently reported in the urology literature (Elliot and Rabinowitz, 1980). It is probable that the COM dumbbells in urine are the result of crystal interaction with urinary polyelectrolytes.

COM crystals nucleated in polyglutamate-free solution but grown in the presence of polyglutamate are shown in Figure 5-25 and 5-26. The crystals form as twinned styloids at σ = 3.71 and T = 37 °C as seen in Figure 5-25. After growing for 80 minutes in .174 μM polyglutamate solution, the habit appears slightly elongated and irregular as seen in Figure 5-26.

5.3 Summary

The observed crystal growth habits of COM are similar to the styloid habits reported in the literature. Raman spectra confirmed the crystals as COM. Styloid COM crystals form with 110, $\underline{1}01$, and 010 faces dominant, and twinned crystals showing these faces form at increased relative supersaturations. A gradual transition in the growth habit is observed as relative supersaturation is increased, with 010 faces gradually replaced by 011 faces. Crystals of COD and COT grow at

relative supersaturations higher than those required for COM growth.

COM crystals grown in the presence of the polyelectrolyte growth modifiers polyglutamate and heparin show distorted growth habits. COM crystals grown in heparin solution show significantly stunted growth on the $\underline{1}01$ faces, while crystals nucleated and grown in polyglutamate solution grow with dumbbell-shaped habits.

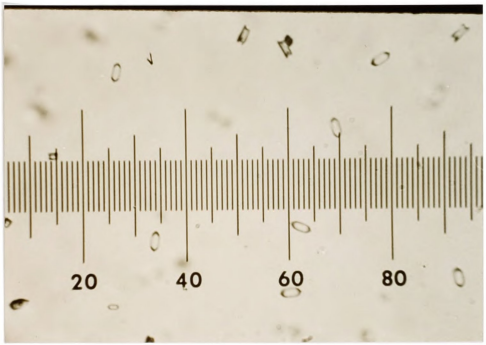

Figure 5-25. COM Crystals Nucleated at σ = 3.71, T = 37 °C at Beginning of Growth Run

Figure 5-26. COM Crystals of Figure 5-25 After Growth in 8 mg/l Polyglutamate at σ = 3.71 and T = 37 °C.

Chapter 6. COM Single Crystal Growth as a Function of Relative Supersaturation and Temperature

Single crystal growth rates of COM were measured over a range of relative supersaturations and temperatures. This information was used to determine empirical rate constants, order of growth for each crystal face, and the activation energy of growth for each face. The results of this analysis are reported in this chapter.

6.1 Calculation of Relative Supersaturation

Four series of experiments were designed to determine to dependence of COM growth on relative supersaturation. The results of computer calculations for these series are presented in Chapter 4 and in Tables A-1, A-2, A-3, and A-4 of Appendix A. In all experiments, the ionic strength was maintained at I = 0.15 M with the addition of KCl, and the pH was set equal to 6.00. Equimolar conditions for the total concentrations of growth ions were used, i. e. $T_{Ca} = T_{Ox}$. Growth was investigated at four different temperatures: 15, 25, 37, and 50 °C. For these temperatures, the ranges of relative supersaturations used were as follows: 15 °C, $3.28 \leq \sigma \leq 6.35$; 25 °C, $1.98 \leq \sigma \leq 7.07$; 37 °C, $1.26 \leq \sigma \leq 6.64$; and 50 °C, $2.02 \leq \sigma \leq 6.74$. The relative supersaturation ranges were limited by heavy nucleation at high σ and slow growth at low σ.

6.2 Measurement of Growth Rates

The methods used to grow COM crystals have been discussed in Chapter 4. The growth of crystals nucleated on the glass cover slip in

the growth cell was monitored photomicroscopically. A series of photomicrographs were taken at regular time intervals during a growth experiment, and these photographs were analyzed to determine the growth rate.

Photomicrographs taken during a typical crystal growth run at 37 °C and σ = 3.71 are shown in Figure 6-1. The magnification in these photographs is 200x with a scale of five microns per division giving a total photograph width of 500 microns. The crystals in Figure 6-1 grew with the typical COM twinned styloid habit as discussed in Chapter 5. The photograph shown in Figure 6-1a was taken at the beginning of the growth run. Sequential photographs were taken at a time interval of 5 minutes. The final picture, taken 35 minutes after the first, is shown in Figure 6-1b. As can be seen from comparison of the photographs, the crystals increased appreciably in size for these experimental conditions.

The growth of crystals such as those of Figure 6-1 was analyzed in one of two ways. In most cases, the distance between parallel crystal faces was used as the dimension for growth measurement. The dimensions used in growth rate measurement are shown in Figure 6-2. The perpendicular distance between the 010 or $\underline{1}01$ faces was used for the measurement of the growth rates for these faces. The distance between the ends of the major axis was used in the measurement of the growth rate of the 110 faces. Since the angle between the 110 and $1\underline{1}0$ faces was approximately constant, growth in the directon of the major axis was geometrically similar to the growth of the 110 faces. Reference to the 110 face growth rate in this dissertation actually indicates growth along this major axis. In each case, the growth was measured with

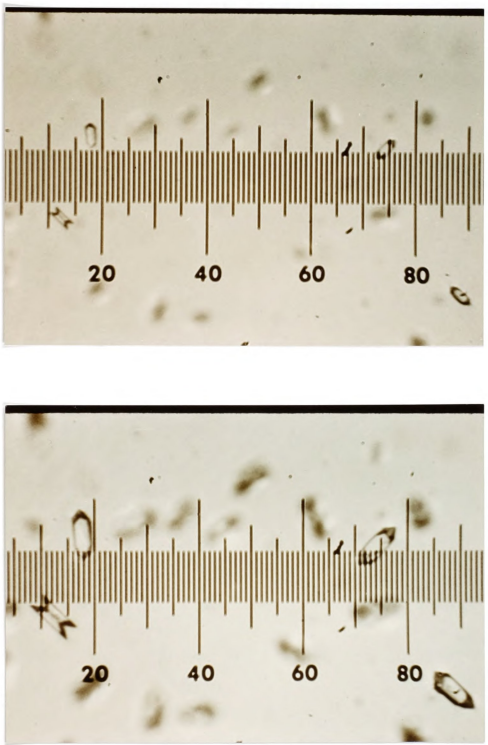

Figure 6-1. COM Crystals Grown at σ = 3.71, T = 37 °C
a) t = 0 min; b) t = 35 min

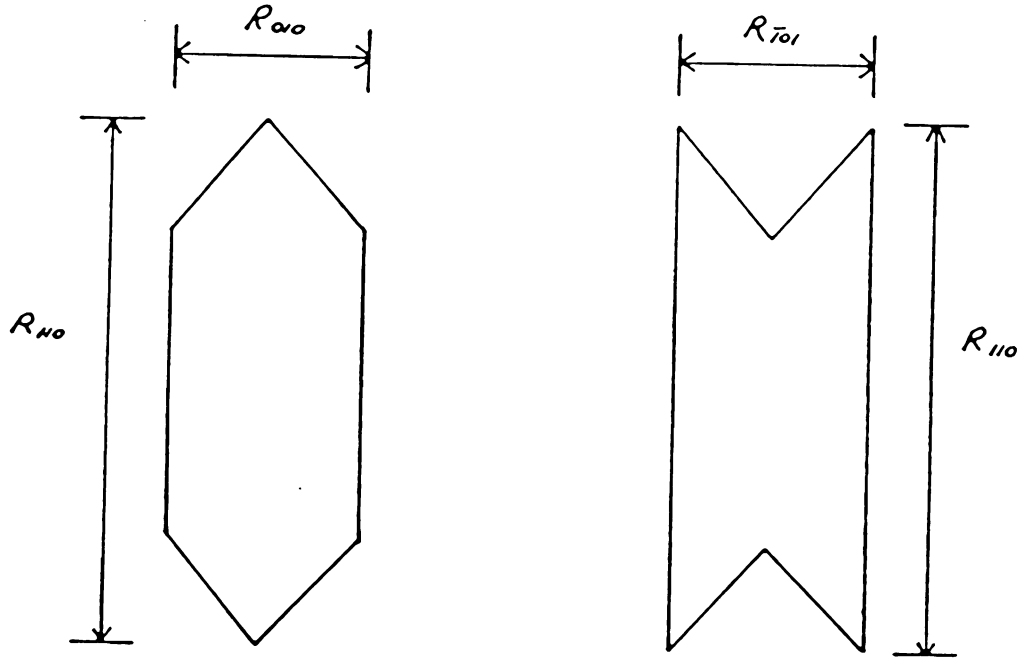

Figure 6-2. Crystal Dimensions Used for Growth Measurements

respect to the midpoint between similar faces; the length measurements were therefore divided by two to get the final length versus time data. For growth of irregularly shaped crystals, the growth rate was measure using the equivalent circular diameter D_{eq}, given by equation (4-1).

Typical growth data taken at 37 °C and various relative supersaturations are shown in Figure 6-3 for the 110 face. The appropriate crystal length was plotted versus the time of growth, and the slope of the plot was calculated using a least-squares linear regression analysis. The slopes of plots such as these were equal to the crystal face growth rates. As seen in Figure 6-3, the plots were fairly linear, with correlation coefficients greater than 0.95 being common.

6.3 Minimization of Mass Transfer Limitations

As may be expected, it was observed that the crystal growth rate seen for given solution conditions was greater if measured at a higher flow rate of growth solution through the growth cell. Such behavior of increasing growth rate versus solution flow rate or velocity was possibly a result of a mass transfer limitation on the growth rate due to the bulk transport of growth ions through the solution (Janssen-van Rosmalen et al., 1975). A second possibility was that growth at higher relative supersaturations was rapid enough to cause significant depletion of growth ions from solution because the flow rate was insufficient to replace ions lost from solution to growth. This would have resulted in a relative supersaturation lower than that desired and consequently a lower growth rate. Regardless of the mechanism of mass transfer limitation, increasing the solution flow to a sufficiently high

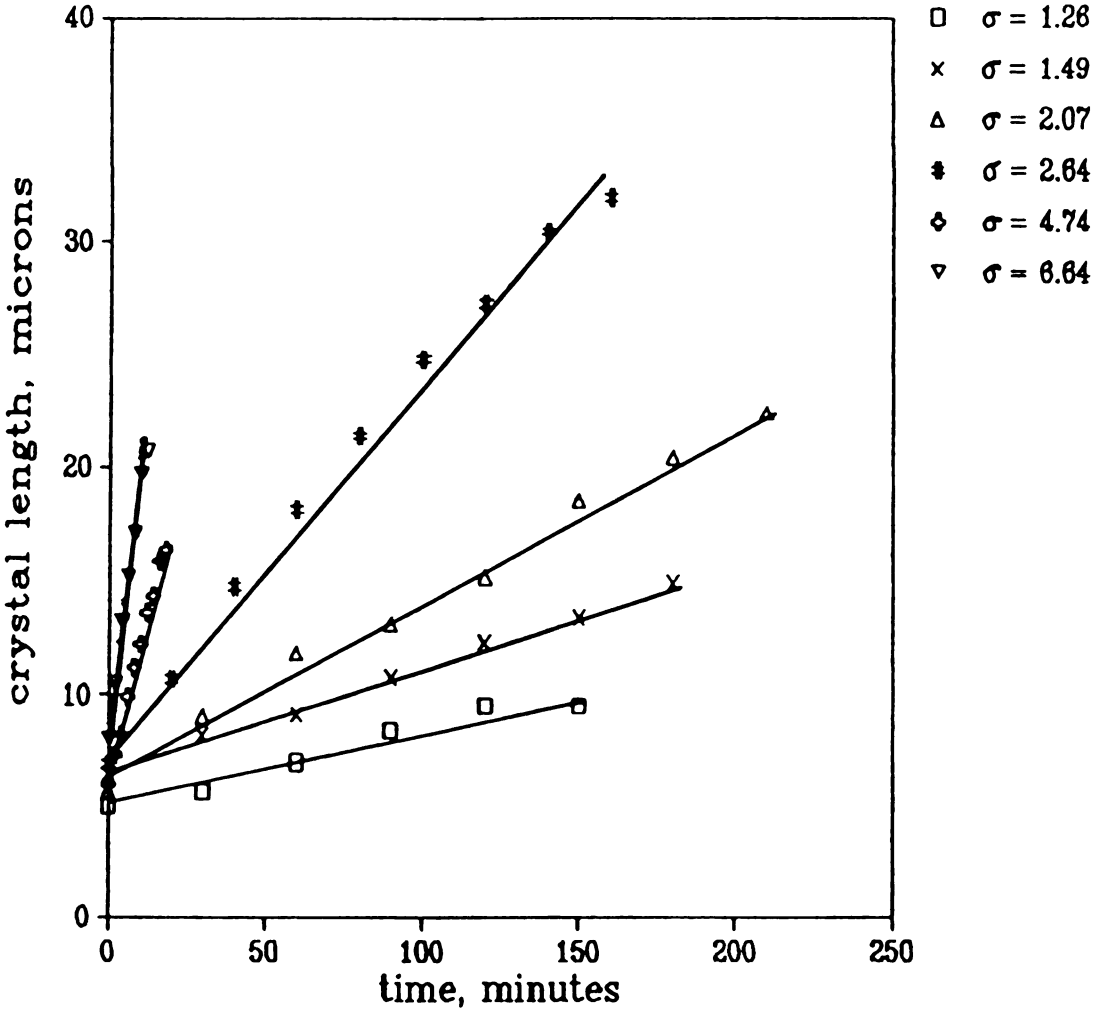

Figure 6-3. COM Crystal Length Versus Growth Time

rate minimized the dependence of crystal growth rate on flow. Growth rate data for a nominal relative supersaturation of σ = 6.64 at 37 °C were plotted versus solution flowrate as shown in Figure 6-4. The measured growth rate was higher at higher flow rates, reaching an asymptotic value of approximately 1.1 microns/minute at high flow rates. The flow rates required for the measurement of crystal growth rates with a minimum of mass transfer limitations were deduced qualitatively from plots similar to Figure 6-4. In general, it was observed that a combined solution flow rate of 20 ml/min was sufficient to minimize the bulk solution mass transfer resistance; at higher temperatures (especially 50 °C) and high relative supersaturations a flow rate of 30 ml/min was used. Use of higher flow rates caused another practical problem: the high shear sometimes caused crystals to move out of the field of view of the camera during a growth experiment thus reducing the number of length measurements available for growth rate determination.

An effectiveness factor for crystal growth, η, defined as the ratio of the actual growth rate to the rate theoretically achievable under conditions of no mass transfer limitation (Garside, 1984a) was calculated to determine a typical value of η for COM growth under flow conditions that minimize bulk solution mass transfer limitations. This calculation is shown in Appendix C. The calculated value of η = .959 shows that some resistance to mass transfer still exists even at the supposedly high flow rate. Garside has noted the difficulty in measuring growth rates free of bulk solution mass transfer limitations. Nonetheless, the relatively high value of η shows that the mass transfer limitation has contributed little to the measured growth rates.

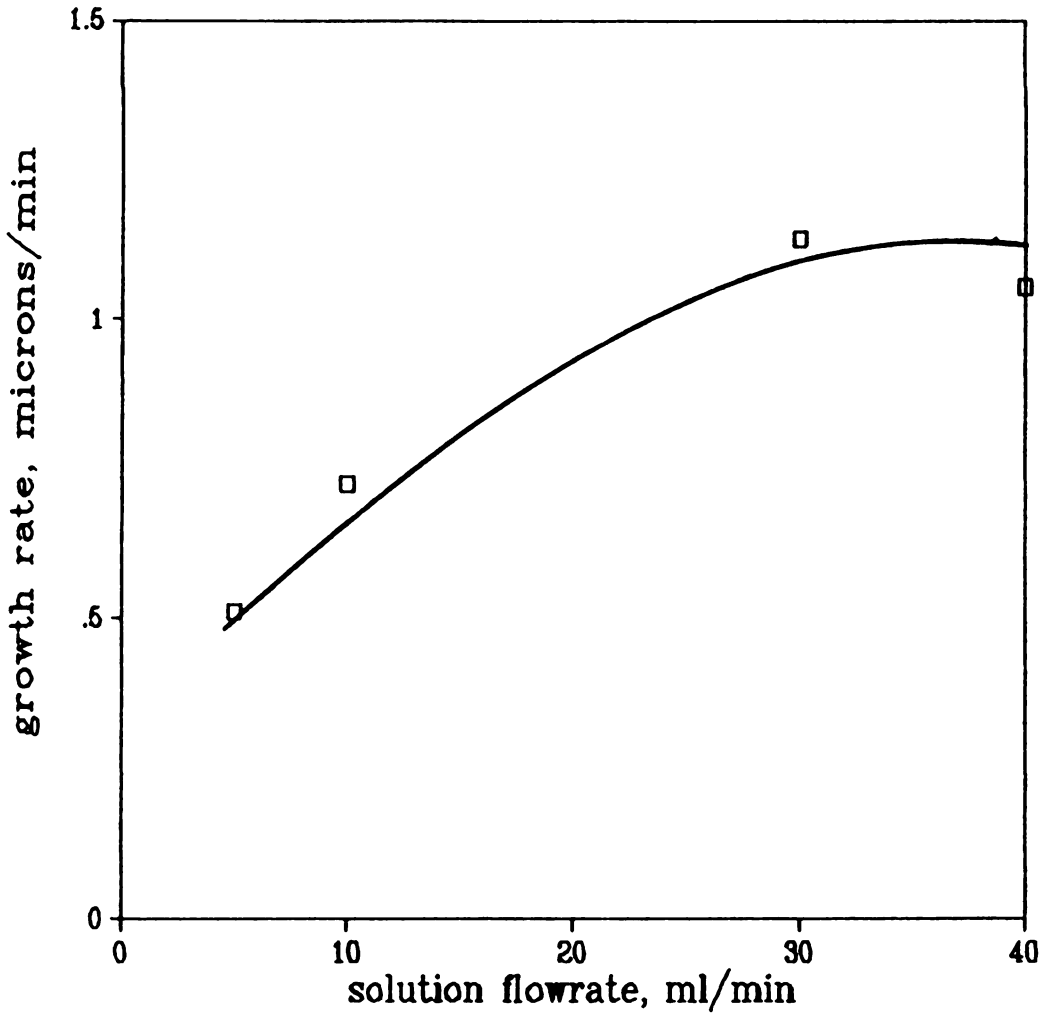

Figure 6-4. Minimization of Bulk Solution Mass Transfer Limitation

6.4 Growth Rate as a Function of Relative Supersaturation for Four Temperatures

COM facial growth rates with a minimum of mass transfer limitations were measured over a range of relative supersaturations for four temperatures. The range of relative supersaturation was limited by the growth rates at the extremes of the range; at low σ, the rates were low and took a long time to measure, while at high σ, dense crystal nucleation caused excess depletion of the supersaturation. In all experiments, the ionic strength was maintained at I = 0.15 M through the addition of KCl, the pH was 6.00, and the total concentrations of the growth ions were equimolar. The results of some of these experiments have been previously reported (DeLong and Briedis, 1985b)

6.4.1 Growth Isotherms

Growth rates in microns per minute for the each of the COM faces were plotted versus the relative supersaturation for the temperatures 15, 25, 37, and 50 °C. Data for the faces 110, 010, and $\underline{1}01$ were plotted as shown in Figures 6-5, 6-7, and 6-8, respectively. Each point represents an average rate for several crystals ($3 \leq N \leq 5$). Figure 6-6 shows typical error for the experiments, with error bars representing the spread in the actual data. In each case, the rate increased monotonically with relative supersaturation over the range studied.

6.4.2 Rate Constants and Growth Order for Each Crystal Face

The growth rate data was fitted to an empirical power law relationship of the form

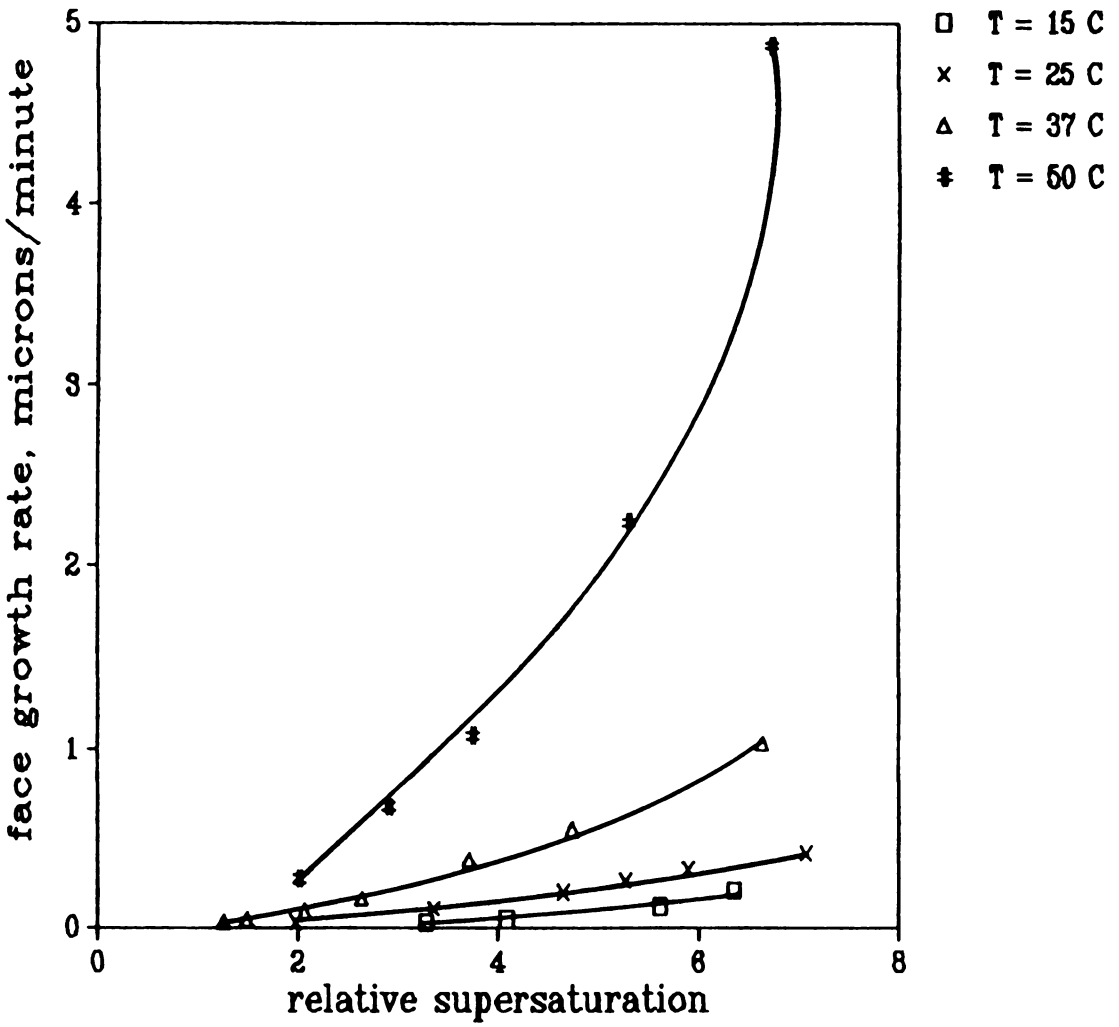

Figure 6-5. COM 110 Face Growth Rate Versus Relative Supersaturation

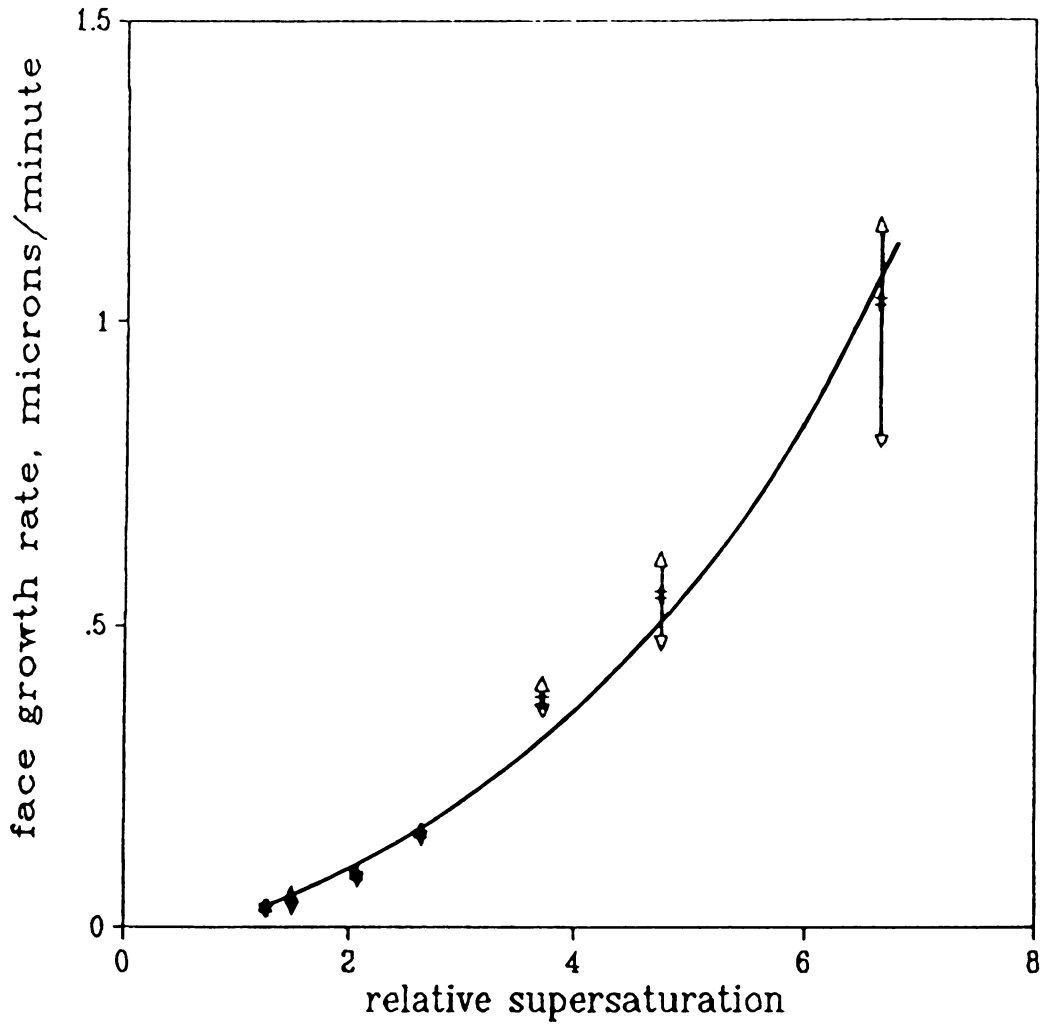

Figure 6-6. COM 110 Growth Data with Typical Error Bars (T = 37 °C)

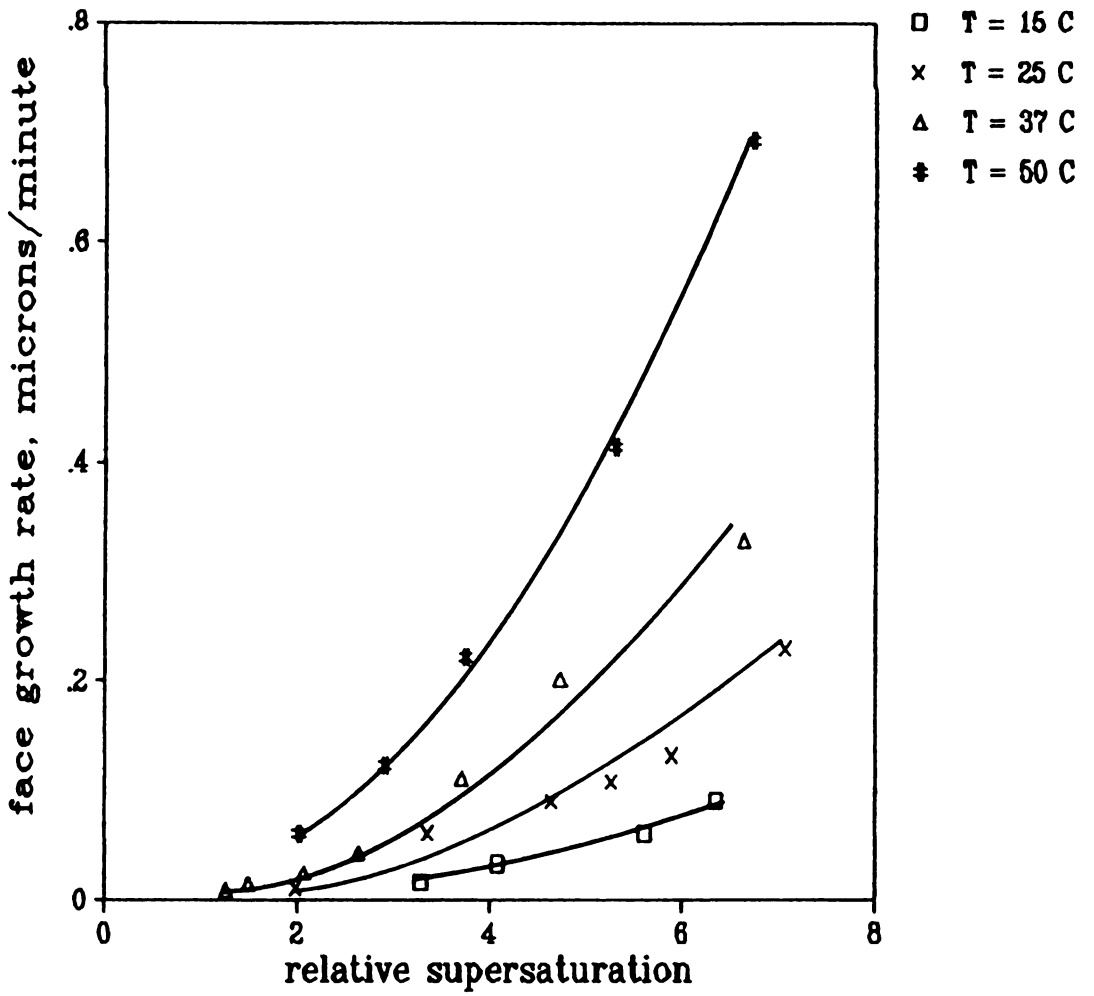

Figure 6-7. COM 010 Face Growth Rate Versus Relative Supersaturation

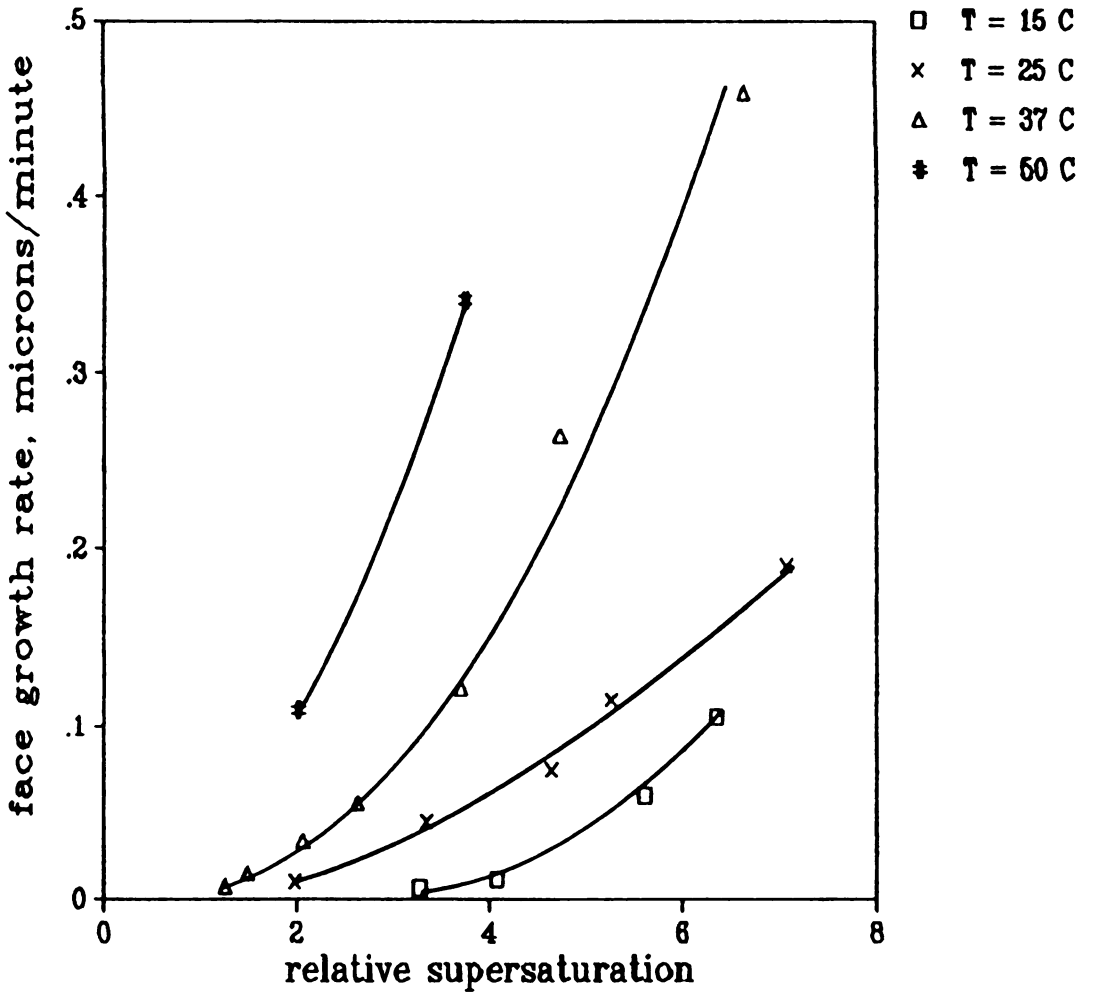

Figure 6-8. COM 101 Face Growth Rate Versus Relative Supersaturation

$$R = k_n \sigma^n \qquad (2\text{-}33)$$

as discussed in Chapter 2. To determine the order of growth and the empirical rate constant, the growth rate data were plotted as log R versus log σ. The slopes of these plots gave the power law exponent, n, and were determined using least squares linear regression analysis. The rate constants were evaluated from the y-intercept of the plots. The calculated growth orders n for each face and temperature are shown with 95 percent confidence intervals in Table 6.1.

Table 6.1. Rate Law Orders n for COM Face Growth

$R = k \sigma^n$

	R-110	R-010	R-$\bar{1}$01
Temp, °C	n	n	n
15	3.03 ± .95	2.39 ± .79	4.38 ± 1.60
25	2.10 ± .22	2.17 ± .55	2.29 ± .45
37	2.15 ± .15	2.20 ± .22	2.47 ± .25
50	2.30 ± .36	2.01 ± .12	1.85 (a)

Error intervals are for 95% confidence.

(a) N=2

In each case, the growth order was very nearly equal to 2, except for data taken at 15 °C where the low rate of growth probably introduced significant experimental error. The second-order rate law indicated a crystal growth mechanism controlled by the surface integration or surface diffusion step as suggested by Nielsen (1984b). Similar second order results for COM growth have been reported by Nancollas and Gardner (1974), Meyer and Smith (1975a), Sheehan and Nancollas (1980), and

Lanzalaco et al. (1982).

As seen by comparing Figures 6-5, 6-7, and 6-8, for a given temperature, growth was most rapid on the 110 faces, with approximately equal rates on the 010 and $\bar{1}01$ faces. This fact could have been deduced from the appearance of the crystals in Chapter 5. The longest dimension of a crystal was typically the distance between the intersections of the 110 faces at either end of the crystal, as seen in Figure 5-6. The larger 110 growth rate tended to elongate the crystals.

6.4.3 Activation Energies

The activation energy, E_a, for the growth of each face was determined from the Arrhenius equation as given in Chapter 2:

$$k_n = A_o \exp(-E_a / R_g T) \qquad (2\text{-}34)$$

In order to calculate an activation energy on a common basis, growth rate constants were determined based on a second-order rate law with n = 2 in equation (2-33). The second-order rate constant k_2 was found by calculating the slope of a plot of R versus σ^2 for facial growth rate. The slopes of these plots were determined by least-squares linear regression. The results of this analysis are shown in Table 6.2.

Based on equation (2-34), plots were made of $\ln(k_2)$ versus (1/T), and the slopes were determined using a least squares linear regression analysis. Plots of this type are shown in Figure 6-8 for each COM face. The calculated activation energies for the 110, 010, and $\bar{1}01$ faces were 65.0 kJ/gmol, 40.8 kJ/gmol, and 45.5 kJ/gmol, respectively.

The average value of E_a = 50.4 kJ/mol may be compared with the 49.0 kJ/gmol reported by Nancollas and Gardner (1974) and 28 kJ/gmol reported by Garside et al. (1982). Fairly good agreement is seen with the former

Table 6.2. Second-order Rate Constants for COM Face Growth

$R = k_2 \sigma^2$

Temp, °C	R-110 1000 k_2	R-010 1000 k_2	R-$\bar{1}$01 1000 k_2
15	5.89 ± 3.90	2.35 ± .85	3.36 ± 1.95
25	8.53 ± 1.23	4.36 ± 1.07	3.90 ± .63
37	23.8 ± 1.8	7.77 ± 1.02	10.9 ± 1.1
50	109 ± 33	15.2 ± .9	23.3 (a)

Units of k_2 are microns/minute

Error intervals are for 95% confidence.

(a) N=2

study, but the latter possibly suffers from interfering effects of agglomeration and coprecipitation with COT. This order of magnitude for E_a indicates a surface-controlled crystal growth mechanism, as suggested by the Nancollas and Gardner study. This agrees with the finding of second-order kinetics discussed above. Crystal growth kinetics controlled by the rate of diffusion with first-order kinetics show a much lower activation energy, about 19.3 kJ/gmol (White and Nancollas, 1982).

6.5 Mechanism of Crystal Growth for Calcium Oxalate Monohydrate

As mentioned in Chapter 2, a second-order rate law for crystal growth usually indicates a crystal growth mechanism controlled by surface diffusion, lattice integration, or, in the case of electrolyte crystal growth, adsorption influenced by double layer effects. This

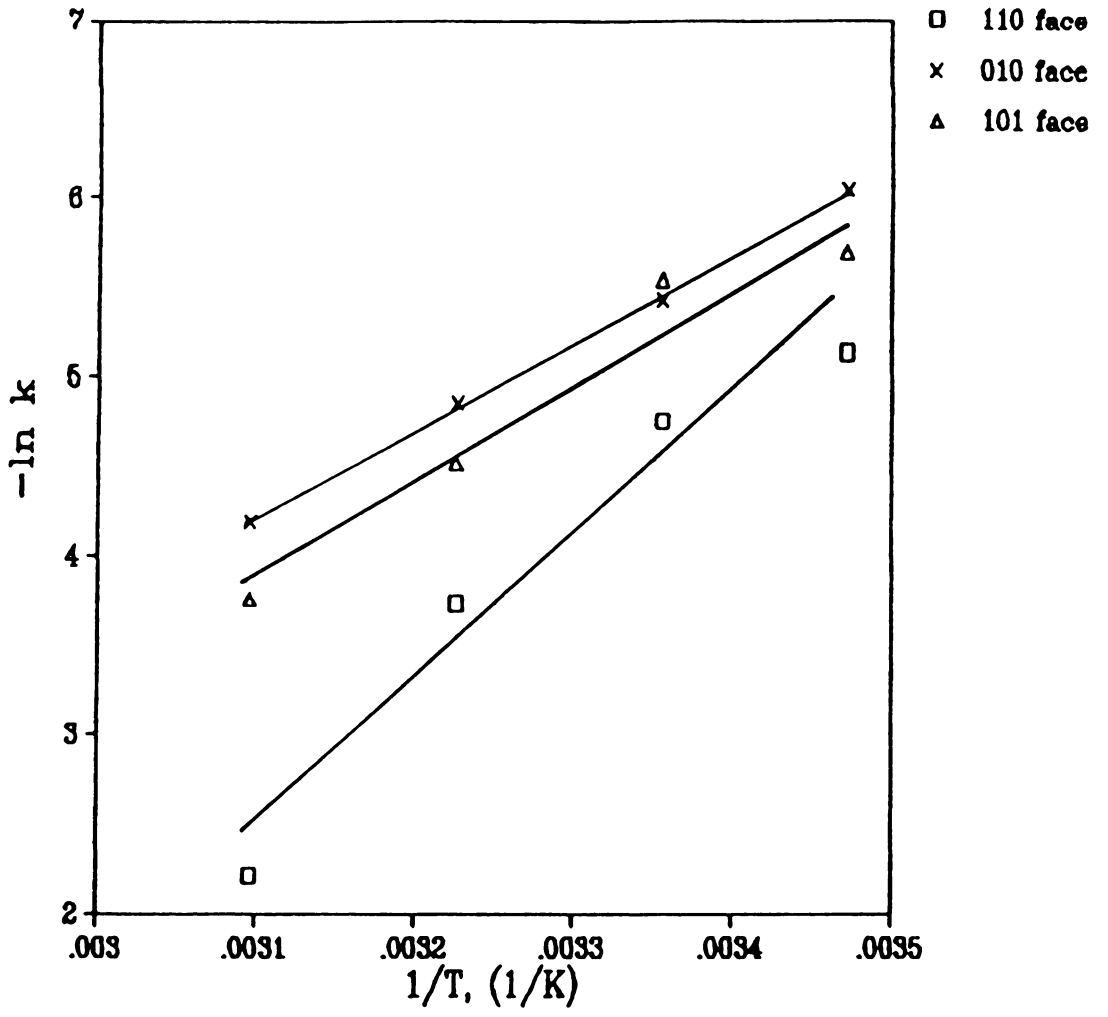

Figure 6-9. Arrhenius Plots for COM Growth Activation Energies

fact, along with the magnitude of the activation energy as discussed in the previous section, presents strong evidence for a surface-controlled growth mechanism for COM. Further evidence is available to conjecture the rate-controlling step in the growth mechanism.

The activation energy for surface diffusion of crystal growth units is in the range of 17 - 38 kJ/mol (Bennema, 1969). This value is lower than the observed COM growth activation energy of 50.4 kJ/mol, so surface diffusion does not appear to be the rate-controlling step.

A better case can be made for lattice integration as the rate-controlling step. Nielsen (1982) has suggested that the rate-controlling step in the crystal growth mechanism of many sparingly soluble salts is the dehydration of the cation upon incorporation into the crystal lattice. If this is the case, it is to be expected that the activation energy should be related to enthalpy of dehydration for the cation. Nielsen has given this enthalpy as approximately 25 kJ/mol, or about one-half of the COM growth activation energy. The activation energy thus accounts for two moles of water lost per mole of calcium ion incorporated into the COM crystal lattice.

The value of the COM growth activation energy therefore supports the idea of crystal growth rate controlled by the dehydration of calcium upon entering the crystal lattice. Since calcium oxalate forms three hydrates, it might be expected that the growth activation energies of each would reflect a proportionate loss of water. Gardner (1975) has shown that the growth of COT is nearly independent of temperature, which suggests a very low growth activation energy. Assuming an approximately zero activation energy for COT, the difference in activation energies between COM and COT is about 50 kJ/mol, which could account for the two

additional moles of water lost for each mole of calcium incorporated into the monohydrate lattice. No activation energy data were found in the literature for COD.

As will be discussed in the following chapter, COM growth rate shows a strong dependence on the ionic strength in solution and in turn on the electrical double layer at the crystal/solution interface. Since, as discussed in Chapter 2, the second-order dependence of growth rate on relative supersaturation can be derived from electrical double layer considerations (Chiang and Donohue, 1987) it must be stressed that the growth rate for electrolyte crystals is strongly influenced by double layer effects. Any discussion of the mechanism must include the effects of the ionic strength and double layer.

Chapter 7. COM Single Crystal Growth Rates as a Function of Ionic Strength and Calcium to Oxalate Ratio

In Chapter 6, the dependence of COM growth rate on the relative supersaturation was discussed. In all of the experiments referred to in that chapter, the ionic strength was maintained at 0.15 M, and the ratio of total calcium to total oxalate was one. The background electrolyte in all cases was KCl. Next, in order to gain some understanding of the ionic interactions occurring during COM crystal growth, it was also important to measure the growth rate at various ionic strengths and various calcium to oxalate ratios. The results of COM crystal growth experiments at various ionic strengths and calcium to oxalate ratios are reported in this chapter. The experimental results discussed in this chapter have been reported previously (DeLong and Briedis, 1987).

7.1 Calculation of Relative Supersaturation

The results of computer calculations to determine the COM relative supersaturation at various calcium to oxalate ratios and ionic strengths with either KCl or LiCl as the background electrolyte were discussed in Chapter 4 and Tables A-5 through A-9 of Appendix A. In all of these calculations, the temperature was held at T = 37 °C, pH = 6.00, and the relative supersaturation was maintained at $\sigma \approx 3.71$. This was the relative supersaturation calculated for the selected base case of T = 37 °C, ionic strength I = 0.15 M with KCl as the background electrolyte, pH = 6.00, and $T_{Ca} = T_{Ox} = 1 \times 10^{-3}$ M.

7.2 COM Growth Rates as a Function of Ionic Strength

COM face growth rates were measured at various ionic strengths. Three series of experiments were performed with a different background electrolyte used for each, KCl, LiCl, and $KClO_4$. In each set of experiments, equimolar free growth ion concentrations, $[Ca^{2}]/[C_2O_4^{2-}]$ = 1, were maintained. In all experiments, the solution conditions were $\sigma \approx 3.71$, pH = 6.00, and T = 37 °C.

The results show an enhancement of crystal growth rate as ionic strength is increased. This effect of ionic strength on the growth rate of the 110 face of COM is plotted in Figure 7-1 as growth rate versus ionic strength for each of three background electrolytes KCl, LiCl, and $KClO_4$. For each electrolyte, the growth rate shows a steady increase with ionic strength towards an asymptote at high ionic strength. Similar effects were seen for the other crystal faces. The data for $KClO_4$ over a range of ionic strengths were limited due to its low solubility. The fact that the curves for the three electrolytes do not superimpose may be partly due to the error involved in calculating the relative supersaturation; this results from uncertainty in the values of the ion-pair stability constants.

Other workers have reported an enhancement of electrolyte crystal growth by ionic strength. Tomazic et al. (1986) measured the growth of calcium hydroxide in the presence of various concentrations of background electrolyte. They found that higher NaCl concentration significantly increased the rate of $Ca(OH)_2$ growth. Brandse et al. (1977) found that higher NaCl concentrations enhanced the growth rate of gypsum ($CaSO_4.2H_2O$). Neither of these studies, however, offered a detailed explanation of the effect. Chiang and Donohue (1987) have

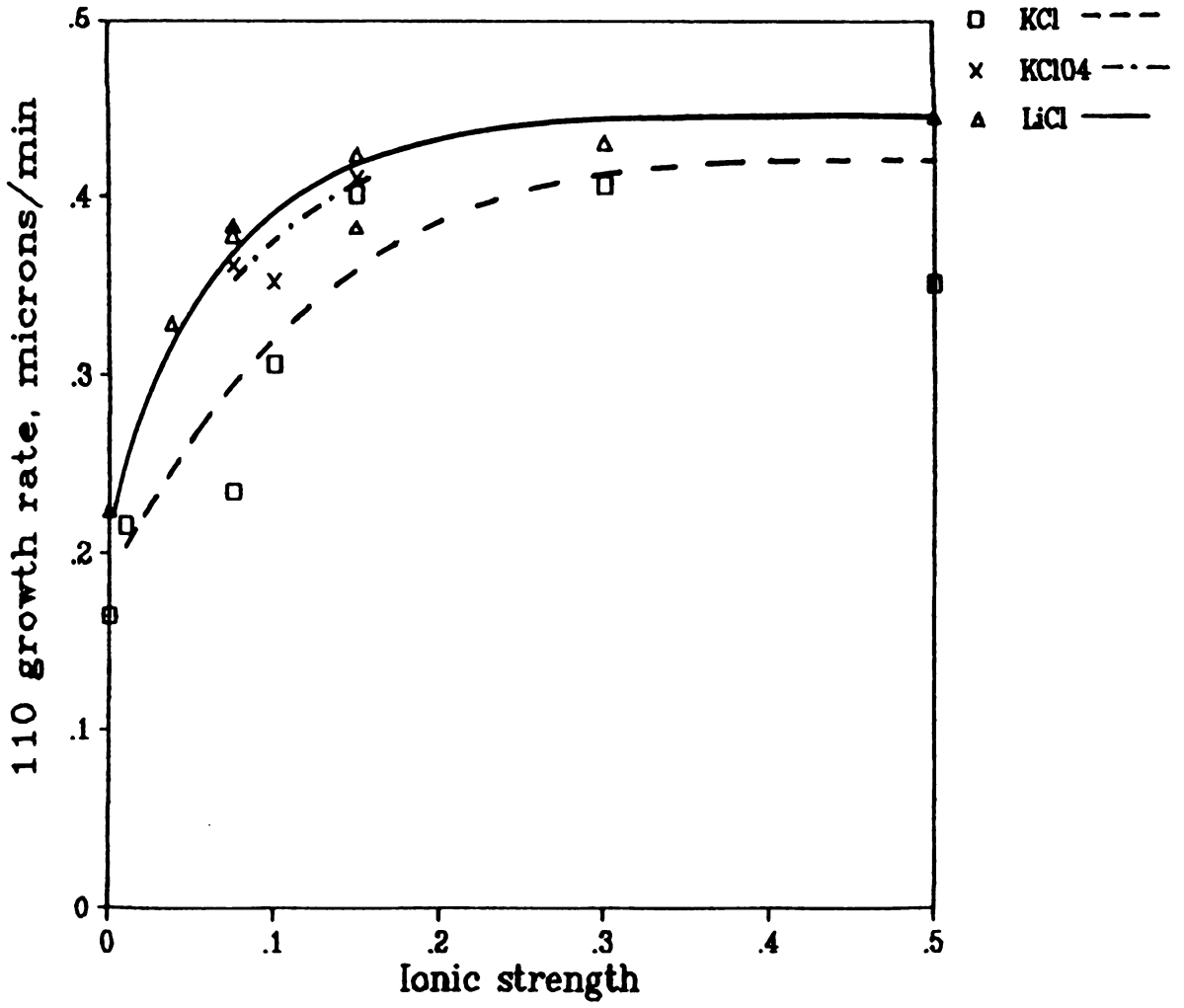

Figure 7-1. COM 110 Face Growth Rate Versus Ionic Strength for Various Electrolytes

discussed a simplified electric double layer theory of crystal growth but have not considered the effects of ionic strength changes. Many studies have investigated the effects of ionic strength on colloid stability (e. g., Adair (1981), Overbeek (1952), Verwey and Overbeek (1948)), but none have considered the non-equilibrium conditions of crystal growth.

It is apparent that present crystal growth theories that have been traditionally used to describe molecular crystal growth are not adequate for modelling electrolyte crystal growth in which the presence of charged species may be an important consideration. At the surface of any phase, there exists a separation of positive and negative charges that creates a region of varying electrical potential and charge distribution. In the specific case of an electrolyte crystal in aqueous solution, a portion of the charged species are typically constituent ions that comprise the "growth unit" for the crystal. Other charged species include non-growth unit ions that can adsorb onto the crystal surface and so-called indifferent ions which do not adsorb and act only to increase the ionic strength. Electrokinetic effects of the charged growth units must be taken into account when modelling electrolyte crystal growth.

Double layers are strongly affected by ionic strength. Honig and Hengst (1969) have described a situation in which an increase in the concentration of indifferent electrolyte (and hence the ionic strength) in an ionic solution causes an increase in the capacity of the electrical double layer at the surface of a crystal in the solution. They further suggest that the increase in capacity increases the amount of constituent ions (in this case, growth ions) which can be adsorbed on

the crystal surface for a given constant electrical potential difference between the crystal and the solution. As discussed in Chapter 2, the adsorption of growth ions is one of the steps in the crystal growth mechanism. It follows that an increase in electrical double layer capacity resulting from an increase in ionic strength may lead to increased crystal growth rates with all other relevant solution properties held constant.

The observed trend of increasing growth rate as a function of ionic strength as seen in Figure 7-1 may be predicted by double layer theory. The qualitative discussion of this effect of ionic strength above can be quantified by considering a simple model of the relationship between the surface charge of a particle and its electrical potential difference in solution given by the Gouy-Chapman treatment of the double layer (Adamson, 1982). More complex models are available, but presently their use is not justified.

In the Gouy-Chapman treatment of the electrical double layer, the region in solution near the solution/solid interface of a particle is visualized to exist as a double layer of charge as shown schematically in Figure 7-2. One charge predominates on the particle surface as the first layer due to crystal lattice structure. In response to the surface charge, oppositely charged solution ions orient themselves next to the surface such that a net charge exists near the surface. This total net charge is balanced by the equal and opposite charge in the bulk solution. The situation described is modelled as a double layer of charge, one layer localized near the surface of the particle, and the other developed in a diffuse region extending into the solution but visualized as being localized at a fictitious distance (the double layer

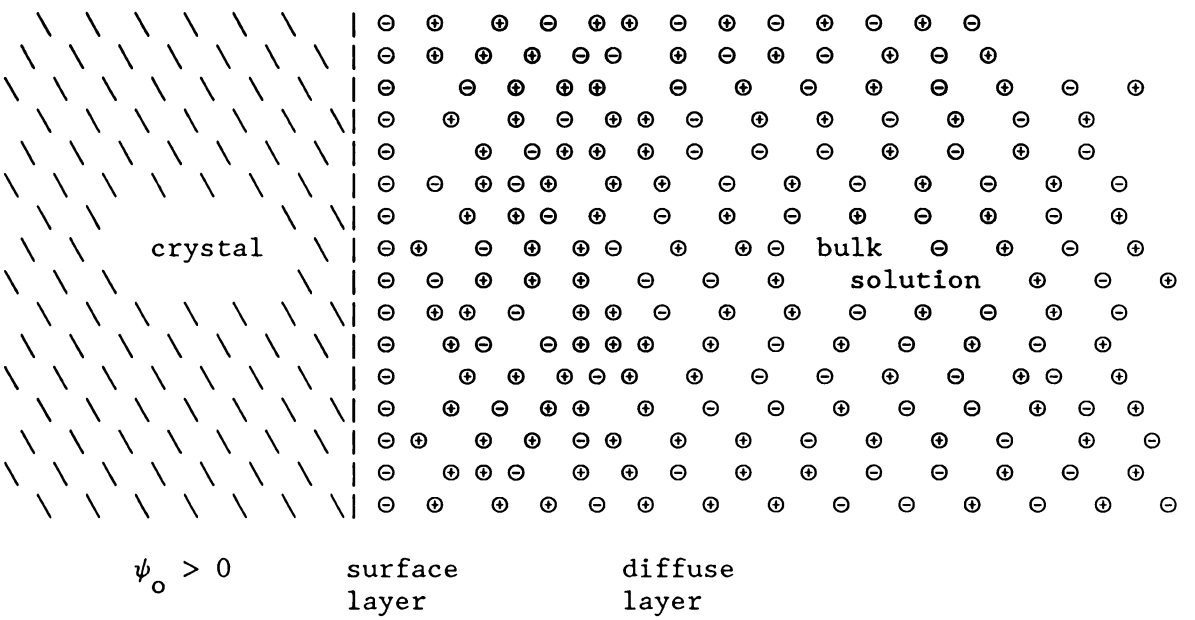

Figure 7-2. Schematic Representation of the Electrical Double Layer

thickness) from the surface. The surface charge density is related to the gradient of the electrical potential at the surface by

$$\sigma_o = -D/4\pi[d\psi/dx]_o \qquad (7\text{-}1a)$$

where σ_o is the surface charge density, D is the solution dielectric constant, ψ is the surface potential, and $[d\psi/dx]_o$ is the potential gradient evaluated at the surface (x=0). For a flat surface with a small surface potential, the potential is given by

$$\psi = \psi_o \exp(-\kappa x) \qquad (7\text{-}1b)$$

Considering the relatively low equilibrium surface potential of approximately 25 mV for COM (Curreri et al., 1979) and the elongated, flat crystal habits, equation (7-1b) is probably valid for COM. Combining equations (7-1a) and (7-1b) gives

$$\sigma_o = D\,\kappa\,\psi_o / 4\,\pi \qquad (7\text{-}1c)$$

with κ defined below.

Equation (7-1c) is similar to the Helmholtz condenser formula. The capacity of the double layer C_d is therefore given by

$$C_d = D\,\kappa / 4\,\pi \qquad (7\text{-}2)$$

The "thickness" of the double layer is given by κ^{-1} where κ is calculated from

$$\kappa^2 = (4\,\pi\,e^2 / D\,k\,T)\,\Sigma\,M_i\,z_i^2 \qquad (7\text{-}3)$$

Here, e is the charge on an electron, k is the Boltzmann constant, 1.3807×10^{-23} J/K, T is the absolute temperature, M_i is the concentration of the i^{th} ion, and z_i is the valence of the i^{th} ion. As can be deduced from equation (7-1c), κ^{-1} is a characteristic length or thickness of the double layer where the potential, ψ, has fallen to 37 percent of its surface value, ψ_o.

κ^2 is therefore related to the ionic strength I in solution since, from Chapter 3,

$$I = 1/2 \Sigma M_i z_i^2 \qquad (3\text{-}17)$$

It follows that the thickness of the double layer is inversely proportional to the square root of the ionic strength, and an increase in ionic strength amounts to a decrease in the quantity κ^{-1}, i. e. compression of the double layer. This compression results in an increased capacity to hold charge in the double layer.

Both the surface potential, ψ_o, and the surface charge density, σ_o, of an ionic crystal in equilibrium with a solution of its constituent ions are determined by the so called potential-determining ions (Ca^{2+} and $C_2O_4^{2-}$). The surface potential for COM is given by the Nernst equation (Hunter, 1981)

$$\psi_o = (k\ T\ /\ z\ e)\ \ln\ (Ca^{2+})/(Ca^{2+})_{pzc} \qquad (7\text{-}4a)$$

or

$$\psi_o = (k\ T\ /\ z\ e)\ \ln\ (C_2O_4^{2-})/(C_2O_4^{2-})_{pzc} \qquad (7\text{-}4b)$$

In these equations, (Ca^{2+}) and $(C_2O_4^{2-})$ represent ion activities in the bulk of the solution, and $(Ca^{2+})_{pzc}$ and $(C_2O_4^{2-})_{pzc}$ are the solution activities calcium and oxalate ion at the point of zero surface charge (pzc), i.e., the point at which equal amounts of calcium and oxalate ions are adsorbed onto the crystal surface giving a net zero surface charge. Their activities at the point of zero charge are related through the solubility product. The point of zero charge for COM has been determined to be $(Ca^{2+})_{pzc} = 7.85 \times 10^{-6}$ M (Curreri, et. al, 1979) which indicates that all experiments described in this chapter were performed with a net positive surface charge on the COM crystal surface. The background electrolytes used in this study have no effect on the

surface charge or potential and can be classified as indifferent, non-adsorbing electrolytes (Curreri, et al., 1979; Hlady, 1984). Curreri et al. have shown that increasing the background electrolyte concentration of KCl has little effect on the surface potential of COM. The inability of an ion to effect significant change in the sign or magnitude of the surface potential characterizes it as being indifferent.

At a constant relative supersaturation and free ion ratio, the activities of calcium and oxalate are constant; the effect of varying ionic strength is accounted for in the activity coefficient. If it may be assumed that the surface potential of a non-equilibrium growing crystal depends on the solution activities of the potential-determining ions in a manner similar to that described by equations (7-4 a,b), the surface potential, ψ_o, is then constant regardless of the ionic strength for constant relative supersaturation. With the solution activities of the potential-determining ions constant, the surface charge, σ_o, depends only on the ionic strength through the double layer thickness, κ^{-1}, as given by (7-1). The surface charge can also be expressed (Hunter, 1981) as

$$\sigma_o = \Sigma\, z_i\, F\, \Gamma_i \qquad (7\text{-}5)$$

where F is the Faraday constant, 96,485 C/mol, and Γ_i is the surface excess adsorbed amount of the i^{th} potential-determining ion. Comparison of (7-1) and (7-5) shows that as ionic strength increases at a constant relative supersaturation and ion ratio, the double layer thickness decreases, thus increasing the surface charge proportionately. In order to maintain the greater surface charge, the total amount of adsorbed potential-determining ions increases according to (7-5).

If an increase in the amount of growth ions adsorbed is directly related to an increase in the growth rate of a crystal in solution, then it follows from the above discussion of double layer effects that the growth rate should be approximately proportional to the square root of the ionic strength if all other relevant solution properties remain constant. The shape of the curves of growth rate versus ionic strength shown in Figure 7-1 are of the general shape of $y \alpha x^n$ with $0 < n < 1$. The actual values of n for the curve corresponding to each electrolyte are $n = 0.166$ for KCl and $n = 0.135$ for LiCl. No value is available for $KClO_4$ due to an insufficient amount of data. Figure 7-3 shows the parameter κ as calculated using equation (7-3) plotted versus ionic strength. The data for crystal growth in the presence of LiCl is included for comparison. Although complete agreement with the theory requires $n = 0.5$, the observed trends are parallel, and the Gouy-Chapman treatment of the double layer offers a preliminary basis for modelling effects of ionic strength on growth rate. As can be seen in Figure 7-3 the shapes of the curves are similar indicating that a model for growth rate enhancement by increased ionic strength based on double layer theory is feasible. A more complete model might be developed by utilizing more complex treatments of the double layer that have been proposed, such as the Stern-Nernst-Gouy-Chapman theory (Hunter, 1981). In addition, the non-equilibrium nature of crystal growth must be taken into account. More importantly, since double layer theory is based on the assumption of equilibrium at the solid/liquid interface, data that describe the non-equilibrium effects of the electrolyte crystal growth process on surface potential and surface charge are needed. The assumption of constant surface potential must also be experimentally verified.

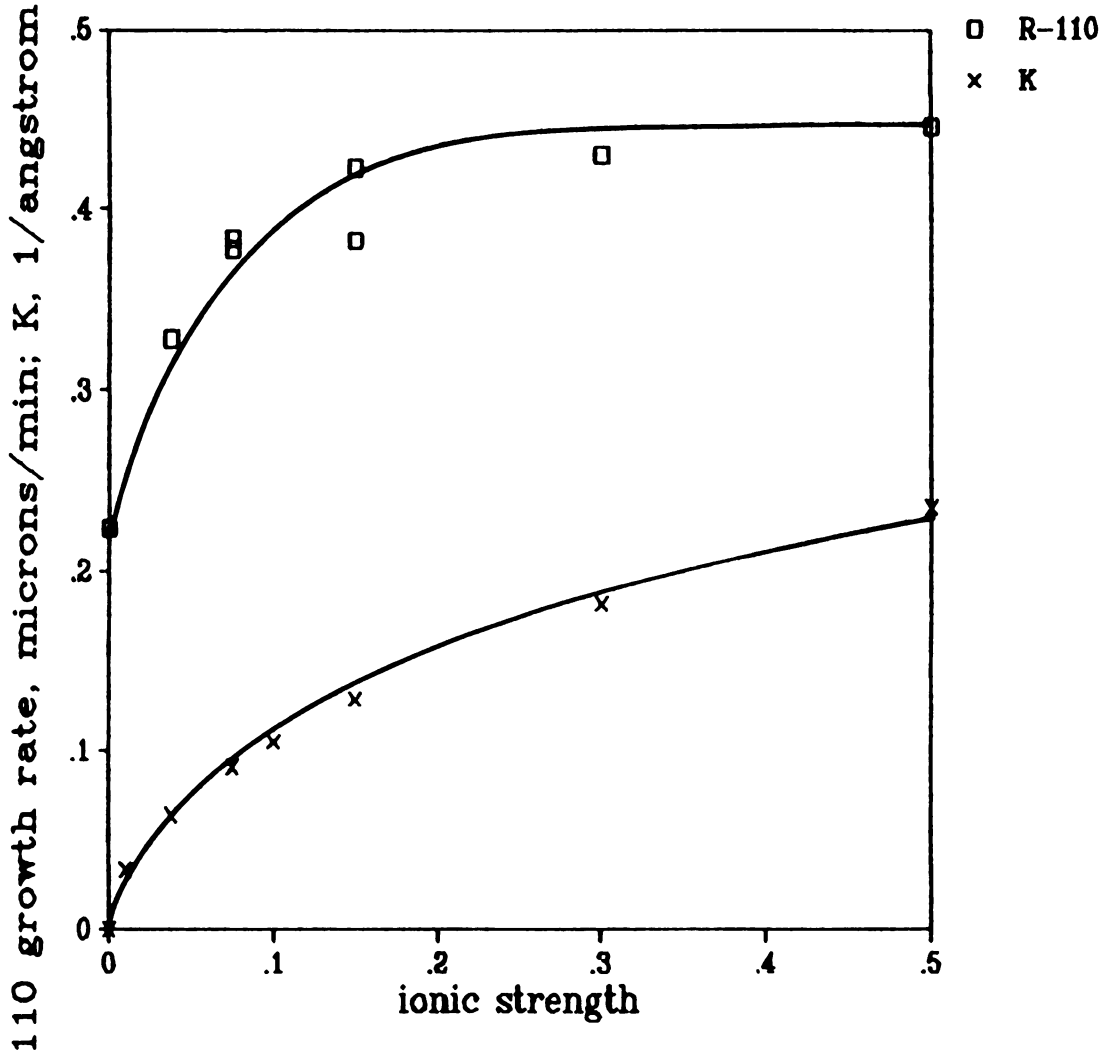

Figure 7-3. Comparison of Trends in Growth Rate and Theoretical Double Layer Thickness as Functions of Ionic Strength

The observed effect of ionic strength on growth rate was easily detectable using photomicroscopic technique. The superiority of this method over others is most apparent when comparing solution effects on the growth rates of different faces. When comparing the effect of ionic strength on the three facial growth rates, it was noticed that the effect is slightly different for one face in the presence of LiCl. Figures 7-4 and 7-5 show the data for KCl and LiCl, respectively, plotted as the relative facial growth rate versus ionic strength for each of the faces 110, 010, and $\bar{1}01$. The relative growth rate, R / R_{max}, is defined as the actual growth rate divided by the maximum rate (for the given face) observed as a function of ionic strength with other solution conditions constant. The trend of steadily increasing growth rate with ionic strength to an asymptote was followed by all faces except for the 010 face in the presence of LiCl. In that case, the curve showed a slower approach to the maximum measured rate and did not approach it asymptotically. Rather, the curve appeared to be increasing and apparently would not have leveled off until a much higher ionic strength. The reason for this observed behavior is unknown; however, it is possible that the small Li^+ ion did not compress the electrical double layer as effectively on the 010 face, leading to a less significant enhancement of the adsorption of growth ions. The difference in growth rate behavior between faces in response to changes in ionic strength would not have been detected using other crystal growth techniques.

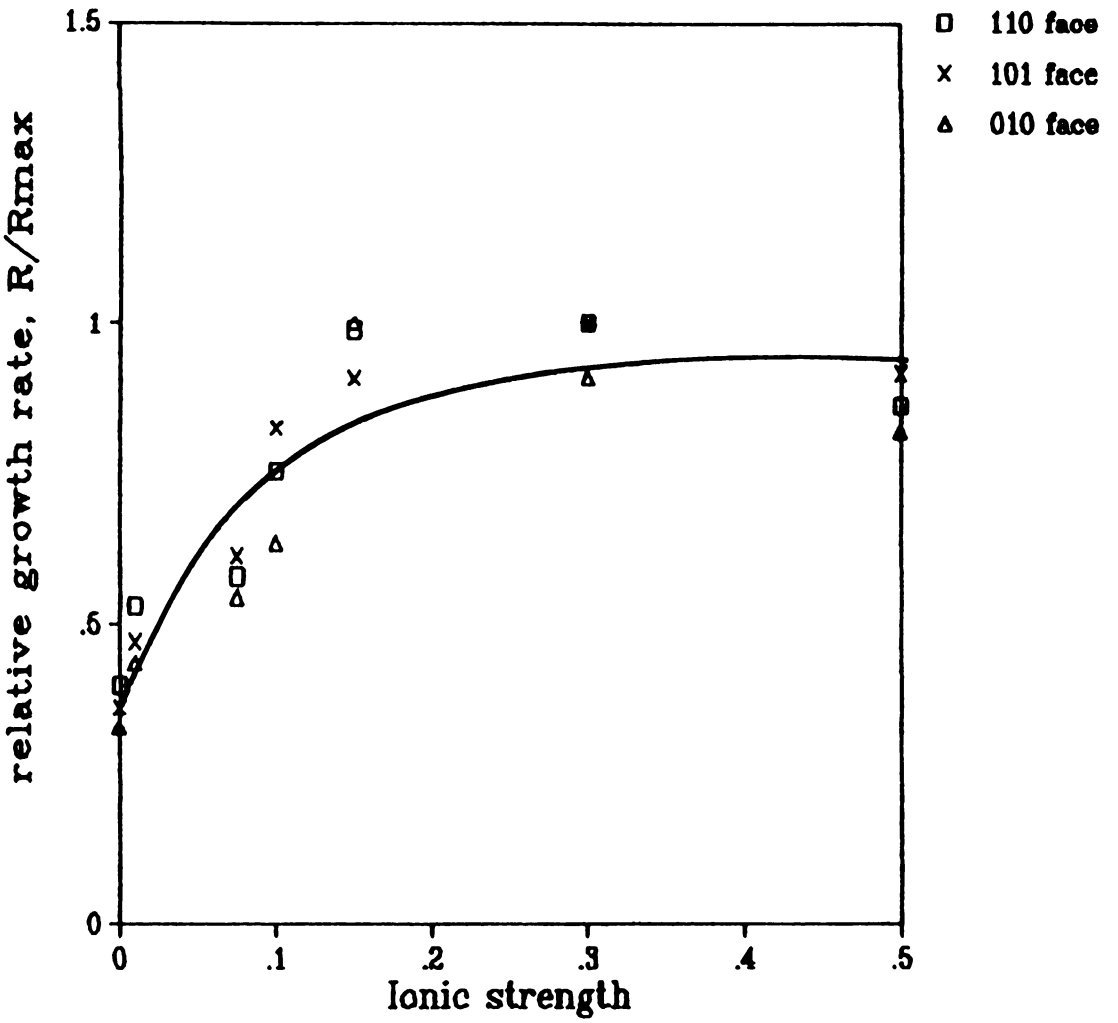

Figure 7-4. COM Relative Growth Rate Versus Ionic Strength in Presence of KCl

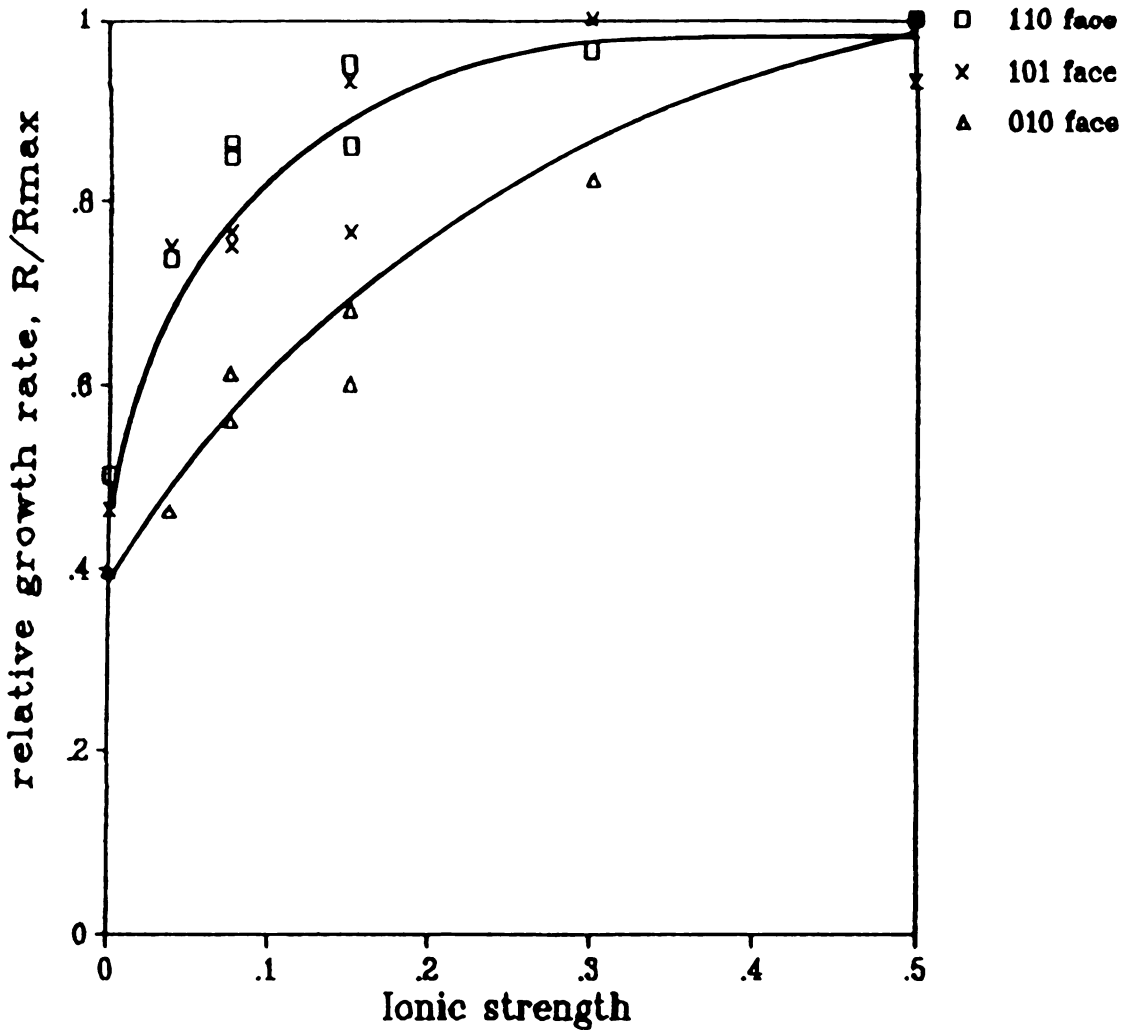

Figure 7-5. COM Relative Growth Rate Versus Ionic Strength in Presence of LiCl

7.3 COM Growth Rates as a Function of Calcium to Oxalate Ratio

COM linear face growth rates were measured at various values of the free calcium to free oxalate ratio, $[Ca^{2+}]/[C_2O_4^{2-}]$, in several series of experiments. In all experiments, the solution conditions were $\sigma \approx 3.71$, pH = 6.00, and T = 37 °C.

In the first series of experiments, the ionic strength was 0.15 M with KCl as the background electrolyte. The crystals formed all had twinned styloid COM habits showing 110, 010, and $\underline{1}01$ faces. The results of this series are shown in Figure 7-6 for each type of crystal face with the linear facial growth rate plotted versus log $([Ca^{2+}]/[C_2O_4^{2-}])$ for the ion ratio range of $0.01 \leq [Ca^{2+}]/[C_2O_4^{2-}] \leq 100$. For each face, the growth rate shows a maximum at the equimolar free ion condition, $[Ca^{2+}] = [C_2O_4^{2-}]$. At ion ratios greater than or less than equimolar, the crystal faces show growth rates less than that at equimolar conditions.

Further experiments were done for various ion ratios at a constant relative supersaturation of $\sigma \approx 3.71$, but without added KCl. Again, the growth rates of the various COM crystal faces were measured as a function of ion ratio in the range $.01 \leq [Ca^{2+}]/[C_2O_4^{2-}] \leq 100$. The results were plotted as growth rate versus the logarithm of the ion ratio as shown in Figure 7-7. As is seen in Figure 7-7, the facial growth rates are fairly constant with ion ratio. There is a slightly greater growth rate at low and high ion ratios with a very shallow minimum in growth rate occurring at equimolar conditions. This minimum in growth rate can be explained by the enhancing effect of ionic strength on growth rate.

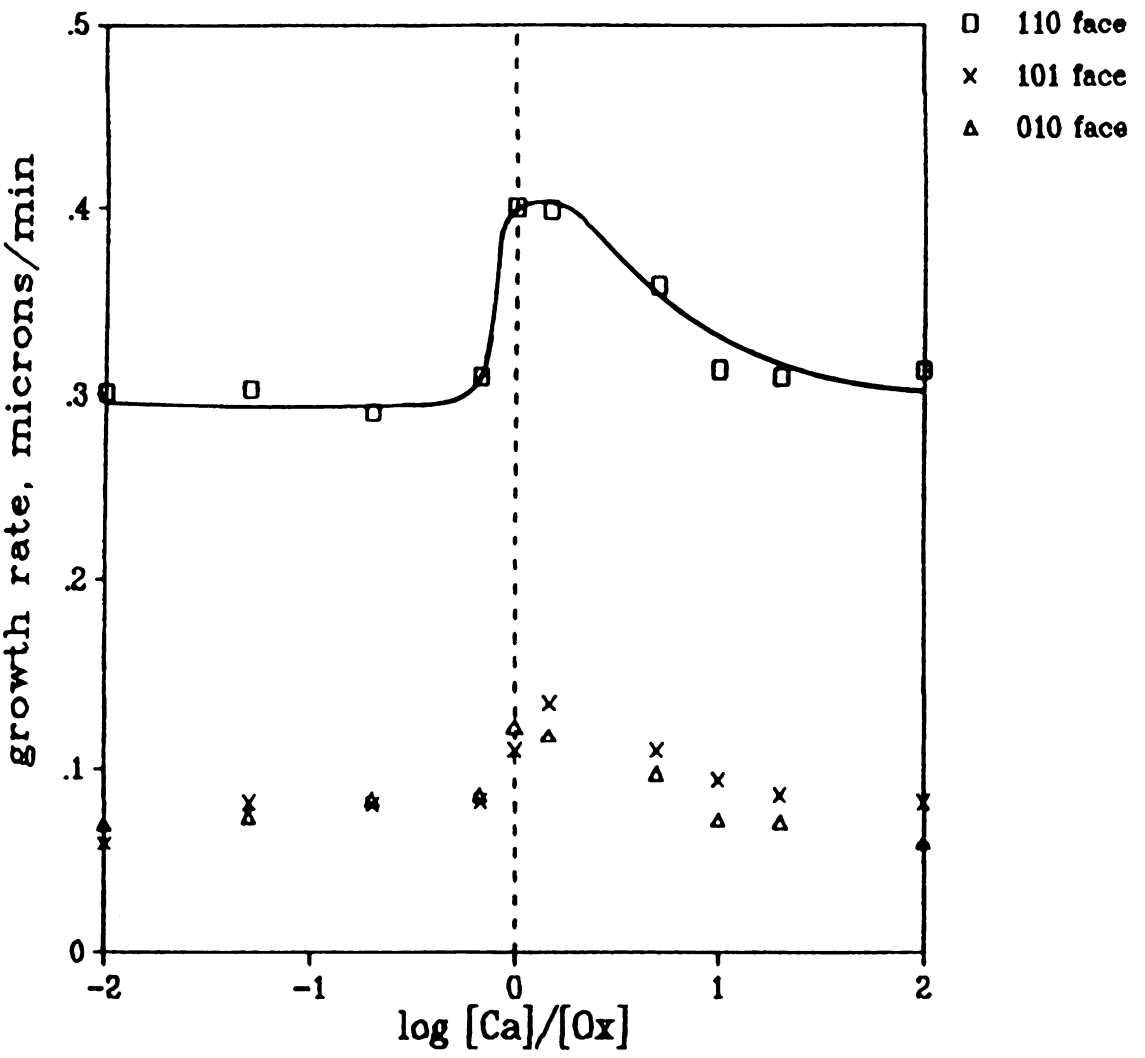

Figure 7-6. COM Face Growth Rate Versus Ion Ratio in Presence of KCl

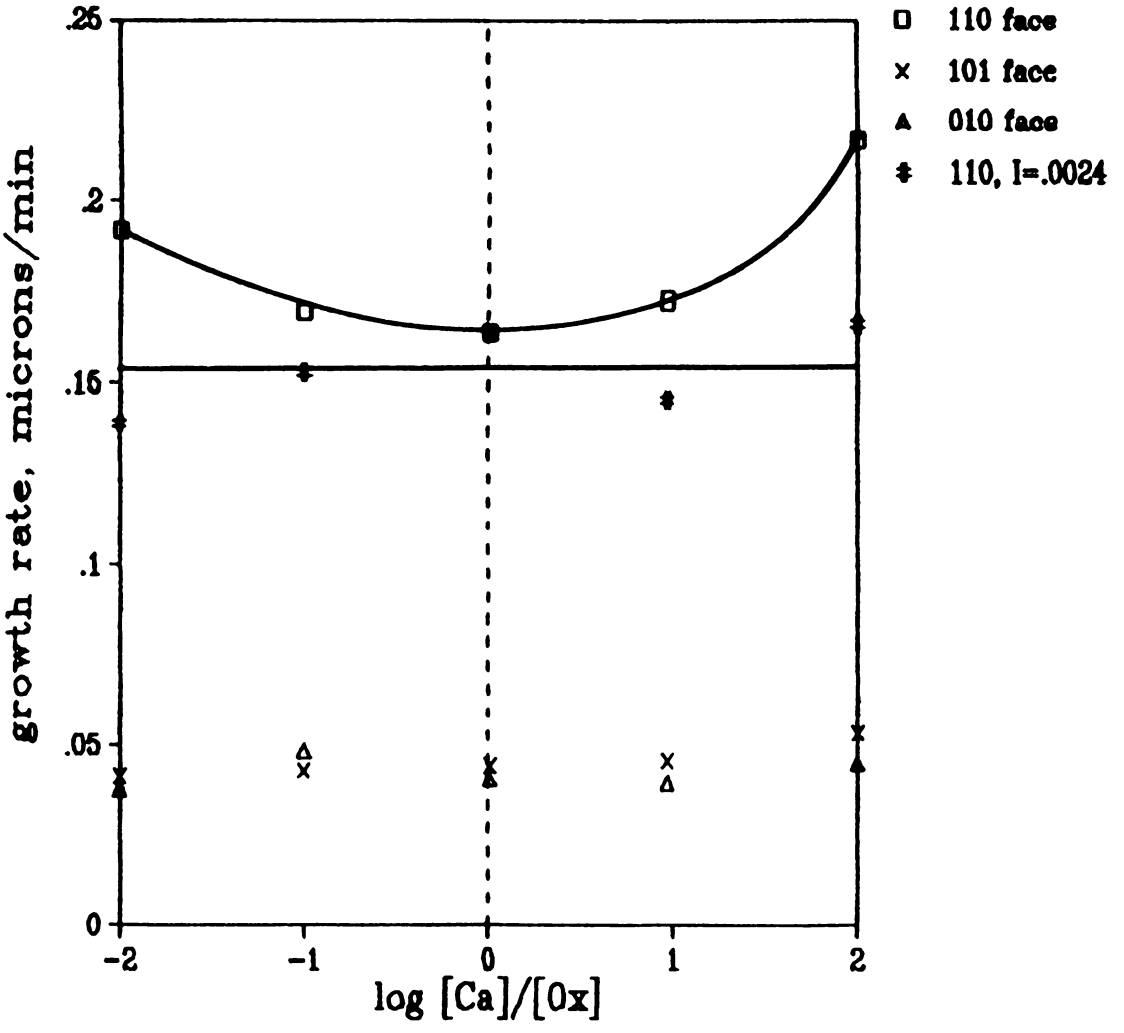

Figure 7-7. COM Face Growth Rate Versus Ion Ratio with No Added KCl with Correction for Non-constant Ionic Strength

Since the data of Figure 7-7 were taken for solutions with no added background KCl, the ionic strength could not be buffered for the different experiments. In each experiment, the amount of reagent added to obtain the required conditions was different which resulted in different net solution ionic strength values. The amounts of oxalate or calcium reagents required to obtain the desired relative supersaturation were substantial at low and high ion ratios, respectively. The total amount of reagent required, including both $CaCl_2 \cdot 2H_2O$ and $K_2C_2O_4 \cdot H_2O$, at the extremes of ion ratio was significantly higher than that required at equimolar ion ratio conditions. The effect was that the ionic strength was lowest at the equimolar ion ratio condition and higher as the ratio was increased or decreased. The higher ionic strengths at low and high ion ratios caused a slight increase in growth rate due to the enhancing effect thought to be caused by double layer compression. This adds further support to the proposed model of ionic strength effect on growth rate via double layer compression.

The curve for the case of no added KCl has been corrected for the effect of ionic strength using the multiplicative scaling factor $(.0024/I)^{.166}$ where .0024 is the ionic strength at the equimolar free ion condition, I is the ionic strength at the given ion ratio, and .166 is the empirically determined exponent of the ionic strength dependence of COM growth rate, as discussed in section 7.2. As seen in the lower curve of Figure 7-7, this correction for the variation in ionic strength for the case of no added KCl eliminates the apparent growth rate minimum.

The curves of 110 face growth rate versus ion ratio for each of the background KCl conditions are plotted together in Figure 7-8. The

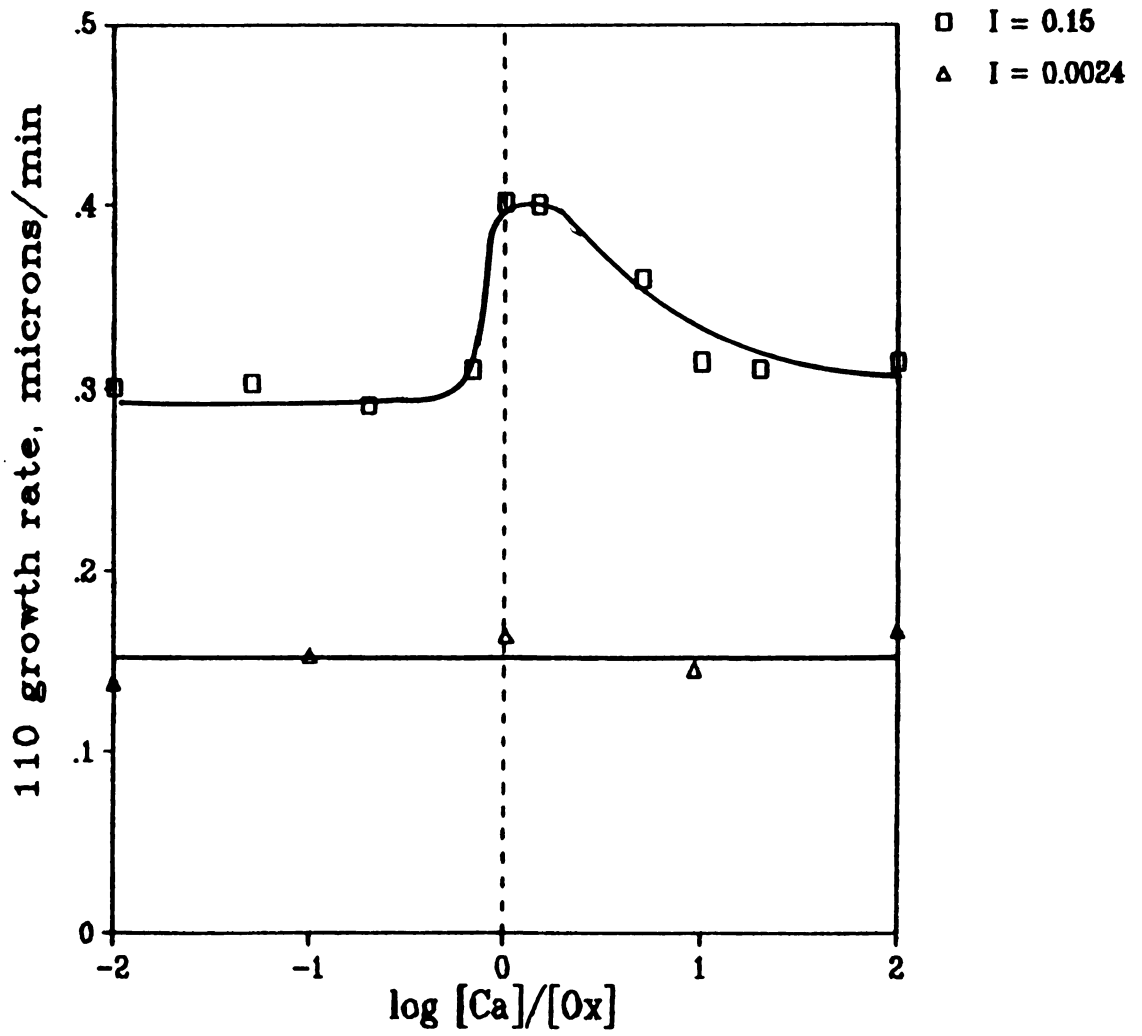

Figure 7-8. COM 110 Face Growth Rate Versus Ion Ratio with and without Background Electrolyte

curve for the case of no added KCl is corrected to a constant ionic strength of 0.0024 M as discussed above. Figure 7-8 illustrates the observed effects of both ionic strength and ion ratio. The growth rate enhancing effect of ionic strength may be seen over the entire range of ion ratio. The enhancement is, however, less apparent at non-equimolar conditions due to the competing effect of ion ratio. Nielsen (1984a) has suggested that COM growth rate should be independent of ion ratio, but his study did not include effects of a concentrated background electrolyte. The present results indicate that the presence of a concentrated background electrolyte induces an ion ratio dependence of growth rate (Figure 7-8, I = 0.15 M). Specifically, growth rate is inhibited at non-equimolar ion ratios by the presence of the background electrolyte KCl. Growth rates measured in solution containing no added background electrolyte (Figure 7-8, I = 0.0024 M) are independent of ion ratio.

It was hypothesized that the addition of background electrolytes other than KCl might offer additional insight into the mechanism of growth inhibition by the electrolyte. To this end, two series of crystal growth experiments were performed using other electrolytes. In the first, potassium perchlorate ($KClO_4$) was used at an ionic strength of 0.15 M. Previous reports (Tomazic, et al., 1986; Voigt, 1987) suggested that the perchlorate anion should not be readily adsorbed on crystal surfaces. It was further assumed that ClO_4^- formed no significant ion-pairs in solution. The results of experiments with $KClO_4$ are plotted for the 110 face as seen in Figure 7-9. As is apparent from this plot, the curves for growth versus ion ratio with $KClO_4$ as the background electrolyte show the same general shape as the curves for

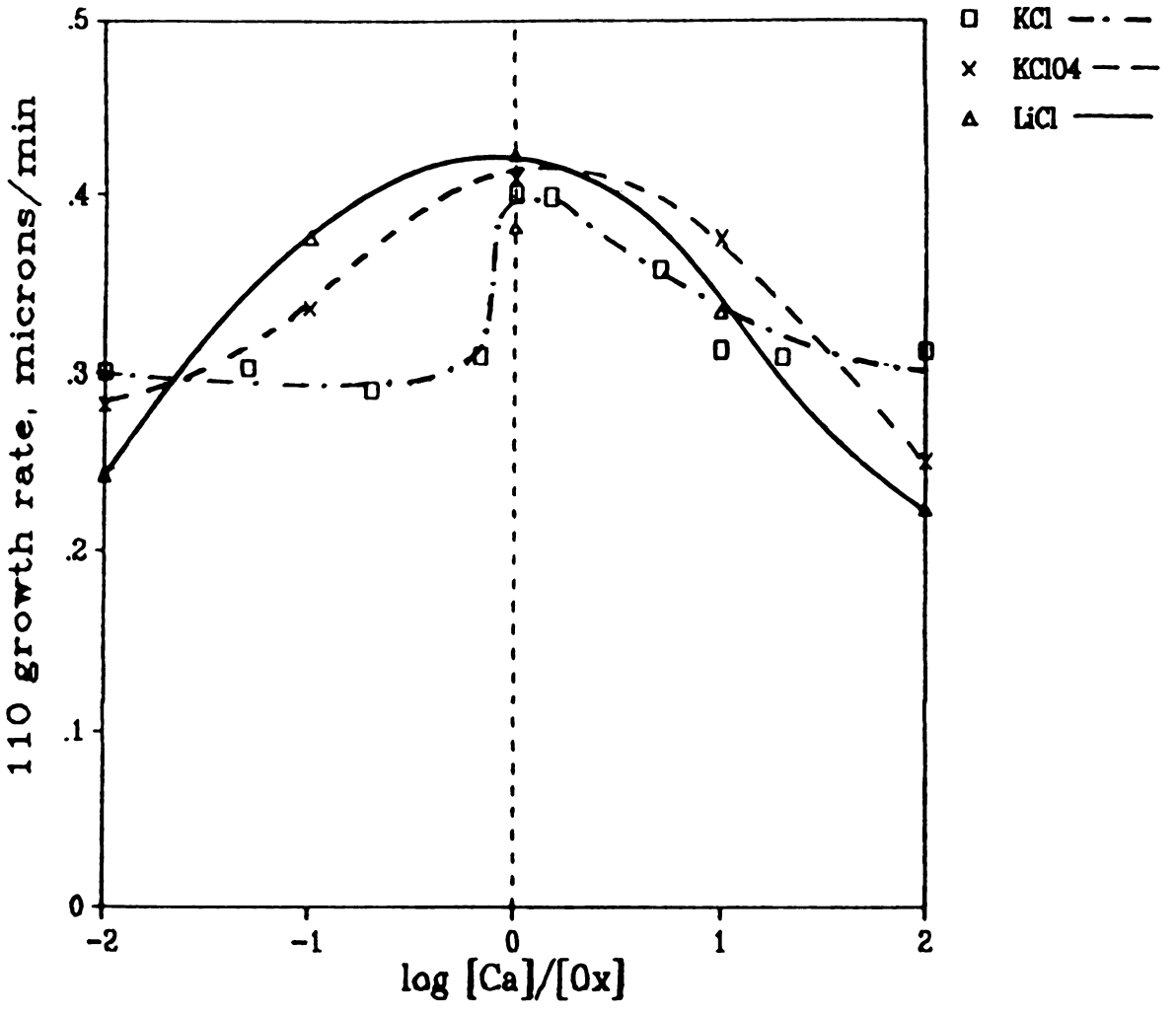

Figure 7-9. COM 110 Face Growth Rate Versus Ion Ratio for Various Electrolytes

growth in the presence of KCl. This confirms the indifferent nature of both electrolytes. In the second series of experiments, lithium chloride (LiCl) was used at an ionic strength of 0.15 M. It was expected that the smaller Li^+ cation might possess a different adsorption potential than the K^+ cation. The results of these experiments are plotted for the 110 face along with those for KCl and $KClO_4$ in Figure 7-9. Again, the trend in growth rate versus ion ratio for LiCl is generally the same as for KCl and $KClO_4$, with a growth rate maximum occurring at equimolar conditions. Apparently, the effect of ion ratio on the growth rate is independent of the type of background electrolyte for the indifferent ions considered.

A few studies exist which report the effect of ion ratio on growth rate. Meyer and Smith (1975a) have reported that the COM growth rate from 0.15 M NaCl solution increased at ion ratios less than or greater than equimolar, with a minimum at equimolar conditions. Nielsen (1984a) has shown that COM growth rates from solution with no added background electrolyte were independent of the ion ratio, similar to the present results. However, Nancollas and Gardner (1974) have found that the growth rate from solution with no added background electrolyte was higher when the cation Ca^{2+} was in excess and explained it as evidence of preferential adsorption of the cation. Such behavior is seen in this work (Figure 7-7), but the increase in growth rate at high ion ratio with no added background electrolyte is probably due to the enhancement of growth rate by ionic strength, and the same effect occurs in the presence of excess oxalate. Furthermore, preferential adsorption of the cation cannot provide the entire explanation of the effect because all experiments in this work were performed under conditions of a positive

surface charge as discussed in Section 7.2. Measurements of electrokinetic parameters of growing crystals are vital for further interpretation of these results.

The source of the ion ratio dependence of growth rate in solution containing 0.15 M KCl is uncertain. At least three possibile explanations exist.

First, inhibition of crystal growth could be caused by adsorption of non-growth units species such as various calcium and oxalate ion-pairs. If this were the cause of the inhibition, it is to be expected that the trends seen in growth rate should parallel changes in ion-pair concentration. Inspection of Table A-7 of Appendix A shows that the ions $KC_2O_4^-$, $HC_2O_4^-$, and $Ca(C_2O_4)_2^{2-}$ all decrease in concentration with increasing $[Ca^{2+}]/[C_2O_4^{2-}]$, while the concentration of the ion $Ca_2C_2O_4^{2+}$ increases with increasing $[Ca^{2+}]/[C_2O_4^{2-}]$. The concentration of the species CaC_2O_4 remains constant. Similar trends in the concentrations of the various ion-pairs are seen for the case of no added background KCl as shown in Table A-8. Since the concentration trends are similar for both cases, with and without background electrolyte, but growth rate is dependent on ion ratio only for I = 0.15 M, it seems unlikely that adsorption of ion-pairs as growth modifiers is the cause of the inhibition.

A second explanation is that a difference in the surface potential accounts for the reduced growth rate observed at low and high ion ratios. As shown in section 7.2, the potential-determining ions, Ca^{2+} and $C_2O_4^{2-}$, fix the surface potential. In the case described in section 7.2 with a constant ion ratio = 1, the activities of Ca^{2+} and $C_2O_4^{2-}$ in the bulk were constant, and, therefore, the surface potential was

constant. However, in changing the ion ratio, these ion activities are not constant, and the surface potential changes accordingly. The surface charge density and, in turn, the amounts of Ca^{2+} and $C_2O_4^{2-}$ adsorbed vary according to equations (7-1) and (7-5).

Two facts seem to refute the idea of inhibition caused by a varying surface potential. Curreri et al. (1979) and Hlady (1984) show that the surface potential increases steadily in positive value at ion ratios greater than about 0.01. It would be expected then that the trend in growth rate should parallel the increase in surface potential rather than pass through a maximum as seen in Figure 7-6 for I = 0.15 M. In addition, the growth rate trend is seen for I = 0.15 M, but not for the case without added electrolyte. Since ion ratio varies for both cases, similar trends in surface potential and, in turn, similar trends in growth rate would be expected for each case. The existence of the growth rate maximum for I = 0.15 M and the lack of any growth rate variability for the case without added background electrolyte refute surface potential as an important factor in this inhibition.

The third and most likely cause of the ion ratio dependence of growth rate is a non-constant driving force for crystal growth. Although the relative supersaturation was held constant throughout all of the experiments, the growth rate did not remain constant. It seems likely that relative supersaturation as expressed by equation (3-3) is not the applicable statement of driving force in this case. Additionally the ionic strength effect on growth rate under conditions of constant relative supersaturation as discussed in Section 7.2 also suggests that relative supersaturation is not the correct driving force in the case of electrolyte crystal growth. The effect of double layer

compression and the as yet undetermined cause of the ion ratio effect on growth rate demonstrate that the driving force for electrolyte crystal growth is not the same as that for growth of crystals composed of neutral molecules.

Chapter 8. COM Single Crystal Growth in the Presence of Polyelectrolytes

8.1 COM Single Crystal Growth from Dilute Polyelectrolyte Solutions

COM single crystal growth rates were measured at 37 °C in the presence of two different polyelectrolytes, polyglutamic acid and heparin. These biopolymers were chosen for study due to their similarity to compounds implicated as urinary crystal growth modifiers. Polyglutamate served as a model growth modifier due to its similarity to the glycoprotein growth modifiers that have many glutamate and aspartate residues (Nakagawa, et al., 1978, 1981, 1983, 1984; Lopez et al., 1986). Heparin is a glycosaminoglycan, a class of compounds which has been shown to influence COM growth in urine (Robertson et al., 1973). The growth of COM crystals in the presence of these polymers was measured in an attempt to understand the mechanism of interaction of these types of compounds with COM crystals during growth.

Single crystal growth rates were measured in a manner similar to that used for unmodified crystal growth. In some cases, however, it was very difficult to identify faces of the growing crystals. This was true especially for the growth of crystals with polyglutamate. Crystals nucleated and grown in the presence of polyglutamate showed distorted habits as discussed in Chapter 5. It was therefore necessary to change the experimental procedure slightly in order to facilitate the measurement of facial growth rates. This was done by initially nucleating crystals from solution at the desired solution conditions but without the growth modifier and then continuing the growth of the same crystals from solution at the same conditions but with the growth modifier.

Two types of growth rates were measured for polyglutamate-modified growth: facial growth rates and equivalent circular diameter (D_{eq}) growth rates. Facial growth rates were measured for crystals nucleated in unmodified solution and grown in solution containing polyglutamate. Growth rates based on D_{eq} were measured for crystals both nucleated and grown in solution containing polyglutamate due to the inability to distinguish crystal faces.

Very dilute concentrations of polyelectrolytes were used in studying their effect on COM crystal growth. This reflected the typically low concentration of polyelectrolyte growth modifiers in urine, such as 5.8 mg/l of glycosaminoglycans (Robertson et al., 1981). The concentrations used were typically on the order of 1 to 100 milligrams per liter. These low concentrations made it unnecessary to alter the method of calculation of the relative supersaturation to take into account the possible binding of ions by the polymers. This assumption was justified by experimental results as will be discussed.

Some of the experimental results discussed in this chapter have been reported previously (DeLong and Briedis, 1985b).

8.2 Effect of Polyglutamate on COM Single Crystal Growth

The effect of polyglutamate on single crystal growth of COM was studied for a range of polymer concentrations, polymer molecular weights, COM relative supersaturations, ionic strengths, and pH. The response of COM growth rate to each of these variables offered valuable insight into the mechanism of polyglutamate interaction with the crystal. These effects will be described in the following subsections.

8.2.1 Effect of Polyglutamate Concentration and Molecular Weight

COM single crystal growth rates were measured using the equivalent circular diameter for a range of polyglutamate concentrations and molecular weights. For this series of experiments, the relative supersaturation was held constant at $\sigma \approx 3.71$, the total calcium and total oxalate concentrations were equimolar at $T_{Ca} = T_{Ox} = 0.001$ M, the ionic strength was maintained at 0.15 M with KCl, and the pH was 6.00.

The D_{eq}-based growth rate was plotted versus the polyglutamate concentration in milligrams per liter for two polymer molecular weights as shown in Figure 8-1. Each data point of Figure 8-1 was plotted using an average for several crystals ($3 \leq N \leq 5$). As can be seen, the single crystal growth of COM is inhibited by the polyglutamate in solution. For each molecular weight, the growth rate decreases steadily towards an apparently asymptotic minimum value as the polymer weight concentration increases.

The D_{eq}-based growth rate curves of constant polyglutamate molecular weight show a more gradual approach to the asymptotic minimum growth rate as the molecular weight increases. As seen in Figure 8-1, the curve of growth rate versus polymer concentration for a molecular weight of 32,000 reaches the apparent minimum growth rate at a weight concentration of about 5 mg/l, while that for 60,000 reaches the minimum at about 10 mg/l or more. However, the minimum growth rate is apparently the same for each molecular weight. This effect can be explained by replotting the growth rate versus the micromolar polymer concentration (10^{-6} moles/liter). This is shown in Figure 8-2. The normalization with respect to molar amounts causes collapse of the constant molecular weight curves forming a single curve of growth rate

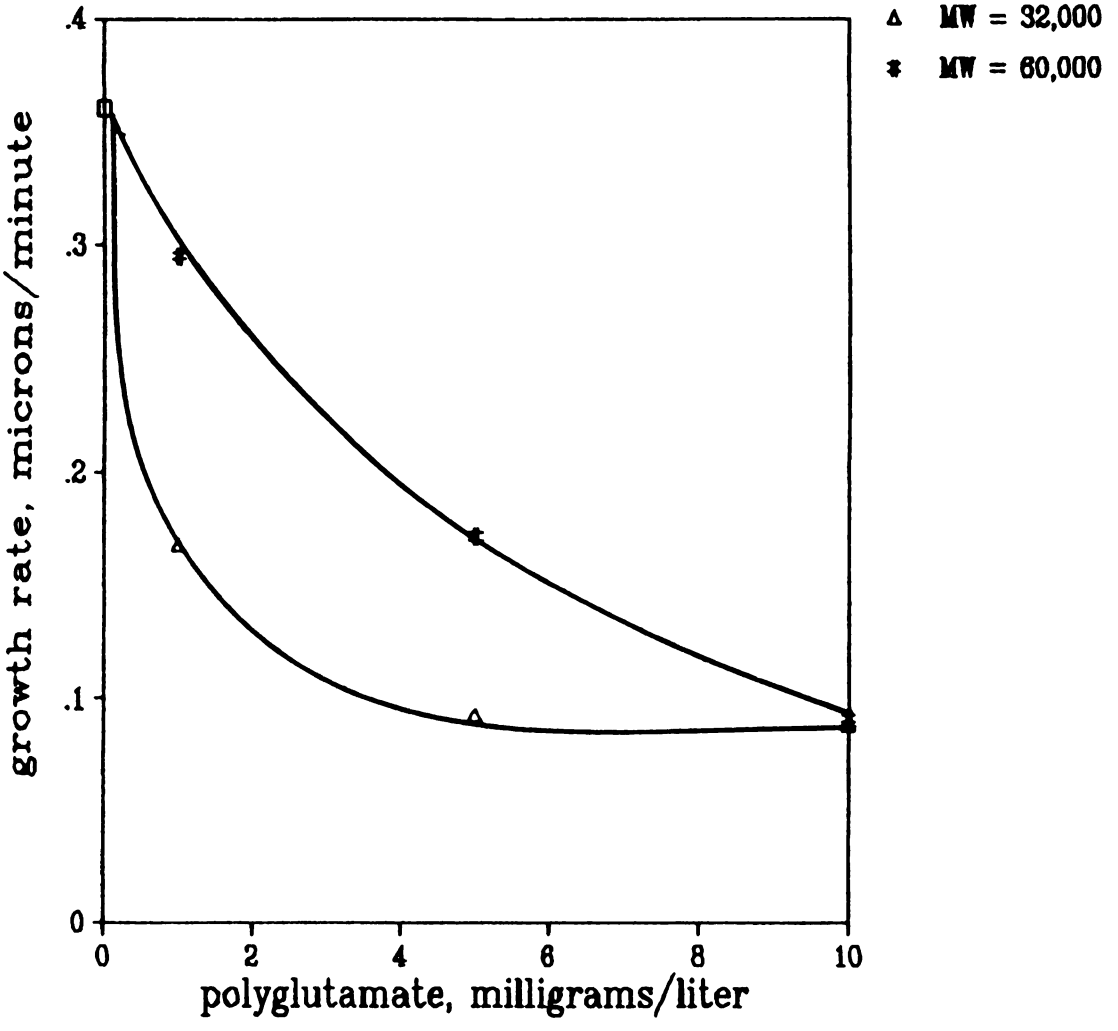

Figure 8-1. COM D_{eq} Growth Rate Versus Polyglutamate Weight Concentration

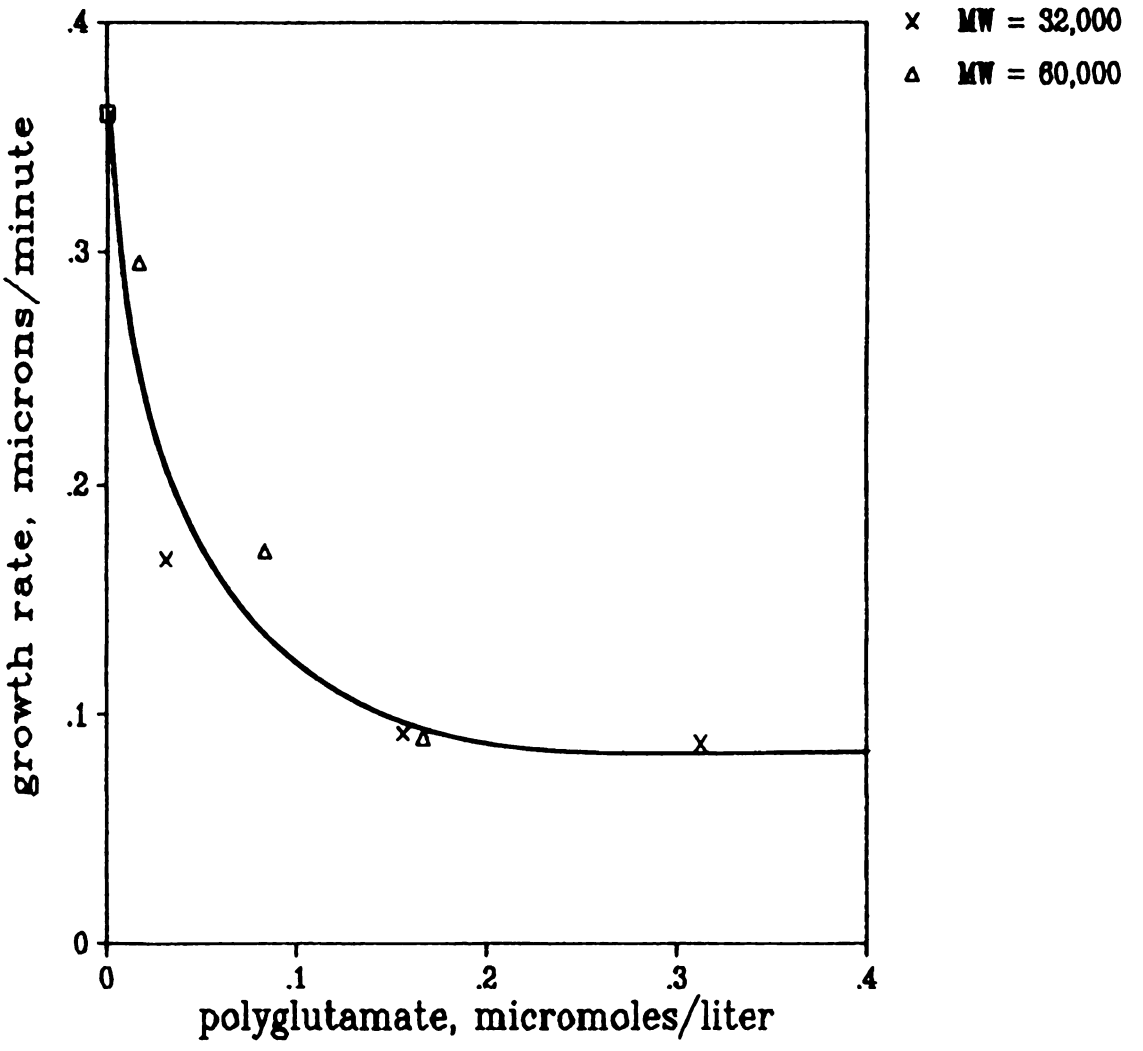

Figure 8-2. COM D_{eq} Growth Rate Versus Polyglutamate Molar Concentration

versus the micromolar polymer concentration (Figure 8-2).

Facial growth rates as a function of polyglutamate micromolar concentration for crystals nucleated in polyglutamate-free solution but grown in dilute polyglutamate solution are shown in Figure 8-3. Similar to the results for D_{eq}-based growth rates, the facial growth rates decrease steadily versus polyglutamate concentration asymptotically approacing a minimum value at high polyglutamate concentration. This trend is followed by the 110, 010, and $\underline{1}01$ faces.

8.2.2 Effect of Relative Supersaturation

In order to determine the effect of relative supersaturation on the ability of polyglutamate to inhibit COM growth, two other series of experiments were performed with constant relative supersaturations of $\sigma \approx 2.64$ and $\sigma \approx 4.74$. Other solution conditions of T = 37 °C, I = 0.15 M, pH = 6.00, and $T_{Ca} = T_{Ox}$ were the same as those used in the series described in the previous section. As will be discussed below, since the molecular weight of polyglutamate was shown to have no influence on inhibitory strength, various molecular weights of the polymer were used in these experiments.

The D_{eq}-based growth rate is plotted versus the polyglutamate micromolar concentration for three relative supersaturations as shown in Figure 8-4. Again, each data point plotted is an average for several crystals. For each relative supersaturation, the growth rate decreases towards an apparently asymptotic minimum as the polymer concentration increases. However, the rate of approach of the curves to the asymptotic minimum is not the same for each relative supersaturation. The polyglutamate concentration required to reach the minimum growth

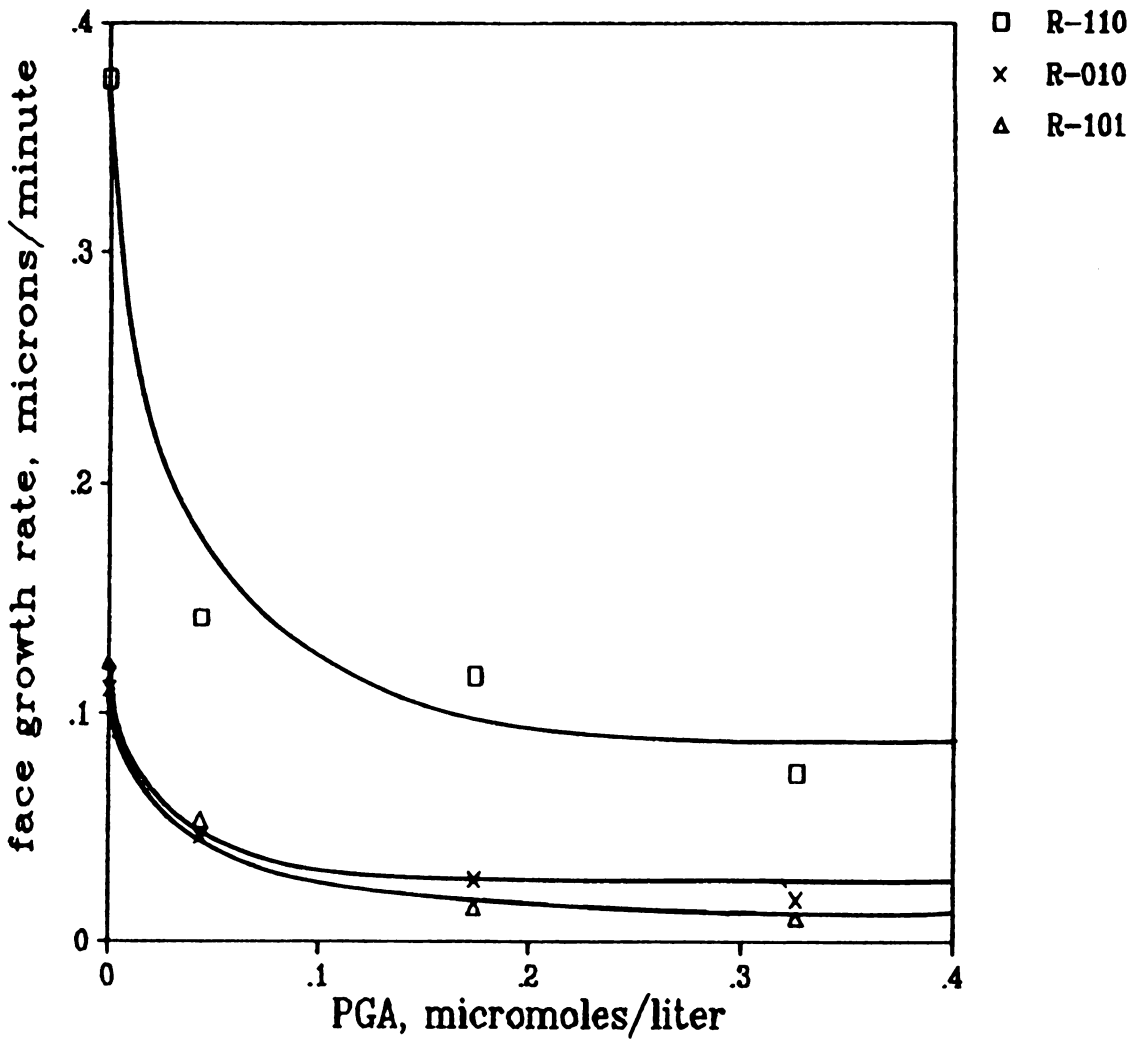

Figure 8-3. COM Face Growth Rate Versus Polyglutamate Molar Concentration

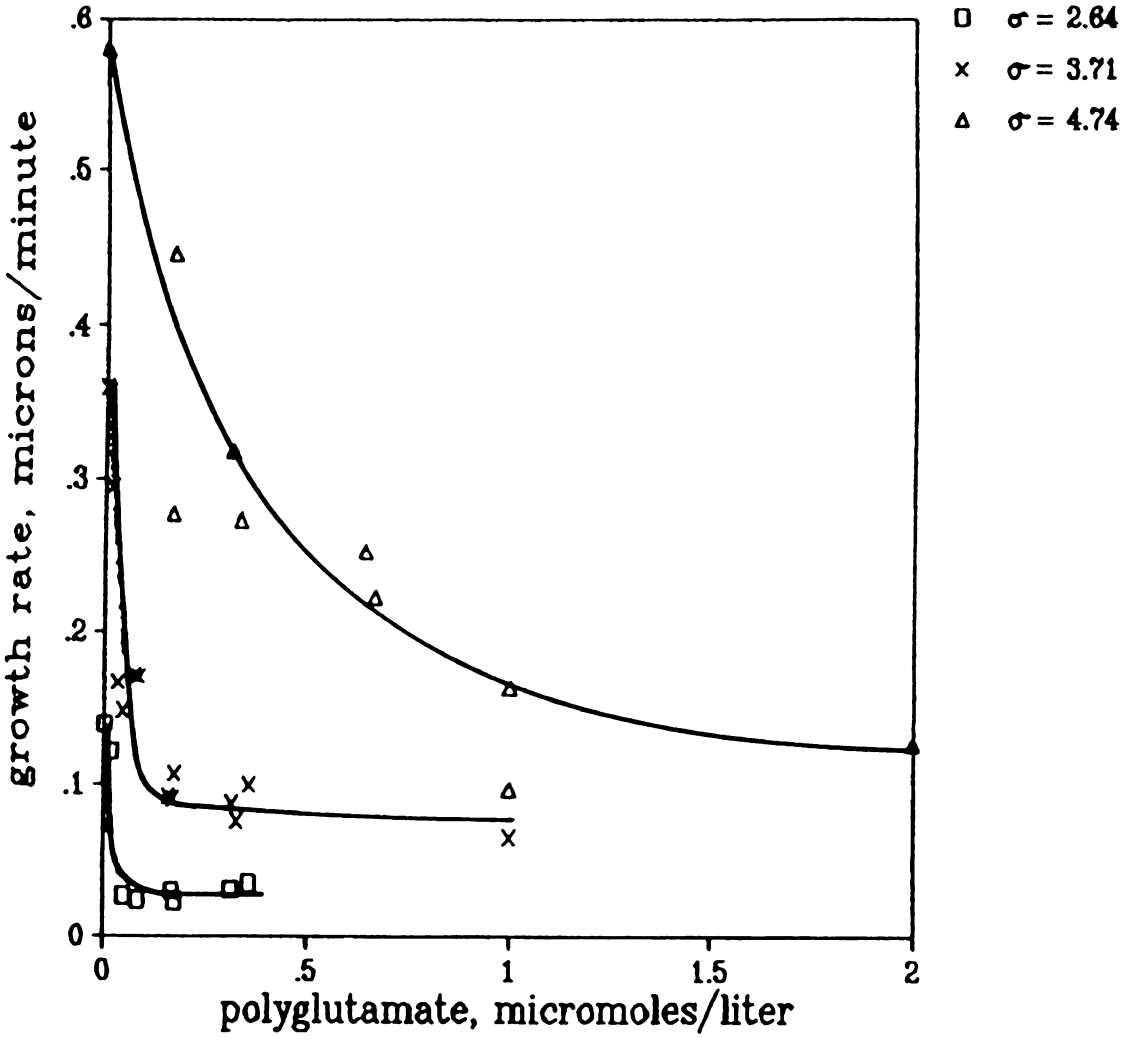

Figure 8-4. COM D_{eq} Growth Rate Versus Polyglutamate Molar Concentration for Three Relative Supersaturations

rate increases with relative supersaturation. For a relative supersaturation of $\sigma \approx 2.64$, the growth rate reaches the asymptote at about 0.1 μM (micromoles/liter), while at $\sigma \approx 3.71$ and $\sigma \approx 4.74$, the growth rate reaches the asymptote at about 0.4 μM and 1.5 μM, respectively.

A similar effect is seen for the face growth rate when measured as a function of polyglutamate micromolar concentration for various relative supersaturations. In Figure 8-5, the growth rate of the 110 face versus polyglutamate concentration is plotted for three relative supersaturations. As was the case for the D_{eq}-based growth rates, the approach to the minimum is more gradual for the higher relative supersaturations.

8.2.3 Effect of Ionic Strength

Since the potential for polyelectrolytes to adsorb onto crystal surfaces is strongly dependent on ionic strength (Hesselink, 1983), two series of experiments were done to determine the effect of ionic strength on the ability of polyglutamate to inhibit COM crystal growth. Facial growth rates were measured as a function of the polyglutamate concentration in the range 0 to 1 μM for two ionic strengths, I = 0.15 M and 0.0025 M. The background electrolyte was KCl. In each case, the solutions were equimolar in calcium and oxalate with T = 37 °C and pH = 6.00.

As discussed in Chapter 8, growth rates of crystals grown in uninhibited solution were dependent on the ionic strength. In order to compare the inhibited growth data, it was therefore necessary to express the data on a relative basis to compensate for the effect of ionic

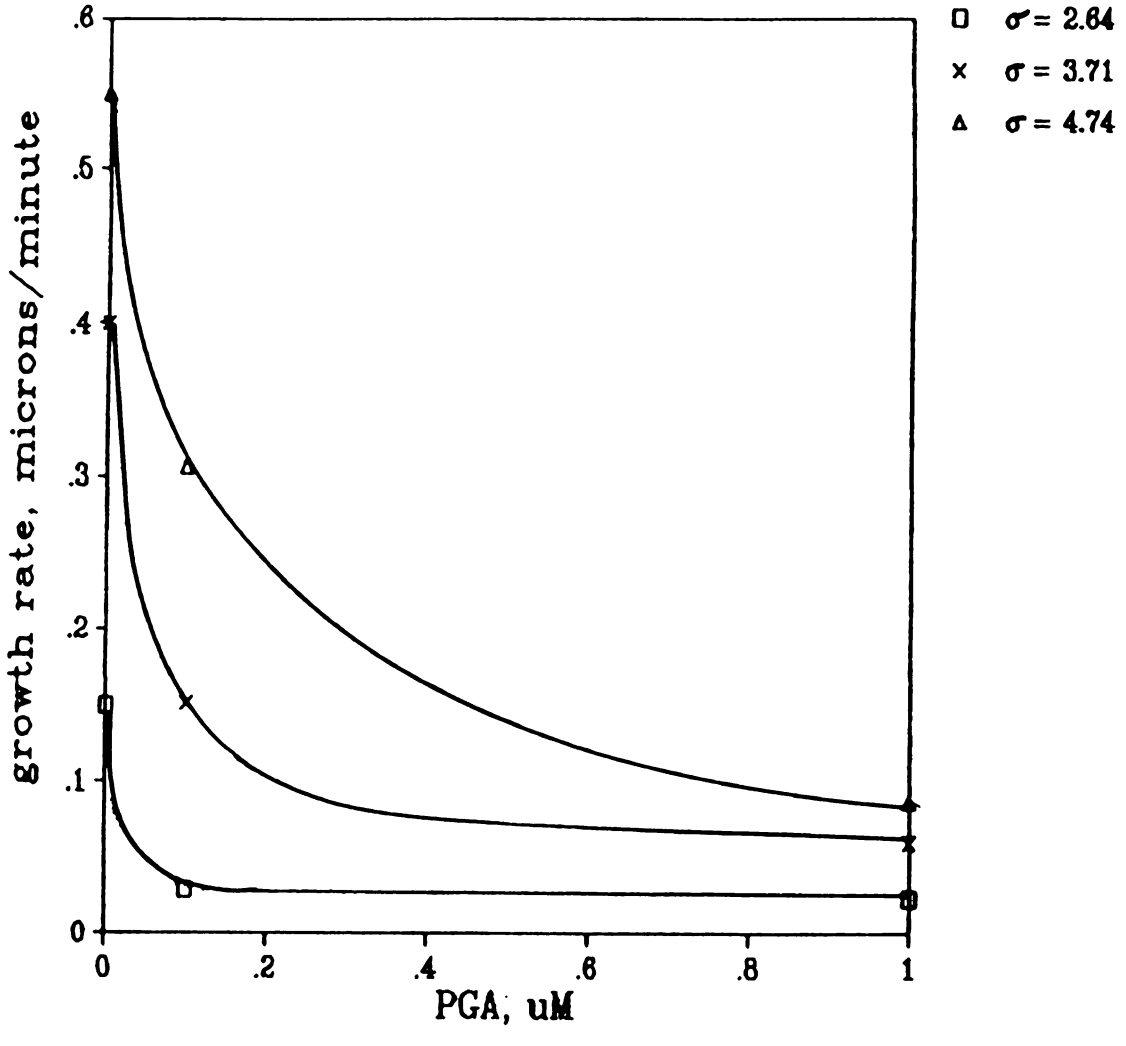

Figure 8-5. COM 110 Face Growth Rate Versus Polyglutamate Molar Concentration for Three Relative Supersaturations

strength on uninhibited growth. This was done by dividing the observed growth rate, R, by the growth rate at the condition of no added polyglutamate, R_{max}, to give the relative growth rate, R/R_{max}.

The relative growth rate, R/R_{max}, for each crystal face is plotted versus the polyglutamate concentration at two ionic strengths, I = 0.15 M and I = 0.0025 M, as shown in Figures 8-6 and 8-7, respectively. In each case, the curves show the usual trend of the growth rate decreasing towards an asymptote with increasing polyglutamate concentration. In order to see the effect of ionic strength on the ability of polyglutamate to inhibit growth on a particular crystal face, the relative growth rate of the given face is plotted versus the polyglutamate concentration for each ionic strength. This is shown in Figure 8-8 for the 110 face. As is apparent, there is little difference in the curves for each ionic strength. Similar effects were seen for the 010 and $\underline{1}01$ faces.

8.2.4 Effect of pH

The potential for polyelectrolytes to adsorb onto crystal surfaces is strongly dependent on the degree of dissociation of the acidic or basic functional groups (Hesselink, 1983). Two series of experiments were carried out In order to determine the effect of pH on the ability of polyglutamate to inhibit crystal growth. Facial growth rates were measured at polyglutamate concentrations of 0, 0.1, and 1.0 μM at pH = 4.00 and pH = 6.00. The pH value of 6 was used due its being a reasonable average for urine, and the pH value of 4 was used because the polyelectrolyte was expected to be less dissociated as compared with pH 6. The other solution conditions were maintained constant at T = 37 °C,

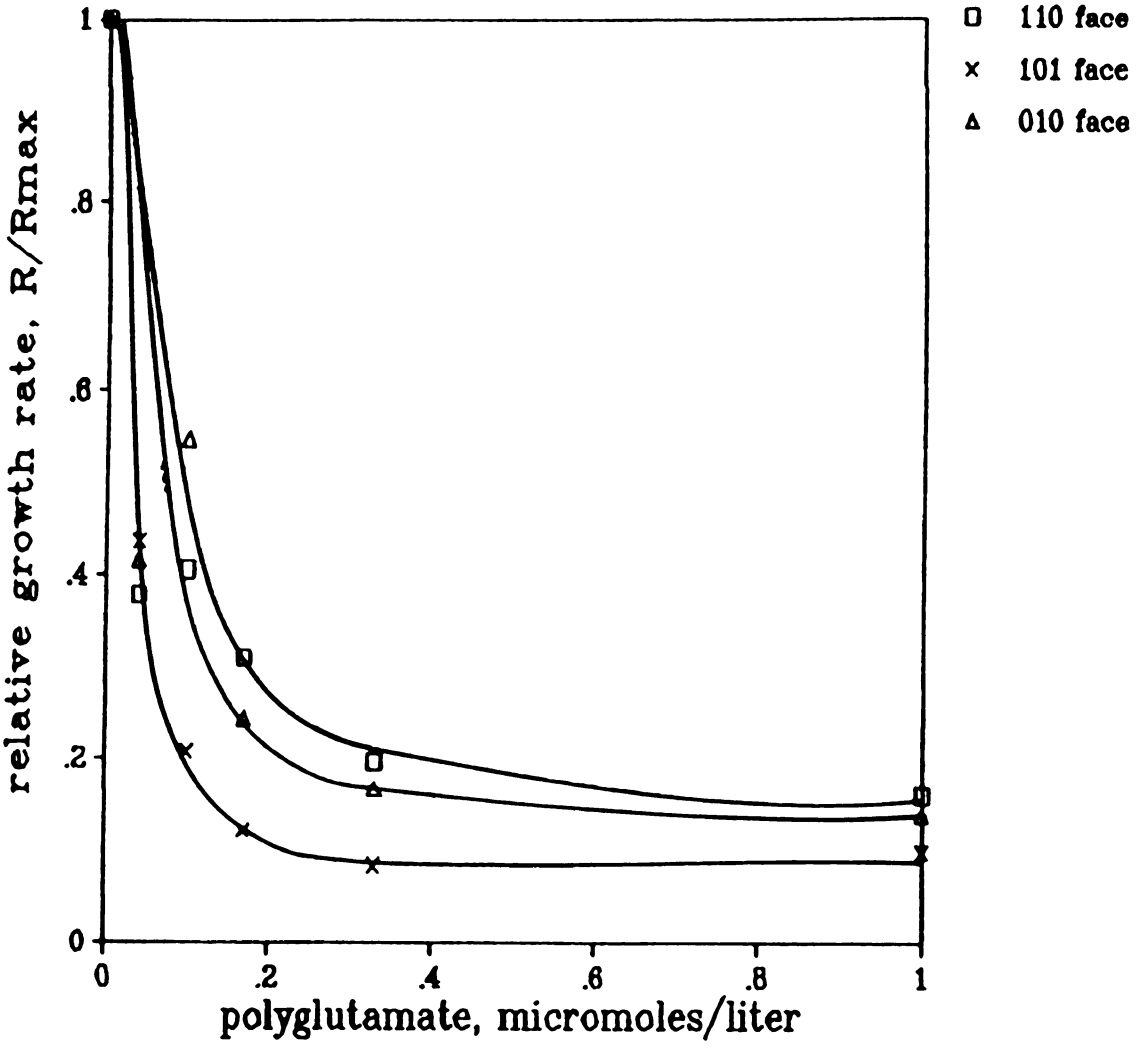

Figure 8-6. COM Relative Growth Rate Versus Polyglutamate Molar Concentration at Ionic Strength = 0.15 M

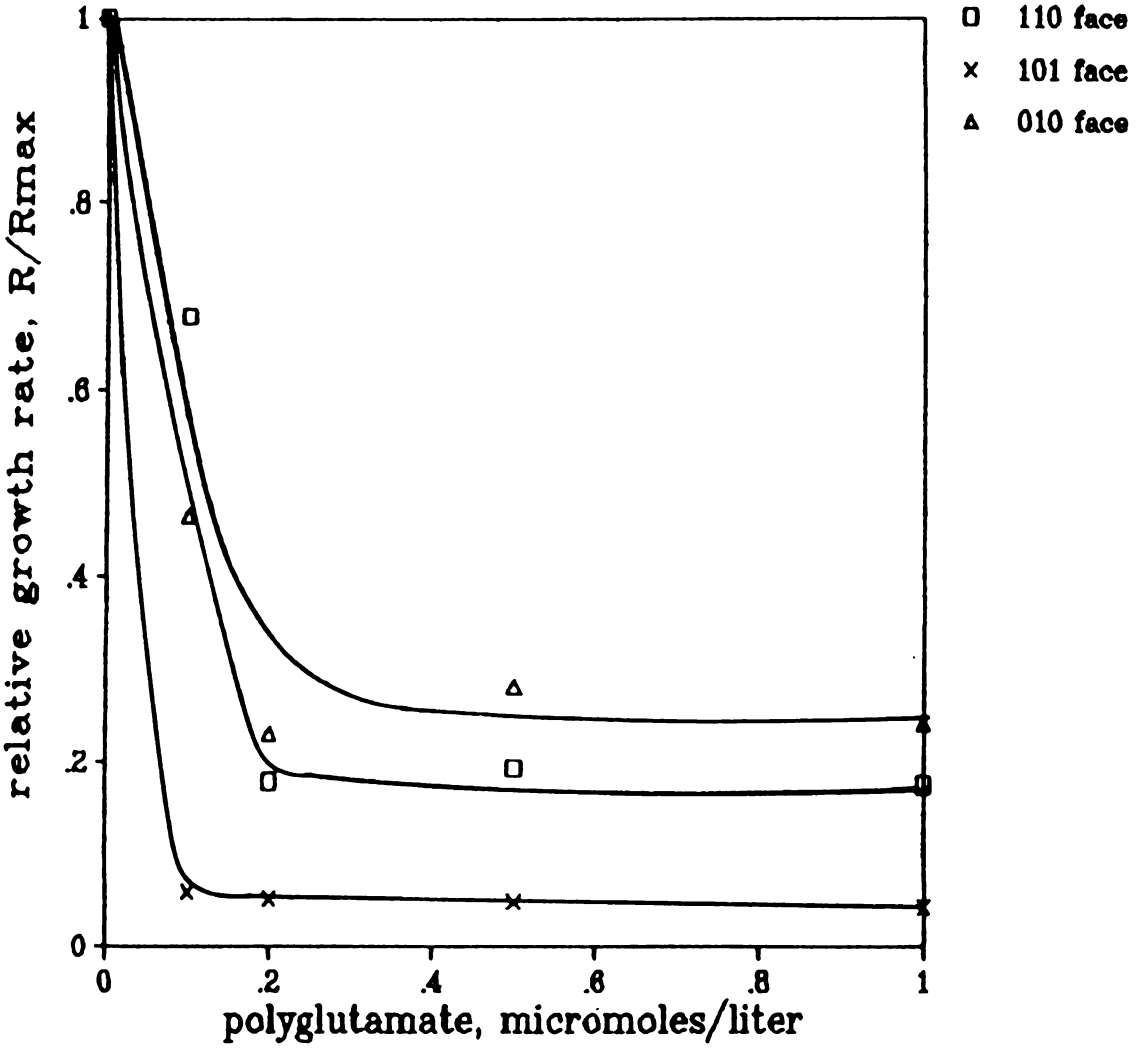

Figure 8-7. COM Relative Growth Rate Versus Polyglutamate Molar Concentration at Ionic Strength = .0025

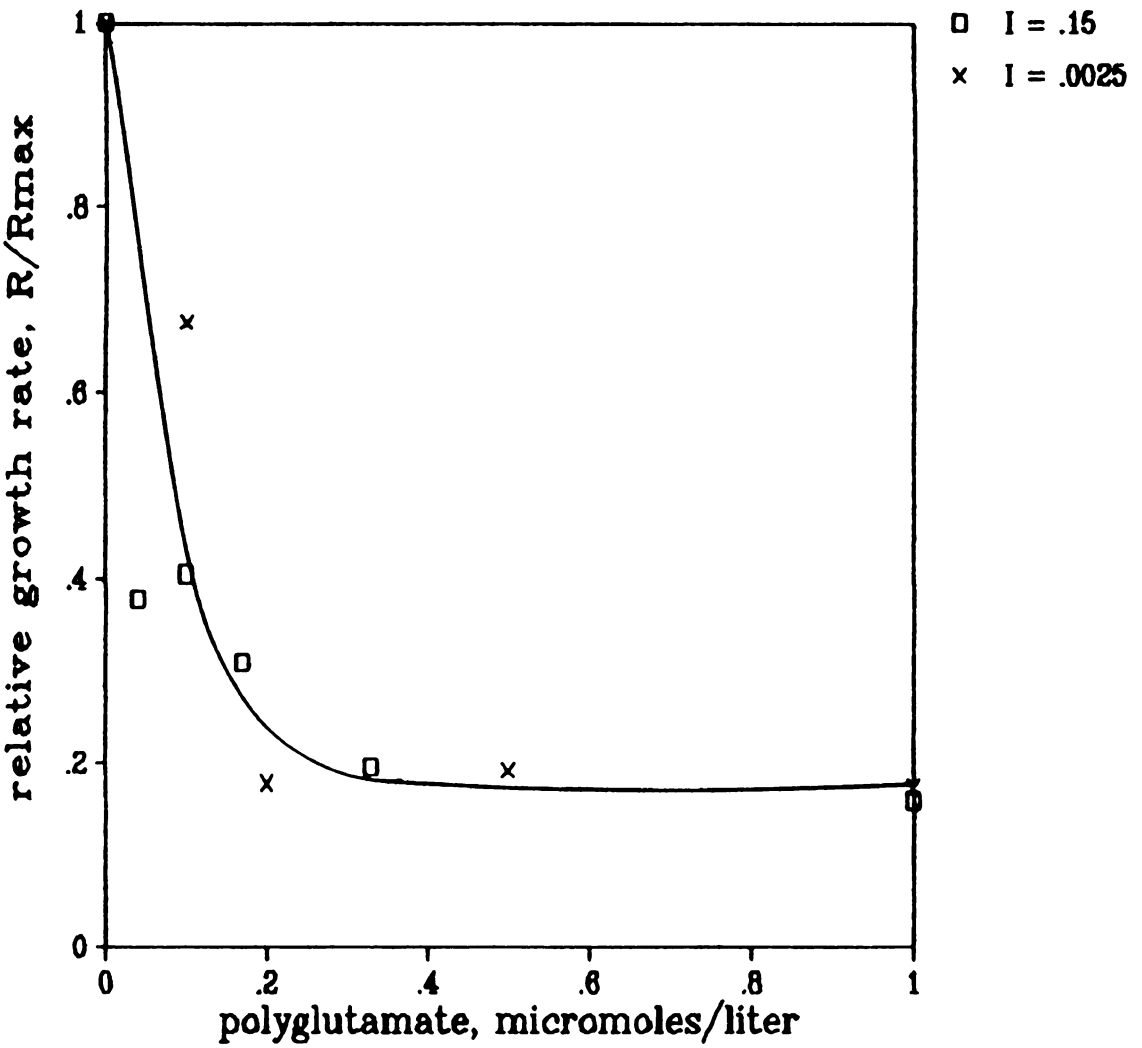

Figure 8-8. COM Relative 110 Face Growth Rate Versus Polyglutamate Molar Concentration for Two Ionic Strengths

I = 0.15 M (KCl), and $[Ca^{2+}]/[C_2O_4^{2-}] = 1$, and $\sigma = 3.71$.

The relative facial growth rate is plotted versus the polyglutamate concentration for pH = 4 and pH = 6 as shown in Figure 8-9 for the 110 face. The curves both show the typical trend of growth rate decreasing towards an asymptotic minimum with increasing polyglutamate concentration. The crystal growth inhibition for pH = 4 is much less than for pH = 6. Similar effects were observed for the other 010 and $\underline{1}01$ faces.

8.3 Effect of Heparin on COM Single Crystal Growth

The study of the effect of heparin on COM single crystal growth was less extensive than that of polyglutamate. Because only one unknown molecular weight was available from the chemical supplier, no molecular weight study was done. Likewise, no studies were done of the ionic strength or pH effect.

The effect of heparin concentration on COM growth rate was investigated in two series of experiments. First, COM facial growth rates were measured over a range of heparin concentrations from 0 to 40 mg/l. The relative supersaturation was held constant at $\sigma = 3.71$ as were the other solution conditions of T = 37 °C, I = 0.15 M (KCl), pH = 6.00, and $T_{Ca} = T_{Ox}$. The results of the first series are plotted as the facial growth rate in microns/minute versus the heparin concentration in mg/l (Figure 8-10). The data of Figure 8-10 were taken for crystals nucleated and grown in the same heparin solution, but, since the resulting crystals retained the general styloid twin habit, it was not necessary to calculate an equivalent circular diameter or to use separate nucleation and growth solutions. As seen in Figure 8-10, the

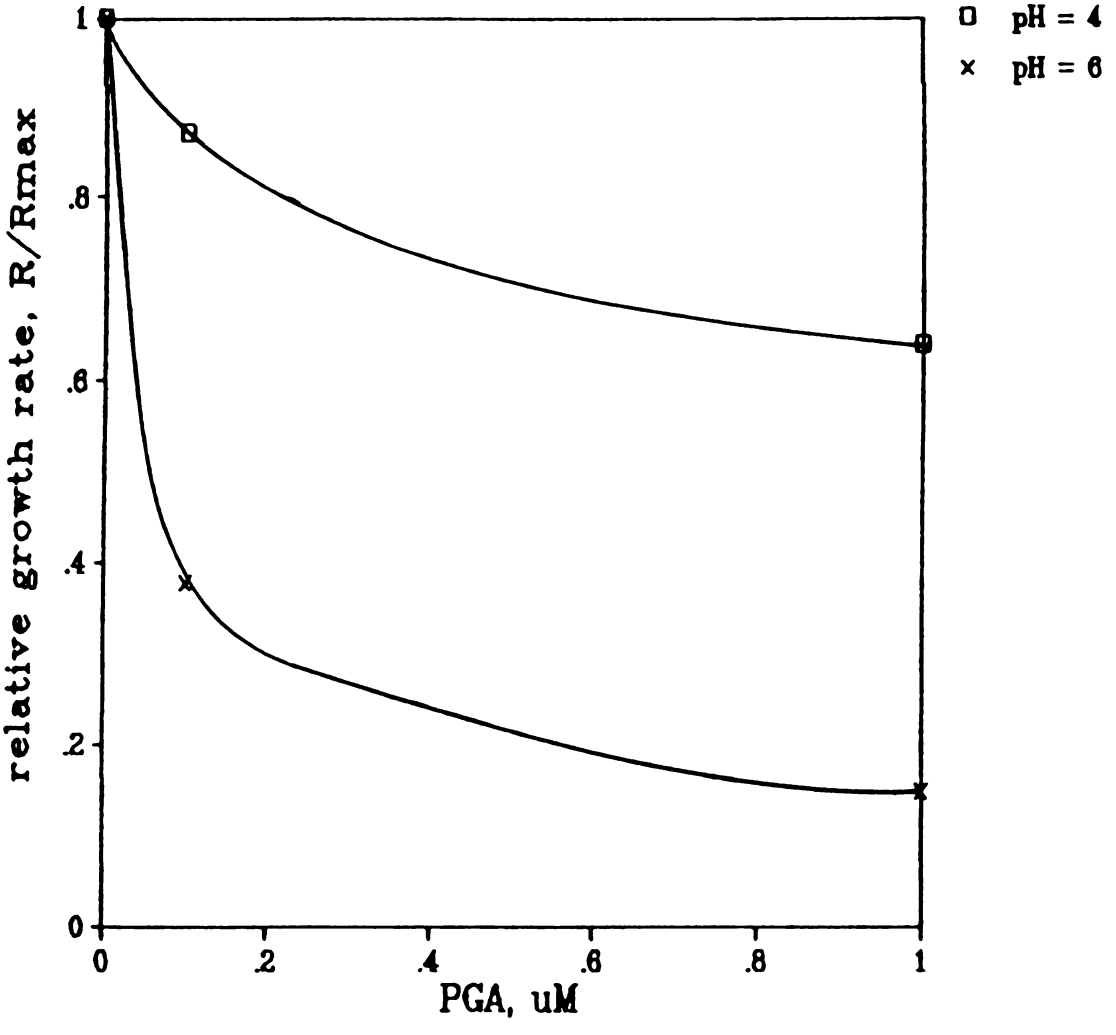

Figure 8-9. COM Relative 110 Face Growth Rate Versus Polyglutamate Molar Concentration for Two pH

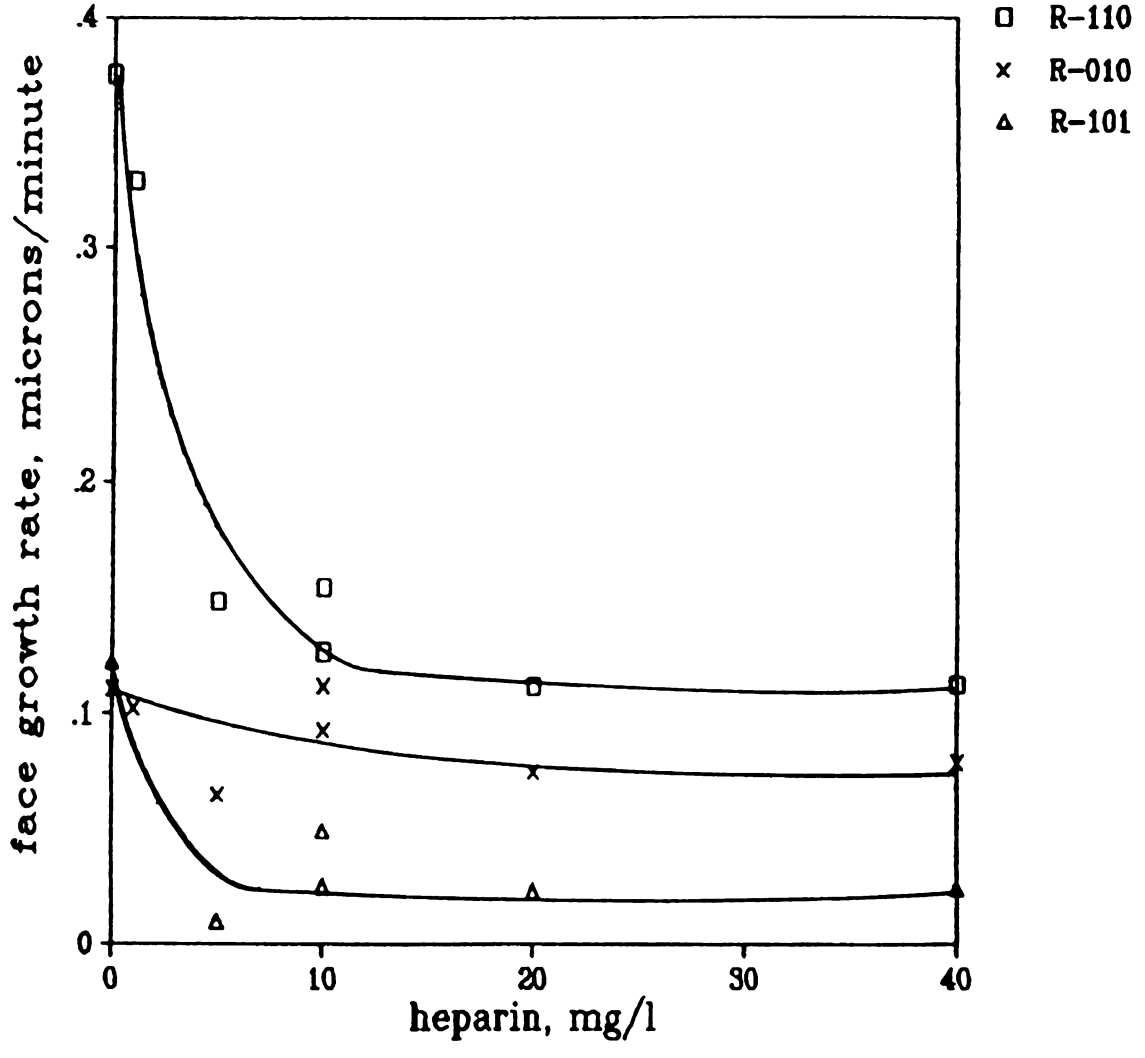

Figure 8-10. COM Face Growth Rate Versus Heparin Concentration

growth rate for each face decreases steadily towards an asymptotic minimum with increasing heparin concentration. This is similar to the effect seen for polyglutamate.

In the second series of experiments, COM facial growth rates were measured at a heparin concentration of 10 mg/l over the range of relative supersaturations $1.49 \leq \sigma \leq 6.64$, all other solution conditions being held constant. The results of these experiments are shown in Figures 8-11, 8-12, and 8-13 for each of the 110, 010, and $\underline{1}01$ faces, respectively. In each of these figures, a curve of facial growth rate versus relative supersaturation is plotted for both 10 mg/l heparin and for no added heparin. The plots for the 110 and $\underline{1}01$ faces show significant growth inhibition by heparin over the entire range of relative supersaturation, while that for the 010 face shows a smaller degree of inhibition, especially at the lower relative supersaturations.

8.4 Mechanism of Crystal Growth Inhibition by Polyelectrolytes

The trends shown in the the COM growth rate data as functions of the various experimental parameters offer a wealth of information about the possible mechanism of growth inhibition by the polyelectrolytes polyglutamate and heparin. Although these are very different compounds chemically, they both exist as polyanions at the solution conditions used. Similarities in their inhibition behavior suggest similar inhibition mechanisms. In addition, certain differences in behavior of polyglutamate and heparin, observed specifically when comparing growth inhibition on the different crystal faces, offer further insight into the inhibition mechanism.

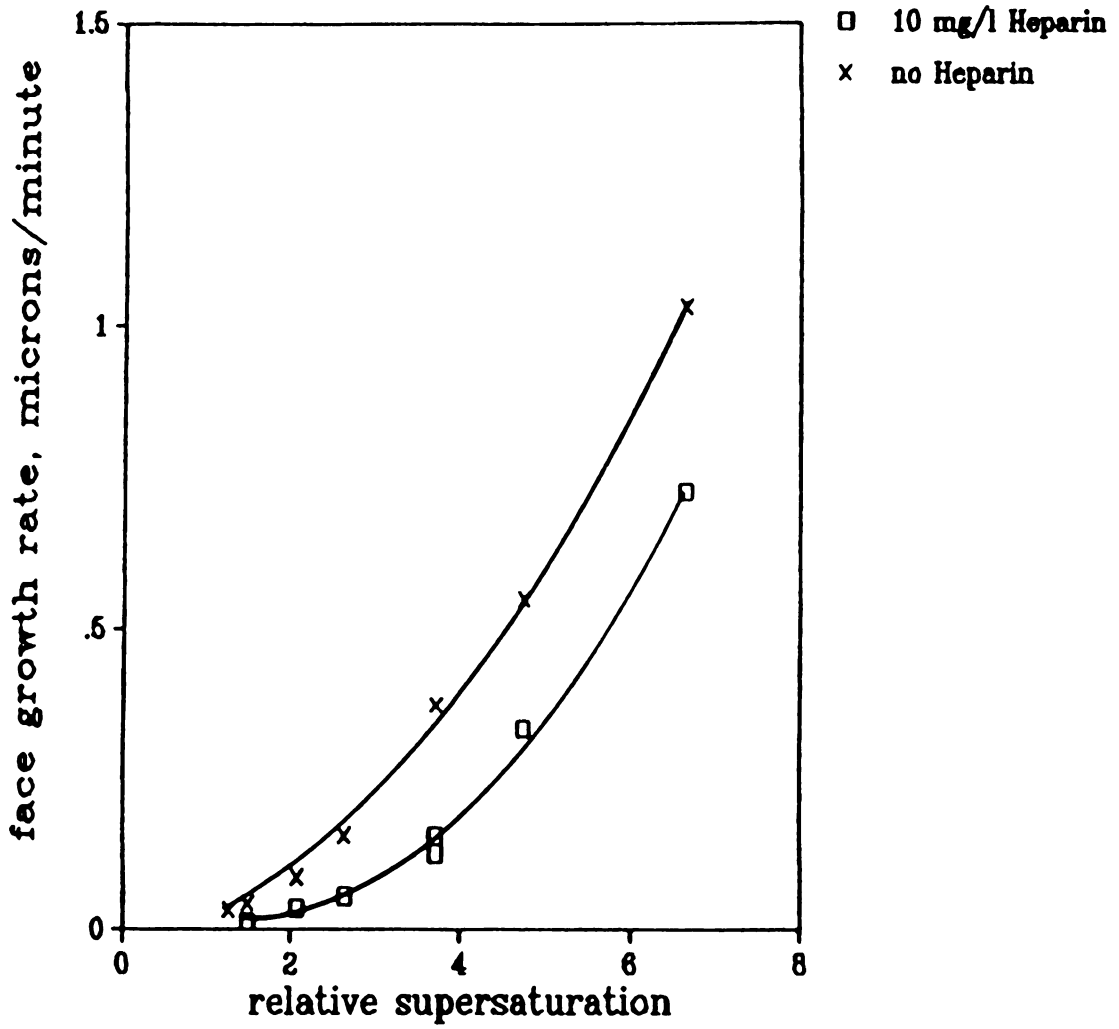

Figure 8-11. COM 110 Face Growth Rate Versus Relative Supersaturation for Two Heparin Concentrations

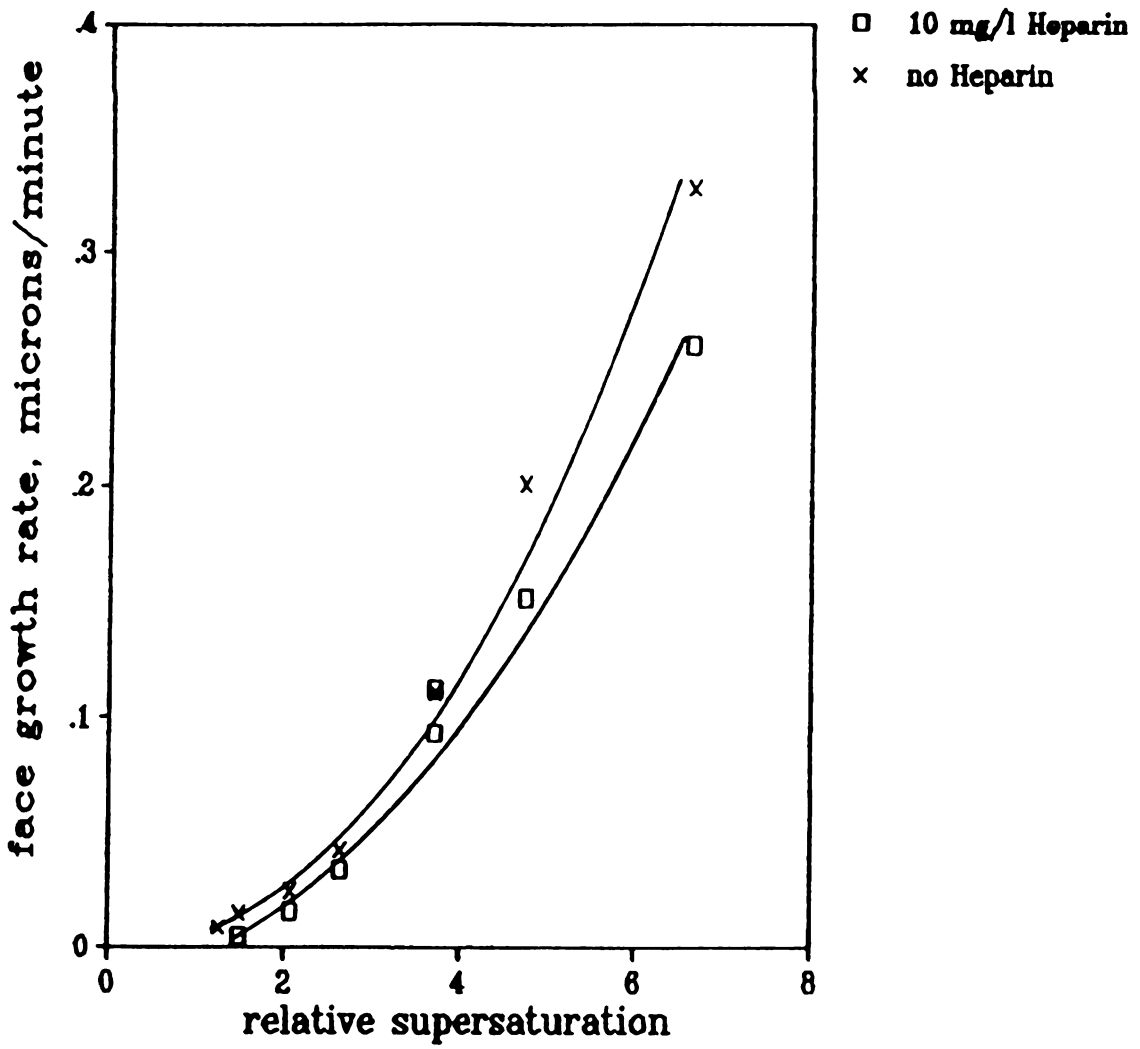

Figure 8-12. COM 010 Face Growth Rate Versus Relative Supersaturation for Two Heparin Concentrations

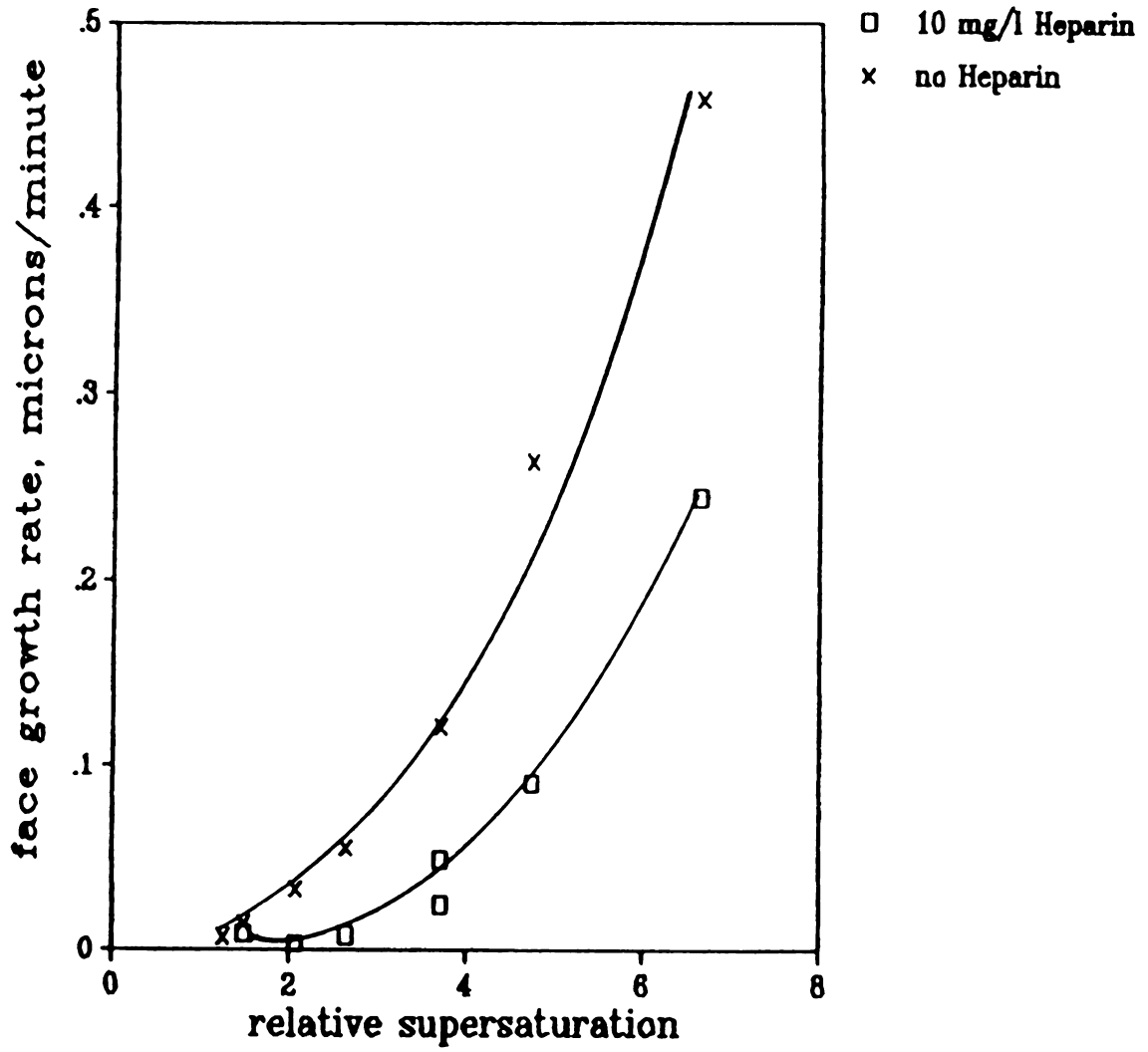

Figure 8-13. COM 101 Face Growth Rate Versus Relative Supersaturation for Two Heparin Concentrations

8.4.1 Growth Inhibition: Polyelectrolyte Adsorption versus Polyelectrolyte Complexation of Ca^{2+}

All of the curves of COM crystal growth rate versus polyelectrolyte concentration show a general trend of growth decreasing towards an asymptotic minimum with increasing polyelectrolyte concentration; this demonstrates growth rate inhibition both by polyglutamate and by heparin. Further analysis of the behavior of growth rate versus polyelectrolyte concentration offers additional information about the way in which the polyelectrolytes interact with the crystal growth mechanism.

The shape of the curves of crystal growth rate versus polyelectrolyte concentration shown in Figures 8-1 through Figure 8-10 shows that the polyelectrolytes interact with the COM crystals in such a way that at high polymer concentrations, the observed growth rate is approximately constant, and further increases in polymer concentration do not significantly decrease the growth rate. This behavior suggests that the COM growth system had somehow become saturated with the polymer. Two possibilities exist that might explain how this "saturation" occurs: solution complexation of Ca^{2+} by the polyelectrolyte or polyelectrolyte adsorption on the crystal surface.

First, the polyelectrolyte could have complexed with free calcium ion Ca^{2+} in solution, thereby reducing the relative supersaturation driving force for crystal growth. The data presented here refute the idea of relative supersaturation reduction as being important in growth inhibition mechanism of COM. Other studies have also suggested that reduction of relative supersaturation through ion complexation is not a significant factor in growth inhibition (Crawford et al., 1968).

The fraction of the Ca^{2+} bound by the polyglutamate depends upon the degree of condensation of the Ca^{2+} counterions onto the polyelectrolyte (Oosawa, 1973). In a mixture of polyvalent counterions such as the mixture of K^+ and Ca^{2+} used in this work, the divalent Ca^{2+} counterions will tend to condense on the polyelectrolyte first, independent of the presence of the monovalent K^+ counterions. The extent of this condensation depends on the expression

$$n^* e^2/\epsilon_o kT\ell = 1/z \qquad (8\text{-}1)$$

where n^* is the number of charged units on the polyelectrolyte minus the number of bound counterions of valence z, e is the charge on an electron, 1.60219×10^{-19} C, ϵ_o is the permittivity (dielectric constant multiplied by the permittivity of vacuum, 8.85419×10^{-12} $C^2/N/m^2$) of the medium, 6.534×10^{-10} $C^2/N/m^2$ for water at 38 °C (CRC, 1977; Levine, 1978), k is the Boltzmann constant, 1.3807×10^{-23} J/K, T is the absolute temperature, K, and ℓ is the polyelectrolyte linear chain length. The number of bound counterions of valence z can be found by calculating n^* from the above expression. For the case of polyglutamate, the distance between the carboxylic side chains on the polypeptide backbone is approximately 3.78 Å based on the average bond radii of the polypeptide chain atoms (Levine, 1978). The linear chain length is then the distance between charged groups times the ratio of the polyelectrolyte to monomer molecular weights, ℓ = 3.78 Å (MW/146). For a polyglutamate molecular weight of 32,000 at a temperature of 37 °C, n^* is calculated to be 4.5. For 32,000/146 = 219 charged monomer groups per chain (assuming complete dissociation of the polyacid at pH 6), this corresponds to about 219 - 4.5 = 214 bound Ca^{2+} counterions per chain. For a polyglutamate concentration of 10^{-7} moles/liter, this

gives a concentration of 10^{-7} x 214 = 2.14 x 10^{-5} moles/liter of bound Ca^{2+} counterions. With the typical Ca^{2+} concentration of 10^{-3} M, this constitutes at most a two percent decrease in the Ca^{2+} available for crystal growth. A measurement of the amount of the fraction of Ca^{2+} bound by polyglutamate showed that less than two percent of the Ca^{2+} was bound by 10^{-6} M polyglutamate at a Ca^{2+} concentration of 10^{-3} M (Barger and Briedis, 1986). The fraction of bound Ca^{2+} is therefore probably within the experimental error of the calculation of relative supersaturation and is not nearly enough to account for the inhibition of COM crystal growth shown in Figure 8-2.

If the complexation of Ca^{2+} were an important factor in the growth inhibition mechanism, the decrease in growth rate would have depended on the number of polyelectrolyte monomer units in solution. Scrutiny of Figures 8-1 and 8-2 shows otherwise. The growth rate behavior of Figures 8-1 and 8-2 suggests two facts about the mechanism of inhibition: first, the degree of inhibition depends not on the number of inhibitor glutamate monomer groups present but on the number of inhibitor polymer molecules. Second, the molecular weight of the polymer has no effect on its ability to inhibit the COM crystal growth rate over the range of molecular weights studied.

This can be understood by considering the following. If the number of monomer glutamate units had been the determining factor in the degree of inhibition, the separate curves of Figure 8-1 would have instead been a single curve of D_{eq}-based growth rate versus the polymer weight concentration because a given weight concentration represents a constant number of monomer units per volume. The observed behavior shows that a given molar concentration of polyglutamate determines the degree of

inhibition, independent of the molecular weight as shown in Figure 8-2. The shape of the curves of D_{eq}-based growth rate versus polymer weight concentration in Figure 8-1 shows that the concentration of glutamate units is not the determining factor in growth rate reduction. Therefore, although complexation of calcium with polyglutamate and reduction of the relative supersaturation does occur to some degree, they are not sufficient to significantly contribute to the inhibition of the crystal growth rate. An analogous analysis for heparin is not possible since only one heparin reagent was available for study.

The second possible explanation of the behavior of the curves in Figure 8-1 through 8-10 is that the polyelectrolyte has adsorbed onto the surface of the crystals, acting to inhibit some step of the crystal growth mechanism. This is the more likely cause of the growth inhibition. Adsorption of polyelectrolytes onto ionic crystal surfaces is a well-known phenomenon and has been discussed by Cafe and Robb (1982), Bain et al. (1982), and Adam and Robb (1983). The adsorption of polyelectrolytes onto calcium oxalate crystals has been studied by Leal and Finlayson (1977) and Hlady (1984).

Several experimental results support the idea of growth inhibition caused by polymer adsorption. The shapes of the curves in Figures 8-1 through 8-10 show that the crystal growth system became "saturated" at high polymer concentrations, i. e., the growth rate stops decreasing significantly even at high polyglutamate concentrations. Theories of the adsorption of polyelectrolytes onto solid surfaces, such as those of Hesselink (1983) and Papenhuijzen et al. (1985a,b), show that polyelectrolyte adsorption follows adsorption isotherms in which the amount of polyelectrolyte adsorbed increases steadily at low polymer

concentrations and levels off at high concentrations, reaching an asymptotic maximum amount of polymer adsorbed. At this maximum, the surface is saturated with the polyelectrolyte and geometric, steric, and chemical factors prohibit further adsorption of polyelectrolyte at the crystal surface. The shape of the curves of Figures 8-1 through 8-10 suggests this type of behavior. At low polyelectrolyte concentrations, the amount adsorbed is low and does not interfere greatly with the crystal growth mechanism. As the polyelectrolyte concentration is increased, the amount adsorbed increases and, in turn, the crystal growth rate becomes more and more inhibited. At very high concentrations, the amount adsorbed and the crystal growth rate both level off. This leveling of the growth rate strongly suggests that the amount of polyglutamate adsorbed at the crystal surface at high concentrations reaches a saturation value.

The polyglutamate molar concentration required to nearly reach the asymptotic growth rate, and thus saturate the surface is greater for a higher COM relative supersaturation as shown in Figures 8-4 and 8-5. This may have been caused in one of least two ways, depending on the mode of interaction of the polymer with the crystal surface. Two possible mechanisms will be discussed below.

According to Garside (1984a), at higher relative supersaturations the surface of a crystal becomes rougher on the molecular scale because of increased step and kink densities, thus offering more "growth sites" for incorporation of growth ions into the crystal lattice. This is the reason that a higher crystal growth rate results from a higher relative supersaturation. The attraction of the polyglutamate for the growth sites may be due to incorporation of the polyglutamate-complexed Ca^{2+} in

calcium lattice sites. If the adsorbing polymer were more readily accommodated by these growth sites than by a smooth crystal surface, then a higher relative supersaturation would give rise to an increased surface capacity for polymer adsorption. In other words, the amount of polymer required to "block" the growth sites and consequently inhibit crystal growth would be higher at higher relative supersaturations. The polymer concentration required to nearly reach the asymptotic minimum growth rate, where the crystal surface would be nearly saturated with polymer, would likewise be increased. This behavior is observed, as seen in Figures 8-4 and 8-5.

Another possible explanation of the effect of relative supersaturation on the inhibitory strength of polyglutamate is that it is due to a kinetic competition between the adsorption of the free Ca^{2+} and the Ca^{2+} bound by polyglutamate. At high relative supersaturations the rate of adsorption of growth ions is greater than that at lower relative supersaturations. Adsorption of the polyglutamate may be non-specific and occur uniformly on the crystal surface as a response to some surface attraction such as surface charge. Assuming that the adsorption of growth ions occurs according to the same mechanism, the higher rate of adsorption of growth ions at a higher relative supersaturation may have retarded the adsorption of the polyglutamate-Ca^{2+} complex of a given concentration when compared with that at a lower relative supersaturation. Consequently, a higher solution concentration of polyglutamate would have been required to achieve adsorption saturation of the crystal surface.

Adsorption of dextran sulfate onto COM crystals has been shown to increase for increasing Ca^{2+} concentration (Hlady, 1984). Similar

effects were seen for other polyanions such as α-globulin, bovine serum albumin, and fibrinogen (Leal and Finlayson, 1977). Electrokinetic data from the former study suggest that COM crystals have an increasingly positive surface charge with increasing Ca^{2+} concentration. The increasing positive charge of the crystal surface may have contributed to the increase in adsorption. In relation to the present study, higher relative supersaturations require higher Ca^{2+} concentrations are used at higher relative supersaturations and a resulting increase in the surface charge may account for the higher polyelectrolyte concentration required to reach adsorption saturation and maximum growth rate inhibition.

8.4.2 Mode of Polyelectrolyte Interference with Crystal Growth Mechanism by Adsorbed Polyelectrolytes

Once the interaction of polyelectrolytes with the crystal surface is reasonably well understood, the effect of this interaction on the crystal growth mechanism must be considered. In the previous subsection, it was concluded that the polyelectrolytes adsorb onto the crystal surface. The mode of inhibition of the crystal growth mechanism by the adsorbed polyelectrolyte theoretically could have been due to interference with any of the growth mechanism steps described in Chapter 3, i. e., diffusion, adsorption, surface migration, or lattice incorporation. The evidence presented here suggests that the interference occurs at the point of incorporation of growth ions into the crystal lattice due to occupation of calcium lattice sites by the polyelectrolyte-bound Ca^{2+}.

The mode of polyelectrolyte interference with the COM crystal growth mechanism can be understood by comparing the inhibition of growth

on the various COM faces both for polyglutamate and for heparin. Figure 8-10 shows the COM facial growth rate versus heparin concentration for each face. There is significant inhibition on the 110 and $\underline{1}01$ faces, but apparently little or no inhibition on the 010 face. This same trend is seen over a range of relative supersaturations as seen in Figures 8-11, 8-12, and 8-13.

The difference in the ability of heparin to inhibit growth rates on different COM faces is best understood by comparing the crystal lattice structure exposed on the 010 and $\underline{1}01$ faces. Figures 2-2 and 2-3 show the lattice structure for each of these faces. The 010 face is parallel to one of the planes of oxalate ions and perpendicular to the other, while the $\underline{1}01$ face cuts across each of these planes of oxalate ions. The $\underline{1}01$ face therefore has oxalate sites from both planes exposed in such a way as to allow association with adsorbing polyelectrolytes, while the 010 face has oxalate sites from only one plane. Oxalate lattice sites situated in the plane parallel to the 010 face cannot as easily accommodate functional groups associated with approaching polyelectrolyte-bound calcium ions because of the geometric orientation of the sites. If carboxylic and/or sulfate functional groups bound to Ca^{2+} ions adsorb through association with the oxalate lattice sites, an adsorbing polyelectrolyte would be more easily accommodated on the $\underline{1}01$ face. As the polyelectrolyte is more easily accommodated, a greater amount is adsorbed. This would lead to a greater degree of inhibition on the $\underline{1}01$ face than on the 010 face. This is the behavior observed in Figure 8-10 for heparin.

Similar behavior is seen for growth inhibition by polyglutamate. The degree of growth inhibition by polyglutamate on the $\underline{1}01$ and 010

faces is apparently the same, as seen in Figure 8-3. However, when plotted in terms of the relative growth rate as shown in Figures 8-6 and 8-7, it becomes apparent that the degree of inhibition is greater for the $\bar{1}01$ face than for the 010 face, similar to the heparin behavior. In contrast to the observed behavior for heparin, however, there is a significant inhibition by polyglutamate on the 010 face. For heparin, the 010 face shows little growth inhibition.

At the prevailing solution conditions of ionic strength of I = 0.15 M and pH = 6, polyglutamate is in an extended random coil conformation (Nagasawa and Holtzer, 1963) rather than the helix prevalent at lower pH and ionic strength. Assuming heparin also exists as a random coil in solution, a significant number of monomer units of either of the adsorbed polyelectrolyte can be assumed to be associated with the crystal in adsorbed "trains" on the surface (Hesselink, 1983). A train of adsorbed polymer is several adjacent monomer units of the same polymer molecule that are adsorbed on a surface. If this adsorption occurs through incorporation of polyelectrolyte-bound Ca^{2+} into calcium lattice sites with subsequent orientation of anionic functional groups in the oxalate lattice sites, adsorption of monomer units in trains would be dependent on the ability of the polyelectrolyte chain to fit into the crystal lattice. Apparently, the bulky heparin polysaccharide backbone and nearness of the anionic functional groups to the heparin backbone preclude significant adsorption on the 010 face due to a steric repulsion of the large cyclic groups by the crystal lattice. For polyglutamate, the smaller polypeptide backbone and greater spacing of the anionic carboxylic group from the backbone presents less steric hindrance. Sarig et al. (1984) have stated that glutamic acid is

structurally compatible with calcium oxalate. An inhibition mechanism in which the carboxylate groups of polyglutamate become intimately associated with the crystal lattice is therefore feasible.

The curves of COM crystal growth rate versus polyglutamate concentration at various ionic strengths and pH offer further evidence that the specific attraction of the anionic functional group-oxalate lattice site is the most significant cause of the crystal-polyelectrolyte interaction. Figure 8-8 shows the effect of ionic strength on the ability of polyglutamate to inhibit COM 110 face growth. Hesselink (1983) states that polyelectrolyte adsorption should increase with increasing ionic strength because of reduced electrostatic interactions which usually oppose adsorption. However, as seen in Figure 8-8, the ionic strength has no discernible effect on the ability of polyglutamate to inhibit growth. This fact implies that electrostatic effects on adsorption were not significant in the growth inhibition mechanism.

The effect of the degree of proton dissociation of polyglutamate on its ability to inhibit COM 110 face growth is shown in Figure 8-9. At pH = 6, the polyelectrolyte is nearly completely dissociated; assuming a pK_a of 4.3 (Stryer, 1981), the polyelectrolyte is approximately 98 percent dissociated following a calculation using the Henderson-Hasselbach equation. At the lower value of pH = 4, the polyelectrolyte is about 33 percent dissociated. As can be seen from Figure 8-9, the growth rate is not inhibited nearly as much for the lower pH. The implication is that the adsorption of polyglutamate occurs more readily at the higher pH, where a greater number of charged carboxylic groups are available to bind Ca^{2+} and subsequently interfere in the crystal

growth mechanism as discussed above. Such behavior is in contrast to theoretical predictions for polyelectrolyte adsorption onto charged surfaces. Hesselink (1983) states that the amount of polyelectrolyte adsorbed usually decreases with increasing degree of dissociation due to electrostatic effects. If that were the case, the growth rate curve for pH = 4 in Figure 8-9 would have been below that for pH = 6. However, experimental results show that the effect of pH on growth inhibition apparently is not the result of electrostatic effects. Instead, a likely cause is the specific interaction of the bound Ca^{2+}-carboxylic groups with the crystal, possibly at the oxalate and calcium lattice sites. A greater number of deprotonated carboxylate groups on the polyelectrolyte increases the number of lattice sites that may be occupied by a polyelectrolyte molecule, thus preventing the incorporation of free growth ions into the lattice. Therefore, at the higher pH, the more deprotonated polyelectrolyte is a better inhibitor of crystal growth.

Incorporation of the polyelectrolyte growth modifier directly into the crystal lattice is seemingly demonstrated in Figure 8-14. In Figure 8-14, COM crystals grown in a polyglutamate solution and then partially dissolved in pH 3.0, zero supersaturation solution containing no polyglutamate are shown. As can be seen, a transluscent, apparently gelatinous mass remains where the mineral portion of the crystal has dissolved. If it is assumed that this mass, which is not apparent in crystals grown without growth modifier, is polyglutamate, then the polyelectrolyte is distributed throughout the crystal and has indeed become part of the crystal during growth. The proposed mechanism for crystal growth inhibition by polyelectrolytes, i.e. adsorption of the

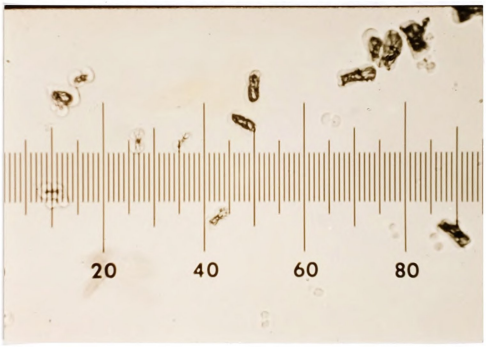

Figure 8-14. Polyglutamate Matrix Remaining After Dissolution of COM Crystals in pH 3.0 Solution

Ca^{2+}-polyelectrolyte complex onto the crystal surface and subsequent incorporation of carboxylate/calcium side groups into the oxalate and calcium lattice sites, is supported by the appearance of the partially dissolved crystals showed distribution of polyglutamate throughout the crystal.

Chapter 9. Summary and Recommendations

The single crystal growth of calcium oxalate monohydrate from solution has been studied under various solution conditions using a photomicroscopic technique. The solution effects studied included the effects of relative supersaturation, temperature, ionic strength, ion ratio, and polyelectrolyte growth modifier concentration. The results of this study have application to the understanding of COM crystal growth and growth inhibition by polyelectrolytes in kidney stone disease and to the growth of sparingly soluble salts in general. The results obtained, especially those such as the differences in inhibitory strength of polyelectrolytes on 010 and $\bar{1}01$ crystal faces, demonstrated the superiority of the photomicroscopic technique over conventional batch and continuous crystallization techniques used to study crystal growth kinetics.

The results of this study are summarized in the following section. Recommendations for future investigations extending and complementing this research follow in section 9.2.

9.1 Summary of Experimental Results

The following is a summary of the results of this study of the single crystal growth of calcium oxalate monohydrate:

1. COM single crystal growth rate shows a second-order dependence on the relative supersaturation with an average activation energy for growth of 50.4 kJ/gmol. These results indicate a surface-integration controlled growth mechanism.

2. Growth is fastest on the 110 faces, followed by approximately equal growth rates on the 010 and $\bar{1}01$ faces. The higher growth rate of

the 110 faces is reflected by the elongated styloid growth habit of COM. A transition in growth habit from styloid to rhomboid is indicative of the decreasing prevalence of the 010 faces as relative supersaturation increases, a phenomenon shown by a decreasing length ratio at 25 °C. The 010 faces are apparently replaced by 011 faces at higher relative supersaturation.

3. COM single crystal growth rate shows a maximum at equimolar ion ratio ($[Ca^{2+}]/[C_2O_4^{2-}] = 1$) for an ionic strength of 0.15 M. The growth rate decreases at low and high ion ratios at this ionic strength. Without added background electrolyte to increase the ionic strength, the growth rate maximum no longer appears and growth rate is independent of the ion ratio. The results suggest that relative supersaturation is not a complete expression of the driving force for electrolyte crystal growth.

4. COM single crystal growth rates measured at constant relative supersaturation and equimolar ion ratio increase with increasing ionic strength, asymptotically approaching a maximum growth rate at high ionic strength (greater than about 0.15 M). This is probably due to a compression of the electrical double layer at the crystal/solution interface, with the general shape of the curve of growth rate versus ionic strength similar to that predicted by an analysis that utilized the Gouy-Chapman theory of the double layer.

5. COM single crystal growth rate is inhibited by the anionic polyelectrolytes polyglutamate and heparin. The shape of the curves of COM growth rate versus polyelectrolyte concentration indicates an inhibition mechanism with adsorption of polyelectrolytes on crystal surfaces rather than reduction of relative supersaturation through

complexation of calcium by the polyelectrolyte.

6. Differences in the degree of inhibition on the 010 and $\bar{1}01$ faces indicate that the mechanism of inhibition is probably through incorporation of polyelectrolyte-bound calcium ions in the crystal lattice with orientation of polyelectrolyte anionic functional groups in oxalate lattice sites. Differences in the orientation of oxalate groups on the 010 and $\bar{1}01$ faces indicates easier accomodation of adsorbed polyelectrolyte into lattice sites by approach of the polyelectrolyte towards the $\bar{1}01$ face rather than towards the 010 face. Results of the measurement of COM growth rate in the presence of polyglutamate at various pH values and ionic strengths support this mechanism.

7. A greater degree of inhibition of growth rate on the $\bar{1}01$ face than on the 010 face is reflected in the growth habits observed for COM crystals grown in the presence of heparin or polyglutamate. Crystals nucleated in polyelectrolyte-free solution but grown in dilute polyelectrolyte solution show thin, elongated styloid habits reflecting a lesser degree of inhibition on the 010 face than on the $\bar{1}01$ face.

8. COM crystals nucleated and grown in the presence of polyglutamate show irregular growth habits that are pinched in the center, reminiscent of the "dumbbell" COM habits frequently reported in the urology literature.

9.2 Recommendations for Future Work

The following are suggested as subjects for future investigations of COM single crystal growth:

1. Evaluate the facial growth rates in terms of the ion lattice structure exposed on each crystal face. Differences in the empirical

rate constant measured for face might be explained in this way.

2. Measure growth rate versus ionic strength with various electrolytes, e.g., the alkali halides with a common cation or anion, to allow a more indepth analysis of the double layer effects on growth rate. This may also lead to an explanation of the anomalous effect of LiCl on the 010 face, which may simply reflect the difference in lattice structure on the different faces.

3. Measure growth rate versus ionic strength at several non-equimolar ion ratios to determine if the effect is the same for equimolar conditions. This may offer more information about double layer effects on crystal growth.

4. As a complement to the measurement of growth rate versus ionic strength, measure growth rate as a function of ion ratio at low ionic strength (about 0.01 M) for various electrolytes, e.g., an alkali halide series, to determine if the effect of ion ratio is due to a reduced adsorption tendency of Ca^{2+} and $C_2O_4^{2-}$.

5. Measure COM growth rate in the presence of heparin at various pH values and ionic strengths to see if the results parallel those observed for polyglutamate.

6. Measure COM growth rate in the presence of other polyelectrolytes including anionic polyelectrolytes such as chondroitin sulfate, hyaluronic acid, and aspartic acid, and cationic polyelectrolytes such as polylysine. Compare face growth rates with those measured in the presence of polyglutamate and heparin.

7. Measure the Raman spectrum of polyelectrolyte-modified COM crystals. Changes in the spectrum when compare to that of unmodified crystals may reflect the presence of the polyelectrolyte and offer

evidence of the mechanism of interaction between the adsorbed polyelectrolyte and the crystal lattice.

8. Measure the zeta potential of growing COM crystals in solutions of various ionic strengths and various $[Ca^{2+}]/[C_2O_4^{2-}]$ to confirm the effects of double layer compression on growth rate.

9. Measure the zeta potential of COM crystals grown with and without polyelectrolytes to determine how surface charge affects growth rate inhibition.

APPENDIX A

Appendix A. Experimental Solution Conditions

Table A-1 Experimental Conditions for Variable σ Series at 37°C

pH = 6.00; T = 37 °C; I = 0.15 M; $T_{Ca} = T_{Ox}$

Reagents: $CaCl_2 \cdot 2H_2O$, $K_2C_2O_4 \cdot H_2O$, KCl

T_{Ca},M	.450	.500	.625	.750	1.000	1.250	1.750
T_{Ox},M	.450	.500	.625	.750	1.000	1.250	1.750
[KCl]	.1473	.1470	.1463	.1455	.1440	.1425	.1395
$[Ca^{2+}]$	.4247	.4689	.5771	.6819	.8822	1.0709	1.4176
$[C_2O_4^{2-}]$	.2857	.3158	.3894	.4611	.5885	.7315	.9795
$[CaC_2O_4]$	.0238	.0290	.0440	.0616	.1037	.1536	.2726
$[K^+]$	.1481	.1478	.1474	.1468	.1457	.1447	.1425
$[KC_2O_4^-]$	.1369	.1511	.1857	.2191	.2827	.3426	.4522
$[HC_2O_4^-]$	.0026	.0029	.0035	.0042	.0054	.0066	.0089
$[Ca(C_2O_4)_2^{2-}]$	.0001	.0002	.0003	.0005	.0011	.0019	.0046
$[H_2C_2O_4]$	0	0	0	0	0	0	0
$[Ca_2C_2O_4^{2+}]$	.0007	.0010	.0018	.0030	.0065	.0117	.0276
I, M	.1501	.1501	.1501	.1500	.1500	.1499	.1496
σ	1.26	1.49	2.07	2.64	3.71	4.74	6.64

All concentrations except [KCl] and $[K^+]$ are multiplied by 1000. I and σ are unmultiplied values. Total potassium includes that from the oxalate reagent.

Table A-2 Experimental Conditions for Variable σ Series at 15°C

pH = 6.00; T = 15 °C; I = 0.15 M; $T_{Ca} = T_{Ox}$

Reagents: $CaCl_2 \cdot 2H_2O$, $K_2C_2O_4 \cdot H_2O$, KCl

T_{Ca}, M	.625	.750	1.000	1.125
T_{Ox}, M	.625	.750	1.000	1.125
[KCl]	.1463	.1455	.144	.1432
$[Ca^{2+}]$	.5843	.6920	.8988	.9982
$[C_2O_4^{2-}]$	.4335	.5143	.6707	.7465
$[CaC_2O_4]$	.0373	.0524	.0887	.1097
$[K^+]$	.1474	.1468	.1458	.1452
$[KC_2O_4^-]$	.1488	.1759	.2277	.2525
$[HC_2O_4^-]$	.0033	.0039	.0051	.0057
$[Ca(C_2O_4)_2^{2-}]$	.0003	.0005	.0010	.0014
$[H_2C_2O_4]$	0	0	0	0
$[Ca_2C_2O_4^{2+}]$	.0016	.0026	.0057	.0078
I, M	.1502	.1502	.1502	.1501
σ	3.28	4.08	5.61	6.35

All concentrations except [KCl] and $[K^+]$ are multiplied by 1000. I and σ are unmultiplied values. Total potassium includes that from the oxalate reagent.

Table A-3 Experimental Conditions for Variable σ Series at 25°C

pH = 6.00; T = 25 °C; I = 0.15 M; $T_{Ca} = T_{Ox}$

Reagents: $CaCl_2 \cdot 2H_2O$, $K_2C_2O_4 \cdot H_2O$, KCl

T_{Ca}, M	.500	.750	1.000	1.125	1.250	1.500
T_{Ox}, M	.500	.750	1.000	1.125	1.250	1.500
[KCl]	.1470	.1455	.1440	.1432	.1425	.1410
$[Ca^{2+}]$	.4714	.6871	.8907	.9883	1.0833	1.2656
$[C_2O_4^{2-}]$	.3345	.4895	.6373	.7088	.7787	.9144
$[CaC_2O_4]$	.0267	.0569	.0960	.1185	.1427	.1959
$[K^+]$	.1479	.1468	.1457	.1452	.1447	.1436
$[KC_2O_4^-]$	.1348	.1959	.2532	.2805	.3072	.3582
$[HC_2O_4^-]$	.0028	.0040	.0053	.0059	.0064	.0076
$[Ca(C_2O_4)_2^{2-}]$	.0002	.0005	.0011	.0015	.0019	.0031
$[H_2C_2O_4]$	0	0	0	0	0	0
$[Ca_2C_2O_4^{2+}]$	.0009	.0028	.0061	.0084	.0110	.0177
I, M	.1501	.1501	.1501	.1500	.1500	.1499
σ	1.98	3.34	4.65	5.27	5.89	7.07

All concentrations except [KCl] and $[K^+]$ are multiplied by 1000. I and σ are unmultiplied values. Total potassium includes that from the oxalate reagent.

Table A-4 Experimental Conditions for Variable σ Series at 50°C

pH = 6.00; T = 50 °C; I = 0.15 M; $T_{Ca} = T_{Ox}$

Reagents: $CaCl_2 \cdot 2H_2O$, $K_2C_2O_4 \cdot H_2O$, KCl

T_{Ca}, M	.750	1.000	1.250	1.750	2.250
T_{Ox}, M	.750	1.000	1.250	1.750	2.250
[KCl]	.1455	.1440	.1425	.1395	.1365
$[Ca^{2+}]$	.6773	.8748	1.0603	1.3997	1.7032
$[C_2O_4^{2-}]$	.4330	.5622	.6853	.9159	1.1295
$[CaC_2O_4]$	.0658	.1104	.1631	.2881	.4330
$[K^+]$	.1468	.1457	.1446	.1425	.1404
$[KC_2O_4^-]$	.2427	.3128	.3786	.4989	.6067
$[HC_2O_4^-]$	.0043	.0056	.0068	.0091	.0112
$[Ca(C_2O_4)_2^{2-}]$	.0005	.0011	.0019	.0046	.0085
$[H_2C_2O_4]$	0	0	0	0	0
$[Ca_2C_2O_4^{2+}]$	.0032	.0069	.0123	.0288	.0527
I, M	.1500	.1499	.1498	.1495	.1490
σ	2.02	2.91	3.75	5.32	6.74

All concentrations except [KCl] and $[K^+]$ are multiplied by 1000. I and σ are unmultiplied values. Total potassium includes that from the oxalate reagent.

Table A-5 Experimental Conditions for Variable I Series with KCl

pH = 6.00; T = 37 °C; $[Ca^{2+}]/[C_2O_4^{2-}] \approx 1$; $\sigma \approx 3.71$

Reagents: $CaCl_2 \cdot 2H_2O$, $K_2C_2O_4 \cdot H_2O$, KCl

T_{Ca}, M	.405	.4702	.7080	.7612	.8400	.9574	.9585
T_{Ox}, M	.405	.4950	.8850	.9950	1.2000	1.6650	2.1300
[KCl]	0	.0071	.0700	.0946	.1438	.2923	.4914
$[Ca^{2+}]$	.2964	.3598	.5939	.6466	.7237	.8390	.8405
$[C_2O_4^{2-}]$	.2910	.3619	.5983	.6501	.7344	.8452	.8428
$[Ca^{2+}]/[C_2O_4^{2-}]$	1.019	.994	.993	.995	.985	.993	.997
$[CaC_2O_4]$	.1037	.1044	.1042	.1038	.1042	.1044	.1040
$[K^+]$	.0008	.0081	.0716	.0964	.1459	.2949	.4945
$[KC_2O_4^-]$	.0019	.0191	.1696	.2276	.3467	.6992	1.1672
$[HC_2O_4^-]$	.0052	.0056	.0063	.0064	.0067	.0069	.0069
$[Ca(C_2O_4)_2^{2-}]$	.0005	.0007	.0011	.0012	.0013	.0015	.0015
$[H_2C_2O_4]$	0	0	0	0	0	0	0
$[Ca_2C_2O_4^{2+}]$	.0022	.0027	.0044	.0048	.0054	.0063	.0062
I, M	.0024	.0100	.0749	.1000	.1500	.3000	.5000
σ	3.71	3.73	3.73	3.72	3.73	3.73	3.72

All concentrations except [KCl] and $[K^+]$ are multiplied by 1000. I and σ are unmultiplied values. Total potassium includes that from the oxalate reagent.

Table A-6 Experimental Conditions for Variable I Series with LiCl

pH = 6.00; T = 37 °C; $[Ca^{2+}]/[C_2O_4^{2-}] \approx 1$; $\sigma \approx 3.71$

Reagents: $CaCl_2 \cdot 2H_2O$, $H_2C_2O_4 \cdot 2H20$ and $LiOH \cdot H_2O$, LiCl

T_{Ca}, M	.4018	.5988	.7051	.8394	.9562	.9557
T_{Ox}, M	.4100	.7900	1.1000	1.6300	2.5500	3.6200
[LiCl]	0	.0334	.0697	.1430	.2906	.4884
$[Ca^{2+}]$	.2935	.4871	.5920	.7244	.8388	.8386
$[C_2O_4^{2-}]$	.2936	.4870	.5960	.7261	.8388	.8384
$[Ca^{2+}]/[C_2O_4^{2-}]$	1.000	1.000	.993	.998	1.000	1.000
$[CaC_2O_4]$	.1035	.1036	.1033	.1031	.1036	.1032
$[Li^+]$	.0008	.0348	.0715	.1455	.2941	.4930
$[LiC_2O_4^-]$	.0044	.1881	.3879	.7863	1.5916	2.6624
$[HC_2O_4^-]$	.0053	.0060	.0063	.0066	.0068	.0068
$[Ca(C_2O_4)_2^{2-}]$	.0005	.0009	.0011	.0013	.0015	.0015
$[H_2C_2O_4]$	0	0	0	0	0	0
$[Ca_2C_2O_4^{2+}]$	.0022	.0036	.0044	.0053	.0062	.0062
I, M	.0024	.0375	.0750	.1500	.3000	.5000
σ	3.71	3.71	3.71	3.70	3.71	3.70

All concentrations except [LiCl] and $[Li^+]$ are multiplied by 1000. I and σ are unmultiplied values. Total lithium includes that from the hydroxide reagent.

Table A-7 Experimental Conditions for Variable $[Ca^{2+}]/[C_2O_4^{2-}]$ Series with KCl, I = 0.15 M

pH = 6.00; T = 37 °C; $\sigma \approx 3.71$

Reagents: $CaCl_2 \cdot 2H_2O$, $K_2C_2O_4 \cdot H2O$, KCl

T_{Ca}, M	.1900	.2768	.3475	.4377	.7150	.8400	1.0000
T_{Ox}, M	10.5700	4.9000	3.4750	2.5300	1.4300	1.2000	1.0000
[KCl]	.1139	.1330	.1377	.1405	.1434	.1438	.1440
$[Ca^{2+}]$	.0726	.1638	.2349	.3255	.5998	.7237	.8822
$[C_2O_4^{2-}]$	7.2696	3.2610	2.2798	1.6357	.8896	.7344	.5995
$[Ca^{2+}]/[C_2O_4^{2-}]$	.0100	.0502	.103	.199	.674	.985	1.472
$[CaC_2O_4]$	.1034	.1047	.1050	.1044	.1046	.1042	.1037
$[K^+]$	.1319	.1413	.1436	.1448	.1458	.1459	.1457
$[KC_2O_4^-]$	3.1045	1.4916	1.0595	.7667	.4200	.3467	.2827
$[HC_2O_4^-]$	.0660	.0296	.0207	.0148	.0081	.0067	.0054
$[Ca(C_2O_4)_2^{2-}]$	.0130	.0059	.0041	.0030	.0016	.0013	.0011
$[H_2C_2O_4]$	0	0	0	0	0	0	0
$[Ca_2C_2O_4^{2+}]$	.0005	.0012	.0018	.0024	.0045	.0054	.0065
I, M	.1500	.1500	.1500	.1499	.1500	.1500	.1500
σ	3.71	3.74	3.74	3.73	3.74	3.73	3.71

Table A-7 continued

T_{Ca}, M	1.7494	2.3250	2.4317	3.3908	7.4803
T_{Ox}, M	.5910	.4650	.4470	.3460	.2610
[KCl]	.1431	.1418	.1416	.1390	.1272
$[Ca^{2+}]$	1.6225	2.1915	2.2975	3.2472	7.2690
$[C_2O_4^{2-}]$	.3222	.2359	.2238	.1539	.0727
$[Ca^{2+}]/[C_2O_4^{2-}]$	5.036	9.290	10.266	21.099	99.986
$[CaC_2O_4]$	.1025	.1014	.1008	.0980	.1036
$[K^+]$	.1441	.1426	.1424	.1396	.1277
$[KC_2O_4^-]$	.1503	.1089	.1031	.0695	.0300
$[HC_2O_4^-]$	.0029	.0029	.0020	.0014	.0007
$[Ca(C_2O_4)_2^{2-}]$	.0006	.0004	.0004	.0003	.0001
$[H_2C_2O_4]$	0	0	0	0	0
$[Ca_2C_2O_4^{2+}]$	.0119	.0159	.0165	.0227	.0538
I, M	.1499	.1499	.1500	.1499	.1500
σ	3.69	3.66	3.65	3.58	3.71

All concentrations except [KCl] and $[K^+]$ are multiplied by 1000. I and σ are unmultiplied values. Total potassium includes that from the oxalate reagent.

Table A-8 **Experimental Conditions for Variable $[Ca^{2+}]/[C_2O_4^{2-}]$ Series with KCl, I ≈ 0 (no added KCl)**

pH = 6.00; T = 37 °C; $\sigma \approx 3.71$

Reagents: $CaCl_2 \cdot 2H_2O$, $K_2C_2O_4 \cdot H20$

T_{Ca}, M	.1512	.2160	.4050	1.0500	3.8701
T_{Ox}, M	4.3700	1.0800	.4050	.2100	.1690
[KCl]	0	0	0	0	0
$[Ca^{2+}]$	.0400	.1078	.2964	.9345	3.7114
$[C_2O_4^{2-}]$	3.9947	.9400	.2910	.0991	.0370
$[Ca^{2+}]/[C_2O_4^{2-}]$	.0100	.115	1.019	9.430	100.308
$[CaC_2O_4]$	.1034	.1049	.1037	.1018	.1037
$[K^+]$	8.5394	2.1450	.8081	.4197	.3379
$[KC_2O_4^-]$	.2006	.0150	.0019	.0003	.0001
$[HC_2O_4^-]$	.0567	.0159	.0052	.0017	.0006
$[Ca(C_2O_4)_2^{2-}]$	.0071	.0017	.0005	.0002	.0001
$[H_2C_2O_4]$	0	0	0	0	0
$[Ca_2C_2O_4^{2+}]$	.0003	.0008	.0022	.0068	.0275
I, M	.0170	.0045	.0024	.0036	.0117
σ	3.71	3.74	3.71	3.67	3.72

All concentrations are multiplied by 1000. I and σ are unmultiplied values. Total potassium includes that from the oxalate reagent.

Table A-9 Experimental Conditions for Variable $[Ca^{2+}]/[C_2O_4^{2-}]$ Series with LiCl, I = 0.15 M

pH = 6.00; T = 37 °C; $\sigma \approx 3.71$

Reagents: $CaCl_2 \cdot 2H_2O$, $H_2C_2O_4 \cdot 2H20$ and $LiOH \cdot H_2O$, LiCl

T_{Ca}, M	.1901	.3402	.8394	2.4335	7.4660
T_{Ox}, M	14.4000	4.8600	1.6300	.5950	.2990
[LiCl]	.1063	.1349	.1430	.1413	.1272
$[Ca^{2+}]$	.0726	.2295	.7244	2.2961	7.2559
$[C_2O_4^{2-}]$	7.2690	2.2959	.7261	.2292	.0725
$[Ca^{2+}]/[C_2O_4^{2-}]$	.0100	.100	.998	10.018	100.081
$[CaC_2O_4]$	.1034	.1033	.1031	.1032	.1031
$[Li^+]$	.1282	.1422	.1455	.1422	.1277
$[LiC_2O_4^-]$	6.9351	2.4301	.7863	.2428	.0690
$[HC_2O_4^-]$	.0659	.0208	.0066	.0021	.0007
$[Ca(C_2O_4)_2^{2-}]$	.0130	.0041	.0013	.0004	.0001
$[H_2C_2O_4]$	0	0	0	0	0
$[Ca_2C_2O_4^{2+}]$	.0005	.0017	.0053	.0169	.0534
I, M	.1500	.1500	.1500	.1500	.1500
σ	3.71	3.71	3.70	3.70	3.70

All concentrations except [LiCl] and $[Li^+]$ are multiplied by 1000. I and σ are unmultiplied values. Total lithium includes that from the hydroxide reagent.

APPENDIX B

Appendix B. Raman Spectra of Calcium Oxalate

Raman spectra of single crystals of each of the three phases of calcium oxalate were taken using a laser Raman microprobe (Spex 1406) with a laser of wavelength 5145 Å. These crystals were grown using the photomicroscopic technique and appeared similar to the crystals shown in Chapter 5. Raman spectra over the frequency range of approximately 1380 cm^{-1} to 1580 cm^{-1} are shown in Figures B-1, B-2, and B-3 for the monohydrate COM, the dihydrate COD, and the trihydrate COT, respectively.

The characteristic band in this frequency range for calcium oxalate is due to the symmetric stretching of the oxalate carboxylate groups (Shippey, 1981; Duval and Chondrate, 1985). For COM, this peak appears at 1470 cm^{-1} for the $\underline{1}01$ and at 1496 cm^{-1} for the 010 face as shown in Figure B-1. An identical spectrum was taken of a commercially available COM (Berglund, 1985). Single carboxylate symmetric stretch peaks for both COD and COT are located at 1483 cm^{-1} as shown in Figures B-2 and B-3, respectively.

The appearance of the carboxylate symmetric stretch double peak for COM is due to the two types of oxalate lattice positions (Shippey, 1981). These two types of oxalate ions were discussed in Chapter 2. The two peaks are observed for both the 010 and $\underline{1}01$ faces, but the relative intensities are reversed. Apparently, the intensity of the peak is related to the orientation of the oxalate ion with respect to the crystal face, with the greater intensity arising from ions lying parallel or at an angle to the given face, and the lesser intensity due to oxalate ions lying perpendicular to a face. Following this reasoning,

the greater intensity of the 1470 cm^{-1} peak for the $\underline{1}01$ face is due to the oxalate ions lying parallel to the 100 plane and at a slight angle to the $\underline{1}01$ plane, as shown in Figures 2-2 and 2-3. The less intense 1496 cm^{-1} peak is due to the oxalate ions lying parallel to the 010 plane (perpendicular to the 100 and $\underline{1}01$ planes). Conversely, the more intense 1496 cm^{-1} peak for the 010 face is due to the oxalate ions lying parallel to the 010, while the less intense 1470 peak is due to the oxalate ions lying parallel to the 100 plane.

In the case of COD and COT, the single peak at 1483 cm^{-1} in both spectra suggests a single type of oxalate ion occurring in their respective lattice structures. Such an occurrence has been reported for COD (Tazzoli and Domeneghetti, 1980) but COT has been reported to have two crystallographically distinct types of oxalate ion (Deganello et al., 1981).

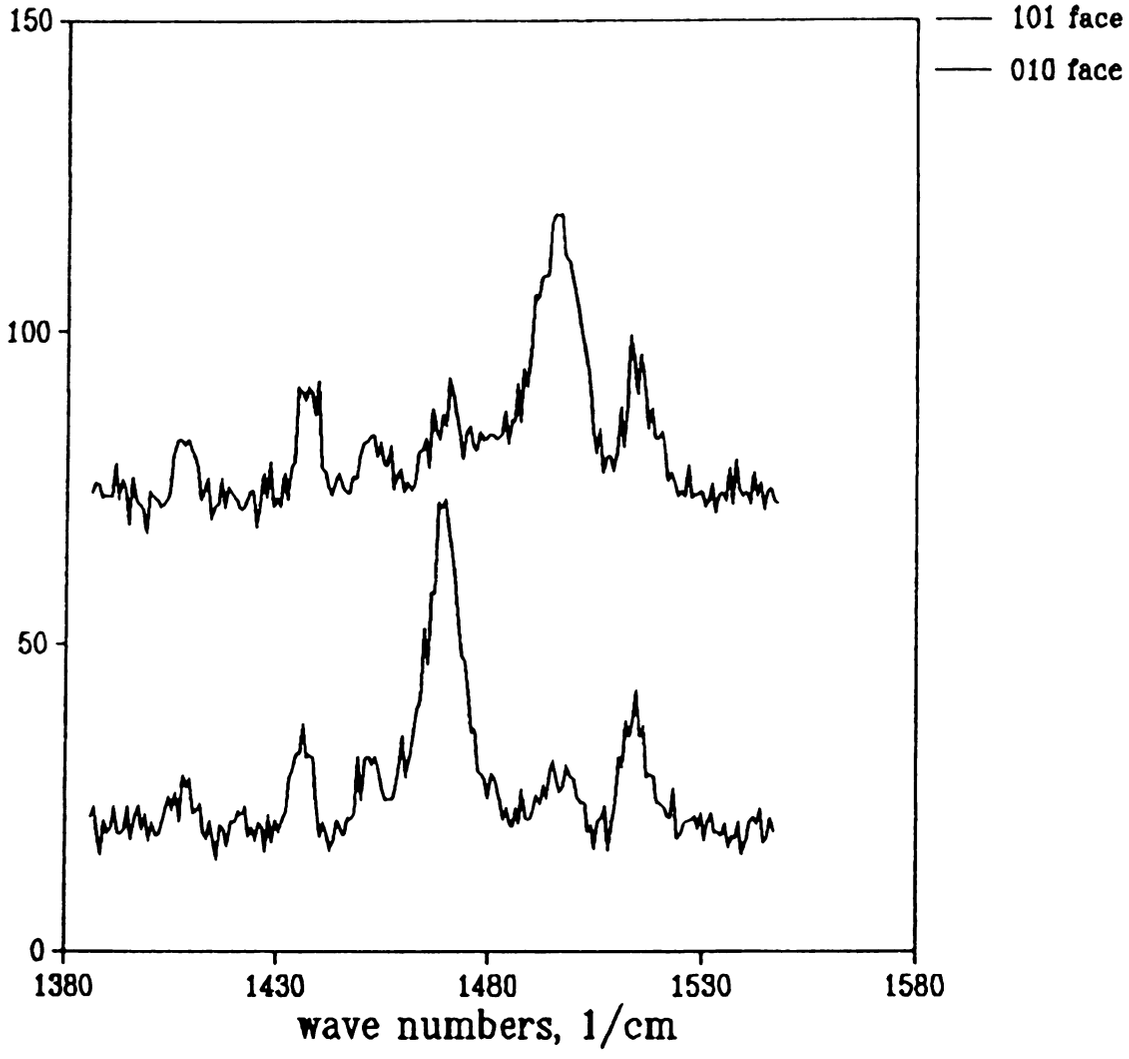

Figure B-1. COM Raman Spectrum

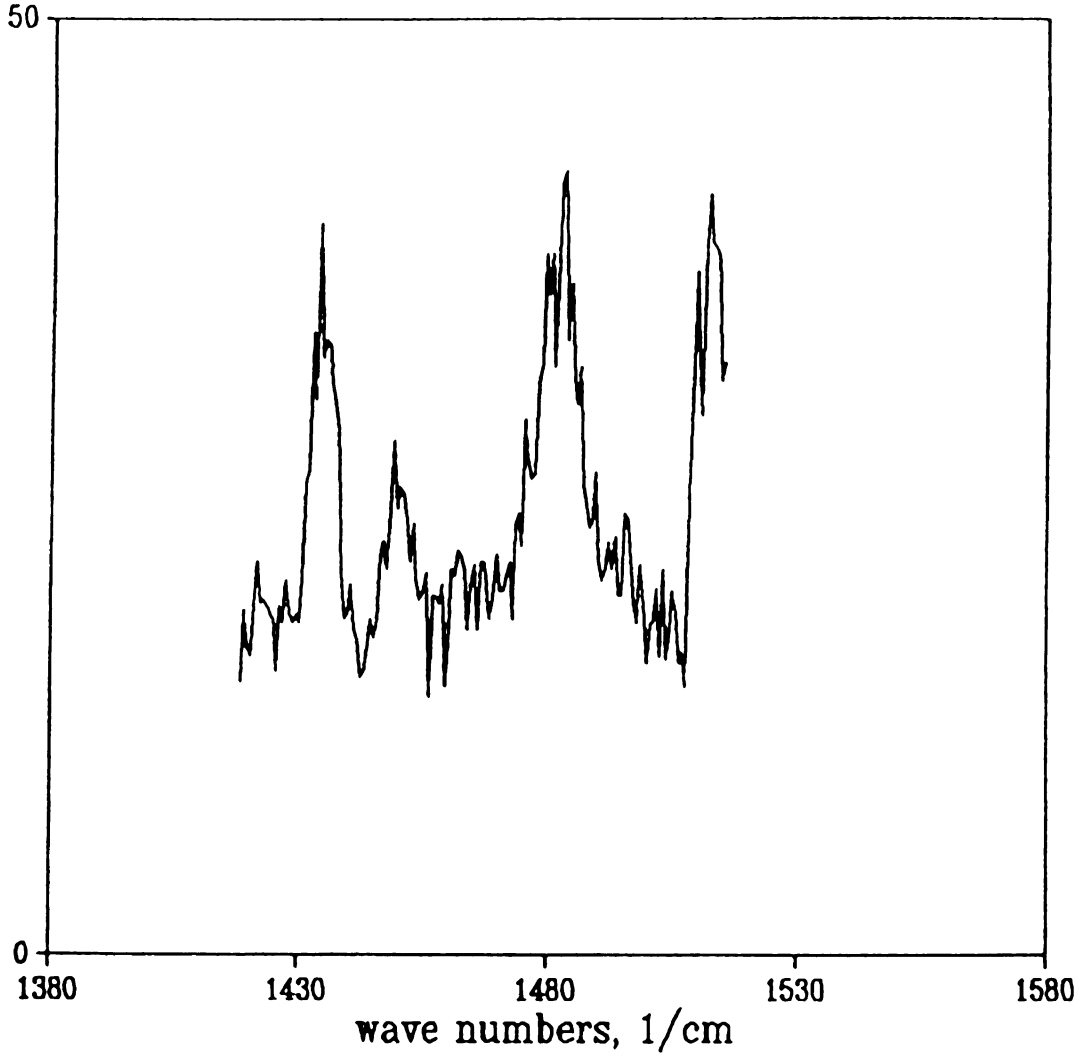

Figure B-2. COD Raman Spectrum

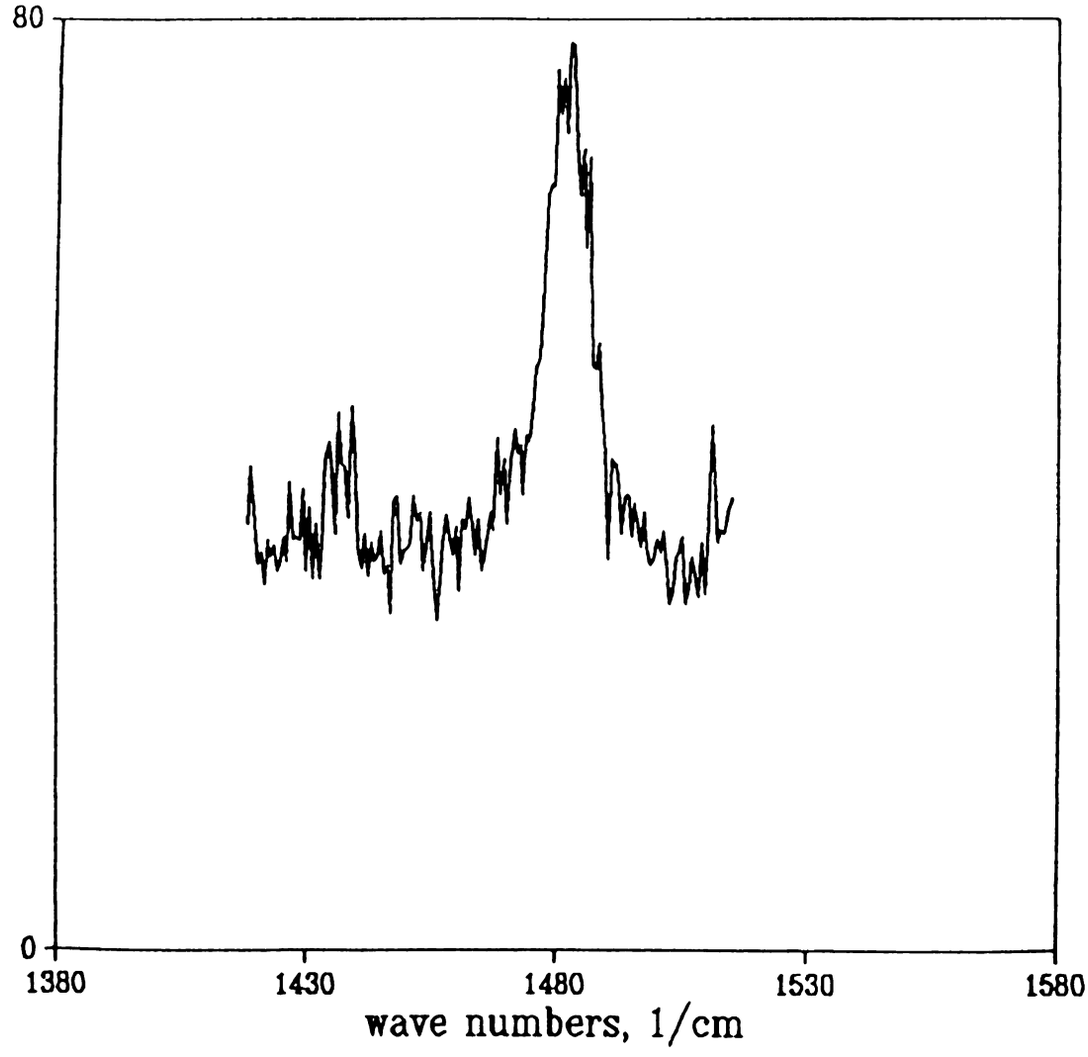

Figure B-3. COT Raman Spectrum

APPENDIX C

Appendix C. Calculation of Mass Transfer Effectiveness Factor

The resistance to mass transfer in a crystallization system can be resolved into contributions from 1) transfer of growth units in the bulk solution from the bulk to the crystal vicinity, and 2) the crystal growth mechanism occuring near the crystal surface, as discussed in Chapter 3. If the solution from which crystals are growing is well mixed, then the rate of diffusive transfer of growth units to the crystal vicinity is negligible compared with their convective transfer. In this case, the concentration of growth ions at the solution/crystal interface is nearly the same as that in the bulk. In order to express the degree of diffusive mass transfer resistance in crystal growth, an effectiveness factor similar to that defined for mass transfer resistance in chemical reaction kinetics can be used (Garside, 1984a).

Using a simple crystal growth rate law based on molar concentrations, the observed crystal growth rate, R_G, for a second-order system is expressed by

$$R_G = k_R (c_i - c_s)^2 \qquad (C\text{-}1)$$

where k_R is the rate constant, c_i is the molar concentration of the growth unit at the interface, and c_s is the concentration at the crystal surface. For a well-mixed solution, the interfacial concentration is equal to the bulk concentration, c_b, and the rate for this condition of no diffusive mass transfer resistance is given by

$$R_B = k_R (c_b - c_s)^2 \qquad (C\text{-}2)$$

The effectiveness factor for crystal growth, η, can then be defined as the ratio of the observed, mass transfer-limited growth rate to the growth rate in a well-mixed solution, or

$$\eta = k_R (c_i - c_s)^2)/(k_R (c_b - c_s)^2) \quad \{C\text{-}3\}$$

The observed growth rate can also be expressed in terms of a mass transfer coefficient, k_c, and a linear concentration driving force

$$R_G = k_c (c_b - c_i) \quad \{C\text{-}4\}$$

If flow near the crystals growing in the growth cell is visualized as flow near a flat plate, k_c can be calculate from the empirical expression (Carberry,)

$$k_c D_{AB}/\delta = .664 \, Re^{1/2} Sc^{1/3} \quad \{C\text{-}5\}$$

where D_{AB} is the diffusion coefficient for growth units, δ is a characteristic length, Re is the Reynolds number, and Sc is the Schmidt number.

Equation {C-4} can be rearranged to give

$$R_G/k_c (c_b - c_s) = 1 - (c_i - c_s)/(c_b - c_s) \quad \{C\text{-}6\}$$

From {C-1} and {C-3}, R_G can be expressed as

$$R_G = \eta k_R (c_b - c_s)^2 \quad \{C\text{-}7\}$$

Combining {C-6} and {C-4} to eliminate R_G gives

$$(c_i - c_s)/(c_b - c_s) = 1 - \eta \, Da \quad \{C\text{-}8\}$$

where the Damkholer number for crystal growth, Da, is given by

$$Da = k_R (c_b - c_s)^2 / k_c (c_b - c_s) \quad \{C\text{-}9\}$$

From equation {C-3}, the effectiveness factor is given by

$$\eta = (c_i - c_s)^2 / (c_b - c_s)^2 \quad \{C\text{-}10\}$$

Combining {C-7} and {C-9} then gives finally

$$\eta = (1 - \eta \, Da)^2 \quad \{C\text{-}11\}$$

Evaluation of the effectiveness factor requires the calculation of the product η Da, which, after combining {C-1}, {C-3}, and {C-8} is given by

$$\eta \, Da = R_G / k_c (c_b - c_s) \quad \{C\text{-}12\}$$

Calculation of the effectiveness factor depends only on the observed

growth rate, the mass transfer coefficient, and the bulk and surface concentrations.

A typical value of the effectiveness factor for crystal growth can be determined by considering growth of the 010 face of COM at a relative supersaturation of σ = 3.7 at 37 °C and I = 0.15 M. In this case, the observed facial growth rate, R_G, is approximately 0.1 microns/minute as seen in Figure 6-7. With a crystal density of 2.2 g/cm^3 (Elliot and Rabinowitz, 1980) and a COM molecular weight of 147 g/mol, this growth rate corresponds to a molar flux of 2.5×10^{-9} mole/cm^2/sec. For a stoichiometric initial mixture of calcium and oxalate, i.e., $T_{Ca} = T_{Ox}$ at σ = 3.7, the effective "growth unit" concentration, c, can be written as

$$c = ([Ca^{2+}][C_2O_4^{2-}])^{1/2} \qquad (C\text{-}13)$$

Using (C-12), the bulk solution concentration c_b is, from Table A-1, $((.8822 \times 10^{-3})(.5885 \times 10^{-3}))^{1/2} = .721 \times 10^{-3}$ M. With K_a for COM given as 2.49×10^{-9} M^2 from Table 2.2 and an activity coefficient of γ_2 = .3237, $c_s = (2.49 \times 10^{-9} / (.3237)^2)^{1/2} = .154 \times 10^{-3}$ M.

For a typical flowrate of 20 ml/min into the growth cell through a 1/8 inch (.3175 cm) inlet tube, the solution velocity near the surface of the glass cover slip is (20 cm^3/min) / (π (.3175)^2 / 4) = 4.2 cm/sec. A typical characteristic length for the crystal can be calculated from Figure 6-1b for the 010 face. With facial dimensions of approximately 25 microns by 50 microns, a geometric average size is $((25)(50))^{1/2}$ = 35 microns.

Other parameters needed for the calculation of the effectiveness factor are:

diffusion coefficient of Ca^{2+} = $.8 \times 10^{-5}$ cm^2/sec

viscosity of water at 37 °C = .007 g/cm/sec

density of water at 37 °C = 1 g/cm^3

Then, Re = (4.2 cm/sec)(.0035 cm)(1 gm/cm^3)/(.007 g/cm/sec) = 2.1

Sc = (.007 g/cm/sec)/(1 g/cm^3)/(.8 x 10^{-5} cm^2/sec) = 875

k_c = (.8 x 10^{-5} cm^2/sec)/(.0035 cm)

x $(2.1)^{1/2}$ $(875)^{1/3}$ = .21 cm/sec

$c_b - c_s$ = (.721 - .154) x 10^{-3} mol/l x .001 = 5.67 x 10^{-7} mol/cm^3

ηDa = (2.49 x 10^{-9} mol/cm^2/sec)/(.21 cm/sec)/(5.67 x 10^{-7} mol/cm^3)

= .00112

The effectiveness factor, η, is then

$\eta = (1 - .00112)^2$

= .959

This shows that for the conditions typical of the experiments performed in this work, the measured crystal growth rates reflect the crystal growth mechanism characteristic of COM and not bulk solution diffusion-limited growth.

BIBLIOGRAPHY

BIBLIOGRAPHY

Adair, J., Ph. D. Thesis, University of Florida, 1981.

Adam, U., and I. Robb, J. Chem Soc Faraday Trans I 79 (1983), 2745.

Adamson, A., Physical Chemistry of Surfaces, Wiley, New York, 1982.

Arnott, H., Biological Mineralization and Demineralization, G. Nancollas, ed., Springer-Verlag, New York, 1982.

Azoury, R., B. Goldwasser, Y. Wax, S. Perlberg, N. Garti, and S. Sarig, Urological Research 13 (1985), 199.

Babic-Ivancic, V., H. Furedi-Milhofer, B. Purgaric, N. Brnicevic, and Z. Despotovic, J. Crystal Growth 71 (1985), 655.

Bain, D., M. Cafe, I. Robb, and P. Williams, J. Coll. Int. Sci. 88 (1982), 467.

Barger, A., and D. Briedis, Department of Chemical Engineering, Michigan State University, unpublished data, 1986.

Bennema, P., J. Crystal Growth 1 (1967a), 278.

Bennema, P., J. Crystal Growth 1 (1967b), 287.

Bennema, P., J. Crystal Growth 5 (1969), 29.

Berg, W., J. Schnapp, H. Schneider, A. Hesse and E. Hienzsch, Eur. Urol. 2 (1976), 92.

Berglund, K., Ph. D. Thesis, Iowa State University, 1981.

Berglund, K., Department of Chemical Engineering, Michigan State University, unpublished data, 1985.

Bijvoet, O., L. Blomen, E. Will, and H. van der Linden, J. Crystal Growth 64 (1983), 316.

Blomen, L., E. Will, O. Bijvoet and H. van der Linden, J. Crystal Growth 64 (1983), 306

Boyce, W., American J. Medicine 45 (1968), 673. Brandse, W., and G. van Rosmalen, J. Inorg. Nucl. Chem. 39 (1977), 2007.

Brecevic, L., D. Skrtic, and J. Garside, J. Crystal Growth 74 (1986), 399.

Burns, J., and B. Finlayson, Inv Urol 18 (1980), 174.

Burns, J., B. Finlayson, and A. Smith, in Urolithiasis: Clinical and Basic Research, Smith et al., eds., Plenum Press, New York, 1981.

Burton, W., N. Cabrera, and F. Frank, Phil. Trans. Roy. Soc. A243 (1951), 299.

Cafe, M. and I. Robb, J. Coll. Int. Sci. 86 (1982), 411.

Caldin, E., Fast Reactions in Solution, Blackwell Scientific Publications (Oxford), 1964.

Carberry,J., Chemical and Catalytic Reaction Engineering, McGraw-Hill, New York, 1976.

Chiang, P. and M. Donohue, AIChE Symp. Ser. 83 (253), 1987.

Curreri, P., G. Onoda, and B. Finlayson, J. Coll. Interface Sci. 69 (1979), 170.

Crawford, J., E. Crematy and A. Alexander, Aust J. Chem. 21 (1968), 1067.

Daniele, P., C. Rigano, and S. Sammartano, Thermochimica Acta 62 (1983), 101.

Deganello, S., A. Kampf, and P. Moore, American Mineralogist 66 (1981), 859.

DeLong, J., and D. Briedis, J. Crystal Growth 71 (1985a), 689.

DeLong, J., and D. Briedis, AIChE Symposium Series 240 80 (1984), 105.

DeLong, J., and D. Briedis, Presented at the AIChE National Meeting, Chicago, Illinois, November 13, 1985b.

DeLong, J., and D. Briedis, Presented at the AIChE Spring Meeting, New Orleans, Louisiana, April 7, 1986.

DeLong, J., and D. Briedis, Presented at the AIChE National Meeting, New York, New York, November 18, 1987.

Desmars, J., and R. Tawashi, Bioch. Biophys. Acta 313 (1973), 256.

Dheu-Andries, M., and S. Perez, Carbohydrate Research 124 (1983), 324.

Djarova, M., and P. Kovandjiev, Industrial Crystallization 84, Jancic and de Jong, eds., Elsevier (Amsterdam) 1984, 275.

Drach, G., S. Thorson, and A. Randolph, J. Urology 123 (1980), 519.

Drach, G., S. Sarig, A. Randolph, and S. Thorson, Urological Research 10 (1982a), 165.

Drach, G., Z. Kraljevich, and A. Randolph, J. Urology 127 (1982b), 805.

Duval, D. and R. Chondrate, Physica Status Solidi B 132 (1985), 83.

Eigen, M., Pure Appl. Chem 6 (1963), 97.

Elliot, J., and I. Rabinowitz, J. Urology 123 (1980), 324.

Finlayson, B., Investigative Urology 9 (1972), 258.

Finlayson, B., Kidney International 13 (1978a), 344.

Fleisch, H., Kidney International, 13 (1978), 361.

Frey-Wyssling, A., Am J Botany 68 (1981), 130.

Gains, N., C. Michaels, M. Thwaites, and J. Trounce, Nephron 5 (1968), 352.

Gardner, G., and R. Doremus, Investigative Urology 15 (1978), 478.

Gardner, G., J. Crystal Growth 30 (1975), 158.

Gardner, G., and G. Nancollas, J. Physical Chemistry 79 (1975), 2597.

Garside, J., L. Brecevic, and J. Mullin, J. Crystal Growth 57 (1982), 233.

Garside, J., and R. Ristic, J. Crystal Growth 61 (1983), 215.

Garside, J., AIChE Symposium Series 240 80 (1984a), 23.

Garside, J., Industrial Crystallization 84, Elsevier (Amsterdam), 1984b, 1.

Garside, J., R. Janssen-van Rosmalen, and P. Bennema, J. Crystal Growth 29 (1975), 353.

Garti, N., S. Sarig, and F. Tibika, Inv. Urol. 18 (1980), 149.

Gill, W., J. Karesh, L. Garsin, and M. Roma, Investigative Urology 15 (1977), 95.

Gill, J., and R. Varsanik, J. Crystal Growth 76 (1986), 57.

Gjaldbeck, J., Clinica Chimica Acta 120 (1982), 363.

Hallson, P., and G. Rose, The Lancet (May 12, 1979), 1000.

Heijnen, W., J. Crystal Growth 57 (1982), 216.

Heijnen, W., W. Jellinghaus, and W. Klee, Urol Res 13 (1985), 281.

Hesselink, F., in Adsorption from Solution at the Solid/Liquid Interface, G. Parfitt and C. Rochester, eds., Academic Press (New York), 1983.

Hillig, W., Acta Met. 14 (1966), 1968.

Hlady, V., J. Colloid and Interface Science 90 (1984), 373.

Honig, E., and J. Hengst, J. Colloid Int. Sci. 29 (1969), 510.

Hunter, R., Zeta Potential in Colloid Science, Academic Press (New York), 1981.

Isaacson, L., Investigative Urology 5 (1968), 406.

Ito, H. and F. Coe, Am J Phys 233 (1977), F455.

Janssen-van Rosmalen, R., P. Bennema, and J. Garside, J. Crystal Growth 29 (1975), 342.

Kitamura, T., J. Zerwekh, and C. Pak, Kidney International 21 (1982), 379.

Lanzalaco, A., M. Sheehan, and G. Nancollas, J Urology 128 (1982), 845.

Leal, J., and B. Finlayson, Inv. Urol. 14 (1977), 278.

Leavens, P., American Mineralogist 53 (1968), 455.

Levine, I., Physical Chemistry, McGraw-Hill, New York, 1978.

Lopez, M., Y. Nakagawa, F. Coe, C. Tsai, A. Michael, and J. Scheinman, Kidney Int. 29 (1986), 829.

Meyer, J., and L. Smith, Investigative Urology 13 (1975a), 31.

Meyer, J., and L. Smith, Investigative Urology 13 (1975b), 36.

Mullin, J., Crystallisation, Butterworths, London, 1961.

Nakagawa, Y., E. Kaiser and F. Coe, Bioch. Biophy. Res. Comm. 84 (1978), 1038.

Nakagawa, Y., H. Margolis, S. Yokoyama, F. Kezdy, E. Kaiser, and F. Coe, J. Biol. Chem. 256 (1981), 3936.

Nakagawa, Y., V. Abram, F. Kezdy, E. Kaiser, and F. Coe, J. Biol. Chem. 258 (1983), 12594.

Nakagawa, Y., V. Abram and F. Coe, Am. J. Phys. 247 (1984), F765.

Nagasawa, M., and A. Holtzer, J. Am. Chem. Soc. 60 (1964), 538.

Nancollas, G. and G. Gardner, J. Crystal Growth 21 (1974), 267.

Nielsen, A., Acta Chemica Scandinavica 14 (1960), 1654.

Nielsen, A., Industrial Crystallization 81, Jancic and de Jong, eds., North Holland, 1982.

Nielsen, A., and J. Toft, J. Crystal Growth 67 (1984a), 278.

Nielsen, A., J. Crystal Growth 67 (1984b), 289.

Oosawa, F., Polyelectrolytes, Marcel-Dekker, New York, 1971.

Overbeek, J.Th.G., Colloid Science, H. Kruyt, ed., Elsevier, 1952.

Papenhuijzen, J., H. Van Der Schee, and G. Fleer, J. Coll. Int. Sci. 104 (1985a), 540.

Papenhuijzen, J., J. Fleer, and B. Bijsterbosch, J. Coll. Int. Sci. 104 (1985b), 553.

Randolph, A., and G. Drach, J. Crystal Growth 53 (1981), 195.

Randolph, A., and M. Larson, Theory of Particulate Processes, Academic Press, New York, 1971.

Riskalla, E., and M. Moawad, J. Chem. Soc., Faraday Trans. I 80 (1984), 1617.

Robertson, W., D. Scurr, and C. Bridge, J. Crystal Growth 53 (1981), 182.

Robertson, W., M. Peacock, R. Marshall and F. Knowles, Clin. Sci. Molecul. Med. 47 (1974), 13.

Robertson, W., M. Peacock, and B. Nordin, Clinical Science 34 (1968), 579.

Robertson, W., M. Peacock, R. Marshall, D. Marshall, and B. Nordin, New Eng J Med 294 (1976), 249.

Robertson, W., and D. Scurr, J. Urology 135 (1986), 1322.

Robertson, W., A. Latif, D. Scurr, A. Caswell, G. Drach, and A. Randolph, in Urinary Stone, R. Ryall, et al., eds., Churchill Livingstone, Melbourne, 1984.

Robertson, W., F. Knowles, and M. Peacock, Urolithiasis Research, H. Fleisch, et al., eds., Plenum, New York, 1976b.

Robertson, W., M. Peacock, and F. Knowles, Urinary Calculi, L. Cifuentes Delatte, et al., eds., Karger, Basel, Spain, 1973.

Robertson, W., M. Peacock, and B. Nordin, Clinical Science 40 (1971), 365.

Rodgers, A. and J. Garside, Investigative Urology 18 (1981), 484. Rose, A., Urinary Stones: Clinical and Laboratory Aspects, MTP Press, Lancaster, England, 1982.

Ryall, R., R. Harnett, and V. Marshall, J. Urology 135 (1986), 174.

Sallis, J., and M. Lumley, Inv Urol 16 (1979), 296.

Sarig, S., D. Hirsch, and N. Garti, J. Crystal Growth 69 (1984), 91.

Sheehan, M. and G. Nancollas, Investigation Urology 17 (1980), 446.

Smith, B., and A. Alexander, J. Colloid and Interface Science 34 (1970), 81.

Smith, L., J. Meyer, and J. McCall, in Urinary Calculus, L. Cifuentes Delatte et al., eds., S. Karger, Basel, Spain, 1973.

Stryer, L., Biochemistry, Freeman, San Francisco, 1981.

Tazzoli, V., and C. Domeneghetti, American Mineralogist 65 (1980), 327.

Tomazic, B., and G. Nancollas, J. Crystal Growth 46 (1979a), 355.

Tomazic, B., and G. Nancollas, Investigative Urology 16 (1979b), 329.

Tomazic, B., and G. Nancollas, J. Coll. Int. Sci. 75 (1980a), 149.

Tomazic, B., and G. Nancollas, Inv Urol 18 (1980b), 97

Tomazic, B., R. Mohanty, M. Tadros, and J. Estrin, J. Crystal Growth 75 (1986), 329.

Valcic, A., J. Crystal Growth 30 (1975), 129.

Verwey, E., and J. Overbeek, Theory of the Stability of Lyophobic Colloids, Elsevier, Amsterdam, 1948.

Voight, J., Sandia National Laboratory, Albuquerque, New Mexico, personal communication, 1987.

Walton, A., Mikrochimica Acta (1963), 422.

Walton, A., The Formation and Properties of Precipitates, Krieger, New York, 1967.

Werness, P., S. Duckworth, and L. Smith, Inv Urol 17 (1979), 230.

Werness, P., J. Bergert, and L. Smith, J. Crystal Growth 53 (1981), 166.

White, D., and G. Nancollas, J. Crystal Growth 57 (1982), 267.
Whitney, K., and H. Arnott, Mycologia 78 (1986), 42.

Will, E., O. Bijvoet, L. Blomen and H. van der Linden, J. Crystal Growth 64 (1983), 297.